Dynamic Monitoring and Life Prediction of Internal Strain-Gage Balances

A Thesis Presented for the
Master of Science
Degree
The University of Tennessee, Knoxville

David Leon Yoder
December 2016

DEDICATION

I dedicate this work to my family and friends who supported me throughout this process. I especially want to thank my wife, Tiffany, who sacrificed much of her time allowing me to focus on this effort, and encouraged me every step along the way. Without her spurring me on, this task would have been even more difficult.

ACKNOWLEDGEMENTS

I would like to thank all those that helped and provided their support during the preparation of this thesis. First and foremost, I would like to thank Mr. Wayne Hawkins for providing the thesis topic as well as the continuous guidance and assistance during the preparation. I would also like to thank Dr. Bill Lawrence, Mr. Chris Curnes, Mr. Stan Richardson, Scott Wieland, Chris Gernaat, and Mr. Rod Stewart for providing countless hours of technical support. Their immense knowledge and work in the area of strain-gage balances and signal processing was a great help to me. I would also like to thank the Major Professor of my thesis committee, Dr. Trevor Moeller, and thesis committee members, Dr. Ahmad Vakili and Dr. Monty Smith. Their support and review during the preparation of this thesis was vital. I would also like to thank Arnold Air Force Base for providing time and resources to complete this thesis.

ABSTRACT

Wind tunnel test customers continue to push the limits by producing air vehicle designs that produce high aerodynamic loads at the desired test conditions. These loads are a combination of steady aerodynamic, unsteady aerodynamic, and inertial forces. A methodology to monitor the health of a wind tunnel strain-gage balance has been developed. The objective of this methodology is to define the stress limits of the balance and monitor these limits so the balance can be safely tested without failure of the balance. A balance failure could result in costly damage to the wind tunnel model, support system, and the wind tunnel facility itself. The health monitoring method incorporates elements of signal processing, finite element analysis (FEA), cycle counting in fatigue analysis, and cumulative damage model theory. From these areas a new balance monitoring methodology that is capable of computing balance loads and stresses, factors of safety, counting fatigue cycles, and providing guidance for inspection of the balance. An example of implementation of this methodology using dynamic balance readings collected from a wind tunnel test is discussed. Results show a maximum load calculation error reduction of 71% and an overall accuracy of at least 95%. Additionally, the new methodology identified 17% more exceedances than the legacy method.

TABLE OF CONTENTS

LIST OF TABLES

LIST OF FIGURES

NOMENCLATURE

AEDC	Arnold Engineering Development Complex
XBAL	X-axis of the balance
BMC	Balance moment center
YM	Yawing moment
NF	Normal force
SF	Side force
PM	Pitching moment
YBAL	Y-axis of the balance
RM	Rolling moment
AF	Axial force
ZBAL	Z-axis of the balance
S_u	Ultimate stress
S_y	Yield stress
S_e	Endurance stress
σ_{max}	Maximum peak stress of a cycle
σ_{min}	Minimum peak stress of a cycle
σ_m	Mean stress of a cycle
σ_a	Alternating stress of a cycle
σ	stress
ε	strain
F	Force
L	Length
A	Area
Δ	delta, change in
R	Resistance
GF	Gage factor
16T	AEDC 16 ft cross section, transonic wind tunnel

1.0 INTRODUCTION

1.1 PROJECT OVERVIEW AND MOTIVATION

In a wind tunnel, a strain-gage balance is frequently used to measure the aerodynamic loads acting on a test article. An important part of using a balance is ensuring the safety of the balance through monitoring the loads exerted upon it. These loads are made up of inertial and aerodynamic loads. Each of these loads can be steady or unsteady. In many cases an aerodynamic phenomenon such as abrupt wing stall, asymmetric vortex shedding, or an inlet unstart is the forcing function that imparts unsteady loads onto the model. This in turn excites unsteady inertial loads based on the frequency modes of the constrained wind tunnel support system attached to the model. All of these loads can be captured via a strain-gage balance.

To protect a balance from failure, knowing the loads acting on the balance is only part of the solution. An understanding of where the balance weak points are located and under what load scenarios failure will occur is also critical. The Arnold Engineering Development Complex (AEDC) mandates that a hazard analysis be a part of each wind tunnel test, and many times a major component of this analysis is the balance stress analysis; thus AEDC has a rich history of implementing algorithms to monitoring balances.

Since much of the AEDC balance inventory is 25+ years old, projects are presently ongoing to modernize the inventory. Although minor changes have been made, the basis for the current (which will be referred to as legacy in this document) AEDC algorithms, used for monitoring the health of a balance during testing, were developed around 25 years ago. These facts, along with balance failures occurring during recent testing, have presented a timely opportunity to examine the legacy balance monitoring process and look for ways to better characterize the health of the balance as it is subjected to loads in a wind tunnel facility. The concept of modernizing balance monitoring and protection has been examined by engineers at ONERA, Boeing, and NASA and their experiences will serve as foundational blocks (REF 1 and 2). The work presented in this thesis sought to understand the AEDC legacy method and proposed solutions to improve these methods based on the current state of technology.

1.2 INTERNAL STRAIN-GAGE BALANCES

An internal strain-gage balance is a measurement device that has been designed in such a way to resolve forces and moment acting on whatever the balance is connected to on the force sensing or metric side of the balance. Balances can be designed to measure from one to six-components of the load, and measurement of all six components is necessary to define the total load. Six-component internal strain-gage balances have been used in wind tunnels since the 1940’s (REF 3). Figure 1 is an example of a six-component strain-gage balance design from 1948 (REF 1). Figure 2 provides some more modern design examples (REF 4-7). These designs incorporate complex internal

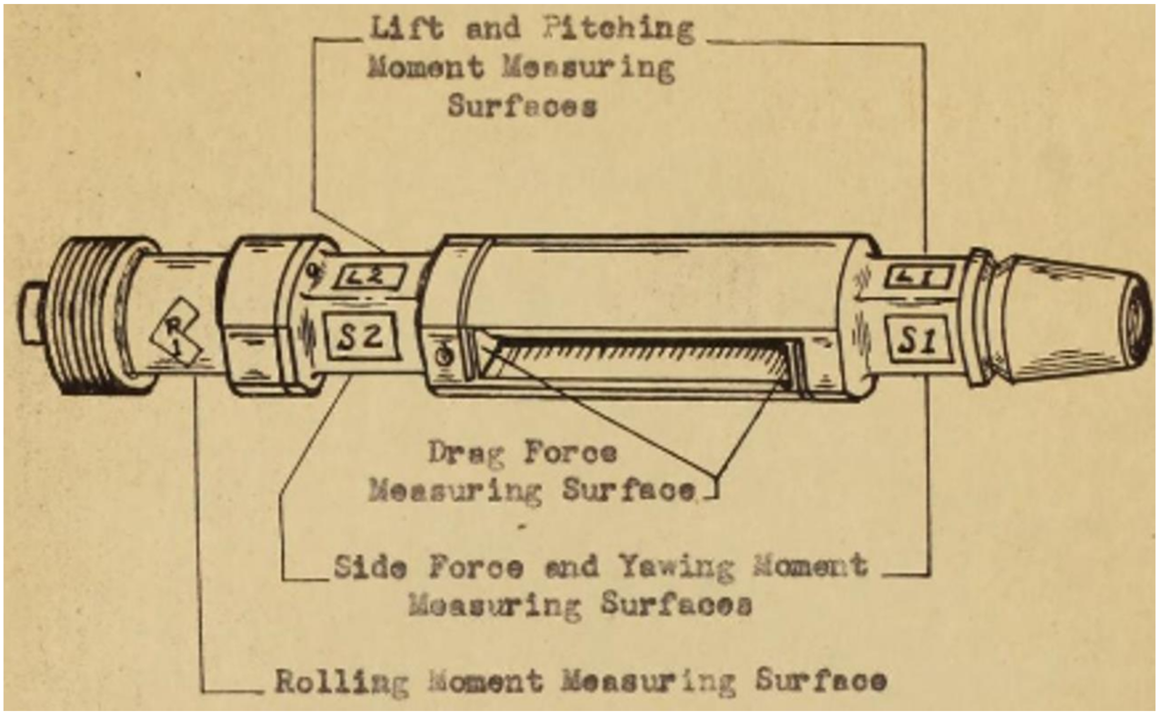

Figure 1. 1948 6-Component Balance Design (REF 1)

Figure 2. Examples of Internal Strain-Gage Balance (REF 4-7)

geometries, advanced materials, and different model attachment methods. Figure 3 provides the axis system definition for the six-component loads. The total loads are a combination of the aerodynamic loads, model weight, and a portion of the weight of the balance itself. A strain-gage balance measures the loads by using strain gages, arranged in a Wheatstone bridge, to measure the strain produced by the loads. A balance measuring six-component loads will have at least six Wheatstone bridges.

The output voltage of a balance bridge changes as a function of the strain at the bridge location which is produced by the applied loads. In order to convert the output voltage into a load, the balance must be calibrated. The balance is calibrated by applying known loads to the balance and recording the output of the various bridges. A numerical relationship, or calibration matrix, between the applied loads and the voltage readings from the balance bridges is then determined. The calibration of the balance is extremely important in the use of a strain-gage balance. The measured loads can never be more accurate than the accuracy of the calibration. It needs to be pointed out that the equipment and techniques used to calibrate a balance greatly affect the accuracy of the loads measured by the balance.

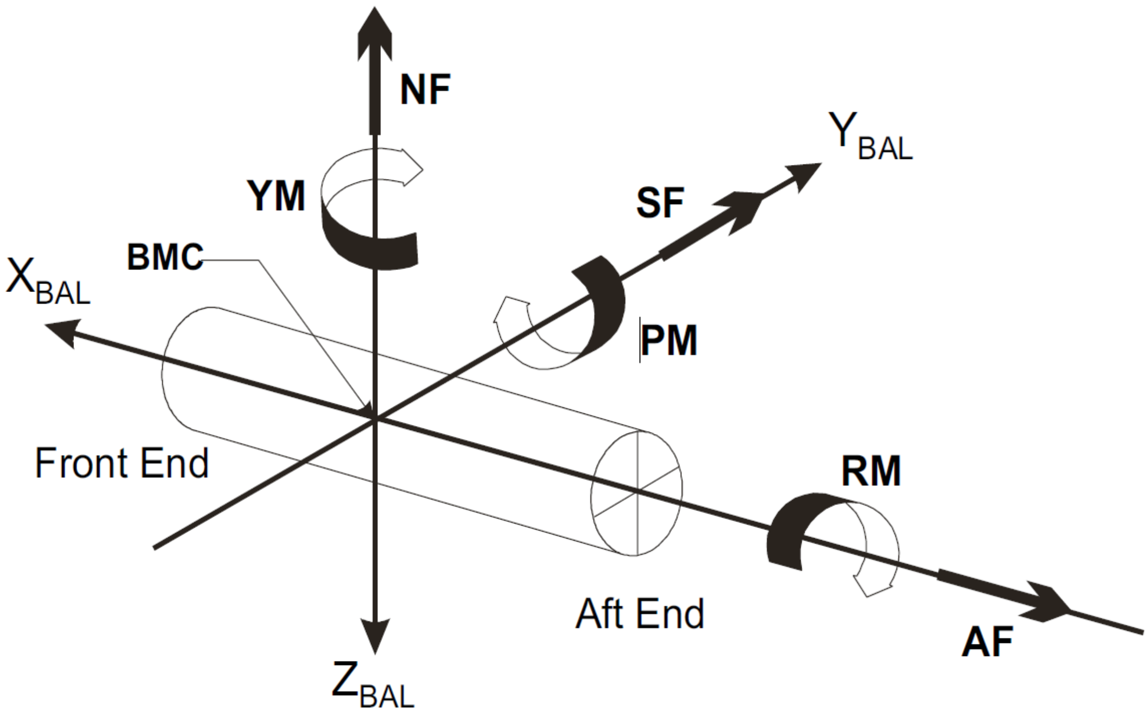

Figure 3. Balance Axis System

2.0 LITERATURE REVIEW

2.1 STRAIN-GAGES

Stress and strain are the results of external forces applied to a stationary object. Stress is defined as the object's internal resisting forces, and strain is defined as the displacement and deformation that occur (REF 8). For a uniform distribution of internal resisting forces, stress can be calculated by dividing the force (F) applied by the unit area (A):

$$\text{Stress, } \sigma = F/A \tag{1}$$

Strain is defined as the amount of deformation per unit length of an object when a load is applied. Strain is calculated by dividing the total deformation of the original length (ΔL) by the original length (L):

$$\text{Strain, } \varepsilon = \Delta L/L \tag{2}$$

Typical values for strain are less than 0.001 inch/inch for internal balances and are often expressed in micro-strains (10^{-6}).

Whether compressive or tensile, strain is typically measured by strain-gages. In 1856 Lord Kelvin first reported that metallic conductors subjected to mechanical strain exhibit a change in their electrical resistance (REF 8). It wasn’t until the 1930s that this phenomenon was first put to practical use (REF 8).

The change in resistance (ΔR) is proportional to the strain experienced by a strain-gage. If a wire is held under tension, the cross-sectional area is reduced and the length is increased. Also the specific resistivity, defined as the resistance per unit length for a given cross section, increases for metals used for strain-gages as the tensile strain is increased. The gage factor (GF), which is also called the strain sensitivity, for a gage with unstrained resistance R is given by:

$$GF = (\Delta R/R)/(\Delta L/L) \qquad (3)$$

The ideal strain-gage would change resistance only due to the deformations of the surface to which the strain-gage is bonded. In real applications, temperature, the stability of the material, and the adhesive that bonds the gage to the surface all affect the detected resistance (REF 8).

2.1.1 BONDED RESISTANCE GAGES

The first bonded, metallic wire-type strain-gage was developed in 1938 (REF 8). A metallic foil-type strain-gage consists of a grid of wire filament of approximately 0.001 in. thickness, bonded directly to an insulated backing material which is bonded to the strained surface of the spring material (balance) by a thin layer of epoxy resin. When the carrier matrix is strained, the adhesive transmits the strain to the grid material. The change in the electrical resistance of the grid is measured to quantify the amount of strain. The grid shape is designed to provide maximum gage resistance while keeping both the length and width of the gage to a minimum. A typical gage is shown in Fig. 4. The typical active grid used at AEDC ranges from 0.040 by 0.050 in. to 0.062 by 0.125 in.

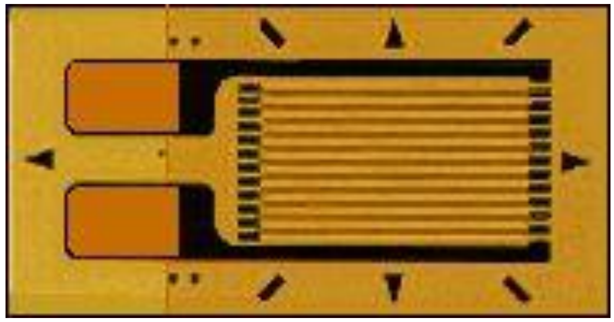

Figure 4. Typical Balance Strain-Gage

Each strain-gage wire material has its characteristic gage factor, resistance, temperature coefficient of gage factor, thermal coefficient of resistivity, and stability. The most popular materials are Constantan (copper-nickel alloy) and Karma (nickel-chrome alloy) foils.

2.2 BALANCE DESIGN

Balances are designed to provide areas of high stress with enough strain to produce a significant resistance change based on the GF. However, one could design a balance that would survive whatever loads it experienced, but would have little to no sensitivity in a strain-gage output, thus the uncertainty in these measurements would be unacceptably large. Hence the design process of a balance is a trade-off between balance accuracy and balance strength. For this reason, balances are designed to meet a defined load case. On a six-component balance one may only be able to define a portion of the desired loads and the remaining components will simply “fall-out” from the other design choices.

In addition to choosing areas with stresses high enough to get sufficient output from a strain-gage, balances are also designed to isolate each component from the other components as much as possible. If the size of the balance is not an issue then this can be accommodated, but in wind tunnel models incorporating an internal balance, size is almost always a driving design constraint, so balances usually have significant interactions between the components. A specific example of an interaction would be if the axial bridge has a change in output when a pure normal force is applied to the balance.

2.2 BALANCE CALIBRATION AND LOAD CALCULATION

A balance is calibrated by applying a known mass and measuring the change in voltage due to resistance changes in the Wheatstone bridges. The masses used at AEDC are determined in a metrology lab and are traceable to the National Institute of Standards and Technology (NIST). The process of applying masses is repeated for a sufficient number of independent conditions to allow determination of the coefficients in the mathematical model chosen to define the device's behavior. A mathematical model is used to estimate the true physical equations that are too complex to derive. A Global process is used to solve for the coefficients that make up a mathematical model representation of the physical process. The defined loading sequence serves as the experimental data to create the math model.

As mentioned previously it is generally not possible to eliminate interactions between the outputs of each bridge so these interactions need to be accounted for in the math model, and therefore the loading sequence. Such interactions are classified as either 'linear' or 'non-linear'. Construction variations (manufacturing tolerances and misalignments arising during assembly of multi-part balances), improper positioning and alignment of the strain-gages, variations of GF, etc. typically cause the linear terms. The non-linear terms are attributable to misalignments resulting from the complex deflections which occur when the balance is loaded (REF 9). Although not required, a total of 96 different coefficients is recommended for consideration in the American Institute of Aeronautics and Astronautics (AIAA) recommended practice when fitting a math model for an internal wind tunnel strain-gage balance (REF 9). These 96 terms come from experience with using and calibrating balances by the American and international wind tunnel test community. Equation 4 provides all the possible terms that are recommended.

$$R_i = a_i + \sum_{j=1}^{n} b1_{i,j} F_j + \sum_{j=1}^{n} b2_{i,j} \left|F_j\right| + \sum_{j=1}^{n} c1_{i,j} F_j^2 + \sum_{j=1}^{n} c2_{i,j} F_j \left|F_j\right| + \sum_{j=1}^{n} \sum_{k=j+1}^{n} c3_{i,j,k} F_j F_k +$$
$$\sum_{j=1}^{n} \sum_{k=j+1}^{n} c4_{i,j,k} \left|F_j F_k\right| + \sum_{j=1}^{n} \sum_{k=j+1}^{n} c5_{i,j,k} F_j \left|F_k\right| + \sum_{j=1}^{n} \sum_{k=j+1}^{n} c6_{i,j,k} \left|F_j\right| F_k +$$
$$\sum_{j=1}^{n} d1_{i,j} F_j^3 + \sum_{j=1}^{n} d2_{i,j} \left|F_j^3\right| \qquad (4)$$

In this form, the model assumes the electrical output reading from the strain-gage bridge for the i^{th} component (R_i) to be related to the applied single and two-component loads (F_j, F_k) by a third-order polynomial function, where 'n' is the number of component loads measured by the balance, and the intercept term a_i represents the output from the i^{th} bridge when all loads (F) are zero. This math model is commonly reffered to as the 6x96 calibration matrix if the balance contains six components. The largest contributors in the 6x96 calibration matrix are the six primary sensitivities, $b1_j$. This term represents the contribution to the voltage change of a bridge when a load is directly applied to that bridge.

Global regression is the commonly used procedure to derive the balance calibration matrix from the calibration data. Although a thorough explanation of global regression will not be explained here, an example of the application of the global regression for a 3-component strain-gage balance can be found in Reference 9. The global regression process solves for the unknown coefficients for each of the 'n' components in the math model of Eq. 4 by the method of least squares. Specifically, the sum of the squares of the deviations between the calculated and measured outputs will be minimized for the calibration dataset. Once the regression process is completed and all the coefficients are known, the resulting math model can predict the voltage change of any of the balance Wheatstone bridges for a given applied load. This relationship is the balance calibration matrix.

Unlike calibration, during a wind tunnel test the applied load is not known, but the voltage change is measured. Thus the inverse of the calibration matrix is required since the independent and dependent parameters have changed. In other words we now want to use Eq. 4 to solve for F_j instead of R_i. Intuitively this cannot be directly accomplished because a 6x96 matrix is not square, thus it can't be inverted. Also examining Eq. 4 it is clear that solving for Fj results in having R_i and F_k on the same side of the equation, but R_i is a function of F_k, thus an iterative scheme is required when using the calibration matrix to calculate load as a function of voltage. Fortunately most balances are predominately linear systems, therefore convergence typically occurs within a few iterations.

2.3 STRESS ANALYSIS

Although the purpose of this thesis is not to focus on all the intricacies and complex details of performing a thorough stress analysis, the reader must understand that the balance monitoring methodology presented is only as good as the understanding of the balance stress limits. For this reason a summary of standard static structural stress equations are presented as well as a discussion on fatigue and the factors that contribute to this type of failure. These topics are complex in their own right, and an expert in material properties and stress analysis should be consulted to perform a thorough and complete stress analysis of a balance to determine the proper monitoring limits. This work conducts a simplified analysis in order to show how it fits into the overall methodology and provide example application results in later sections.

2.3.1 STATIC STRUCTURAL ANALYSIS

Historically at AEDC the balance stress analysis has been executed by performing hand calculations at critical cross sections of the balance to find the highest stressed components. In stress analysis industries, especially in aerospace, hand calculations in structural analysis are a necessity to quickly analyze simple geometries before a part is manufactured. The term hand calculations refers to using classical stress equations to do rough order magnitude assessments of stress levels and sizing requirements. Typically these are performed by a stress engineer using a pencil, paper, and a handheld calculator. Generally some form of the classic stress equations provided in Eq. 1 and 5 through 7 are applied where appropriate. Section 4.4.2 provides example calculations using these equations for the balance chosen in this study.

$$Bending\ Stress = \sigma_b = \frac{Mc}{I} \tag{5}$$

$$principle\ stress = \sigma_1, \sigma_2 = \frac{\sigma_x + \sigma_y}{2} \pm \tau_{max,min} \tag{6}$$

$$\tau_{max}, \tau_{min} = \frac{1}{2}\sqrt{\left(\sigma_x - \sigma_y\right)^2 + 2\tau^2} \tag{7}$$

A particularly useful theory in the prediction of failure due to static loading of ductile materials is the von Mises theory (also known as the distortion energy theory). It is commonly used to predict tensile and shear failure in steel parts (REF 10). The von Mises stress, σ', is calculated from the principal stresses, and an equation for biaxial loading is provided in Eq. 8.

$$von\ Mises\ stress = \sigma' = \pm\sqrt{\sigma_1{}^2 + \sigma_2{}^2 - \sigma_1\sigma_2} \tag{8}$$

The von Mises stress is calculated using finite element analysis (FEA) software and is often the basis for determining factors of safety for a given static load condition. Using the von Mises theory the failure criterion is

$$\sigma' > S_{yt} \tag{9}$$

The factor of safety can then be calculated from taking the ratio of the tensile-yield strength, S_{yt}, over the von Mises stress. This will be the cornerstone method in this research for determining what areas of the balance are the highest stressed, and for determining the overall magnitude of the max stress levels.

2.3.2 FATIGUE

Material fatigue is a phenomenon where structures fail when subjected to a cyclic load. A cycle can simply be considered an event in which two load/stress reversals have occurred, and cyclic loading will contain many cycles. Fatigue structural damage occurs at stress levels that can be far below the static yield strength. Fatigue problems in a dynamically loaded mechanical structure arise at stress concentrations (REF 11). The gross deflections of the structure are related to the applied loads in a linear elastic manner. In other words, there is no general yielding because the global stress is well below the static yield, but plastic strains may occur at the critical locations. For this reason fatigue is the most common source behind failures of mechanical structures (REF 12). The process until a component finally fails under repeated cyclic loading can be divided into three stages (REF 13). The first stage involves a microscopic crack forming at the surface and then, due to a large number of cycles, this crack grows until a macroscopic crack is formed. Once the macroscopic crack is formed it will continue to grow for each cycle until a critical length is reached which is characterized as the second stage. Finally, the last stage results in the component breaking due to the cracked area forming high stress concentrations which can no longer handle the peak load. Sometimes the progression of these stages is not clear because the microscopic crack grows rapidly causing sudden failure. Because of this phenomenon the intent of the balance monitoring methodology will be to limit the loads to below the point where the initial microscopic cracks are formed in the first stage.

In some texts the first stage is considered fatigue and the last two steps are considered fracture mechanics, but for the purposes of this work these areas overlap. The main reason all of these steps were considered as one phenomenon is because the measured number of cycles to fatigue failure often includes the last two stages as well, and this information is critical for understanding the Fatigue Strength and Endurance Limit.

The Fatigue Strength, $S_f^{(N)}$, is the oscillating stress level that a material can endure for N cycles, assuming a zero-mean stress. The oscillating stress level at which the material can withstand an infinite number of cycles is called the Endurance Limit. The Endurance Limit is observed as a horizontal line on an S-N curve, where the Fatigue Strength no longer decreases as the number of cycles increases. In Fig. 5 it occurs at around 10^6 cycles, which is typical for ductile steel. Note that as the S-N curve approaches S_{ut} on the left, the slope decreases and relatively small increases in stress can very significantly reduce the number of cycles to failure. The endurance limit on this S-N curve represents an ideal fatigue strength, but the actual endurance limit can be reduced by several design-specific factors known as Marin Factors shown in Eq. 10.

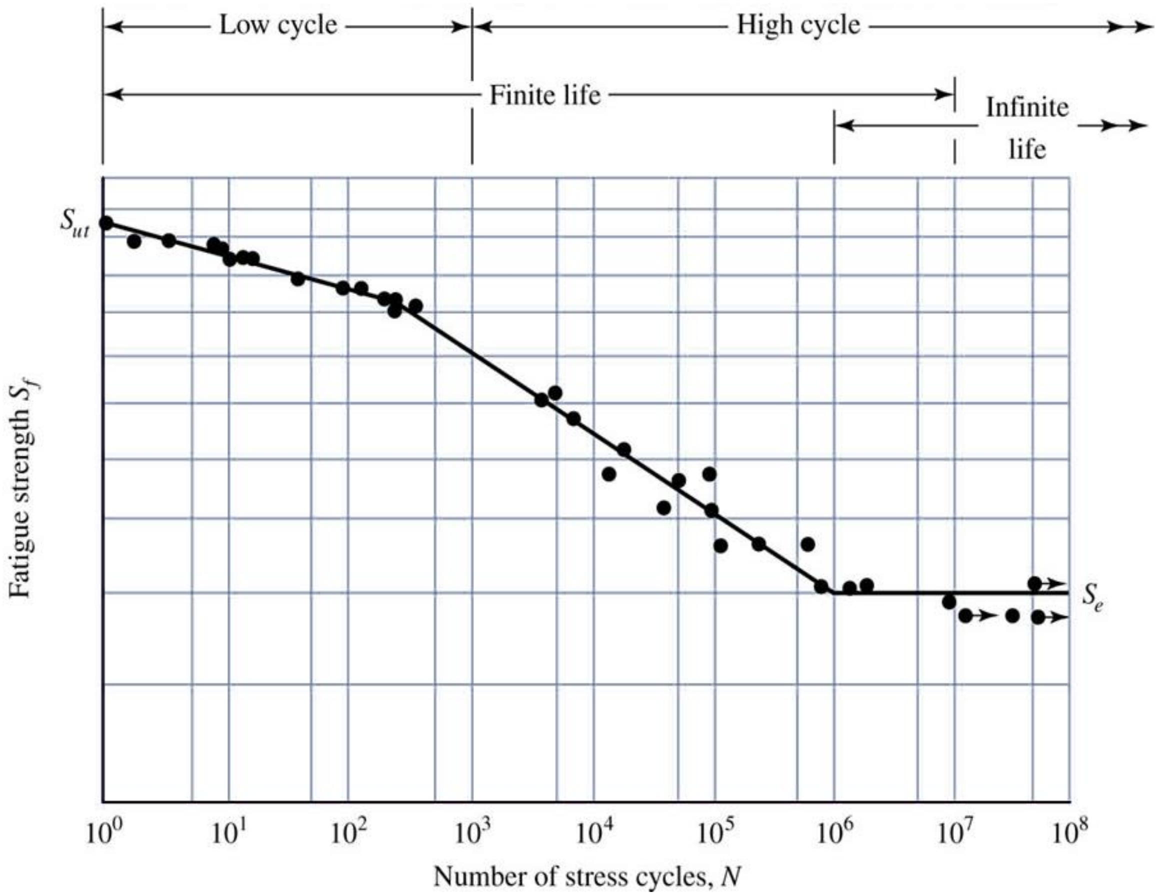

Figure 5. S-N Curve Example

$$S_e = k_a \cdot k_b \cdot k_c \cdot k_d \cdot k_e \cdot S'_e \qquad (10)$$

$S_e \equiv Endurance\ limit\ of\ part$

$S'_e \equiv Endurance\ limit\ of\ test\ specimen$

$k_a \equiv Surface\ factor$

$k_b \equiv Size\ factor$

$k_c \equiv Load\ factor$

$k_d \equiv Temperature\ factor$

$k_e \equiv Miscellaneous\ effects\ factor$

In addition to these factors, AEDC studies have shown that the machining of the balance itself can have a significant impact on the endurance limit. Section 2.3.3 discusses this in further detail.

In Fig. 6 the modified Goodman diagram shows the ultimate, yield, and endurance strength values (S_u, S_y, and S_e) and limiting values of stress components (e.g., max stress, with the max value being the sum of the mean and the alternating stress) (REF 14). The max alternating stress is limited to the endurance stress limit at zero mean stress and linearly progresses to the ultimate stress limit at the intersection with the 45º line shown on the diagram. However, a specified upper limit at the yield stress limit generates a termination in the growth. Operation envelope for estimated “infinite life” is within the area bounded by the solid dark boundary lines. Given a specific mean stress, one can extract the max and min alternating stress limits. The alternating stress limits are shown as σ_a on the diagram.

If the infinite life boundary is crossed then some level of fatigue damage is

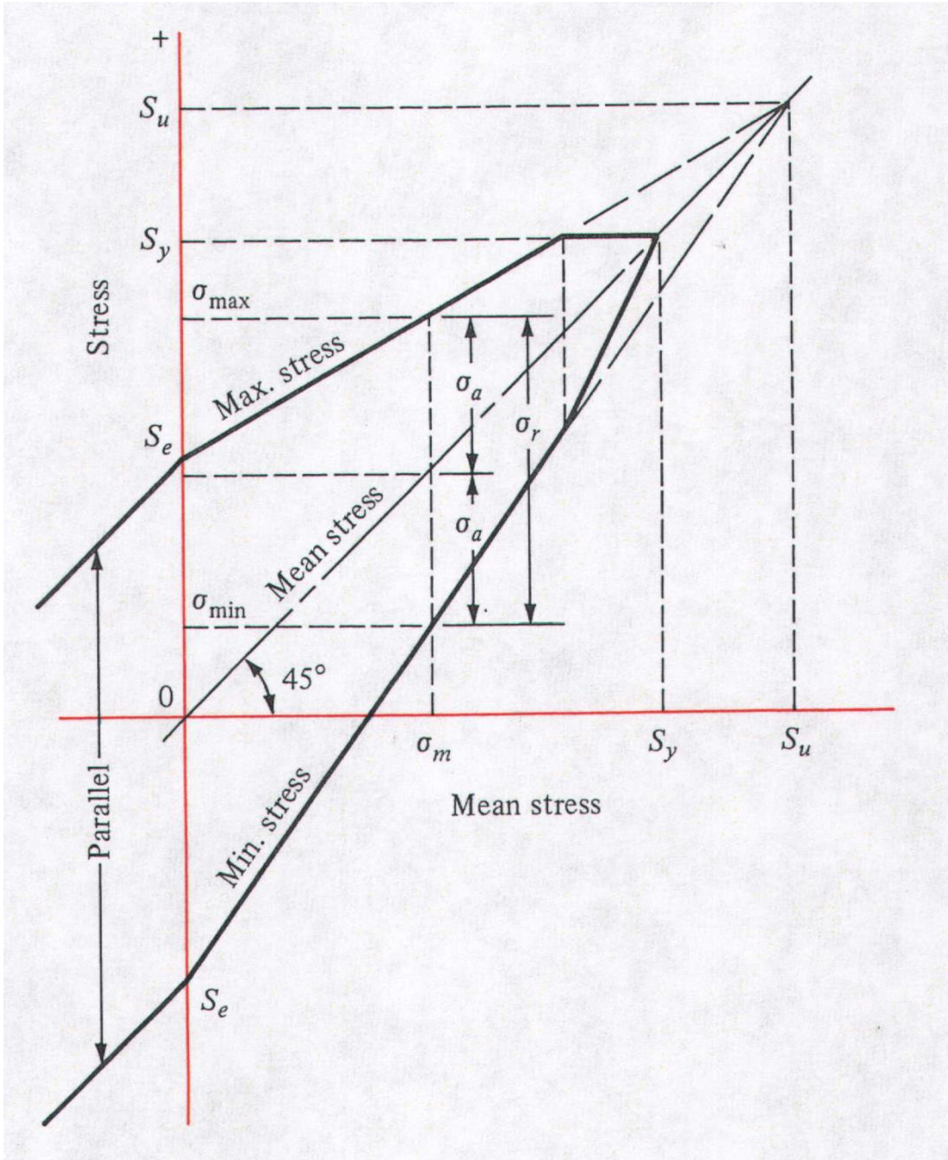

Figure 6. Modified Goodman Diagram (Figure 7-13 from REF 14)

theorized to have occurred. In other words, the expectation of infinite life cannot be supported when an alternating load at the endurance limit magnitude is seen by the specimen. The process of quantifying how much damage has occurred is known as cumulative fatigue (REF 15). For example if a balance is subjected to an alternating stress of σ_1 for n_1 cycles, σ_2 for n_2 cycles, σ_3 for n_3 cycles, etc. the balance will accumulate varying amounts of fatigue damage during each series of cycles. Miner's rule shown in Eq. 11 can be used to evaluate cumulative damage (REF 10).

$$n_1/N_{f1} + n_2/N_{f2} + n_3/N_{f3} + \ldots + N_k/N_{fk} = 1 \tag{11}$$

where N_f is calculated using the Goodman-Basquin equation (Eq. 12) for predicted cycles to fatigue failure.

$$N_f = 0.5\left(\frac{K_t\frac{\sigma_{alt}}{\sigma'_f}}{1-\frac{\sigma_{mean}}{\sigma_{ult}}}\right)^{\frac{1}{b}} \tag{12}$$

σ_{alt} = alternating stress amplitude

σ'_f = fatigue strength coefficient (a material-specific property)

σ_{mean} = mean stress

σ_{ult} = ultimate stress (a material-specific property)

b = fatigue strength exponent (a material-specific property)

K_t = stress concentration factor (geometry dependent)

The σ'_f and b can be provided by the balance material supplier or can be interpolated from curve fits of the ASM Handbook, Volume 1 (REF 16) shown in

Fig. 7 and 8. Miner's rule and the Goodman-Basquin equation will be used in this research to estimate the amount of life remaining on the balance after the infinite life line has been crossed.

2.3.3 MACHINING EFFECTS

Machining effects have been studied by AEDC engineers in the past and need to be considered when doing a stress analysis to predict fatigue life. A specific method of manufacturing known as electrical discharge machining (EDM) can be particularly problematic. In many modern balance designs the roll and drag flexures must be machined using either a plunge-type EDM technique or a wire EDM technique. The EDM process leaves an undesirable "recast" layer of thickness ranging from less than 0.001-inch up to approximately 0.004-inch in extreme cases. Additionally, there is an undesirable heat-affected zone (HAZ) of annealed (soft), low-strength material lying below the recast layer of approximately the same thickness as the recast layer. When considering that the drag flexures on some of AEDC's balances are less than 0.018-inches thick and that opposing surfaces of these flexures are machined using an EDM process, approximately 22% of the thickness of each drag flexure lies within the recast and HAZ.

The EDM recast layer often contains microscopic cracks, the presence of which is unacceptable in balance flexures that are, by design, highly stressed and subject to alternating stresses. These microscopic cracks can propagate into the undisturbed areas of the flexures resulting in premature component failure. The

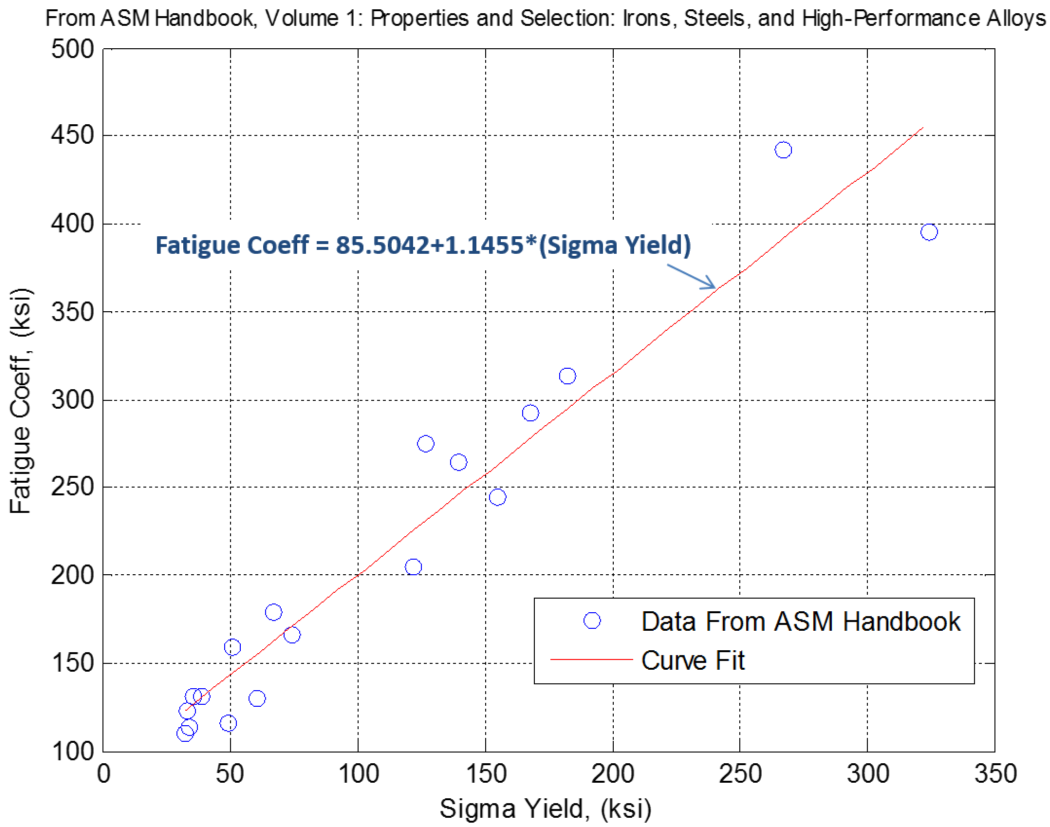

Figure 7. Fatigue Strength Coefficient Correlation

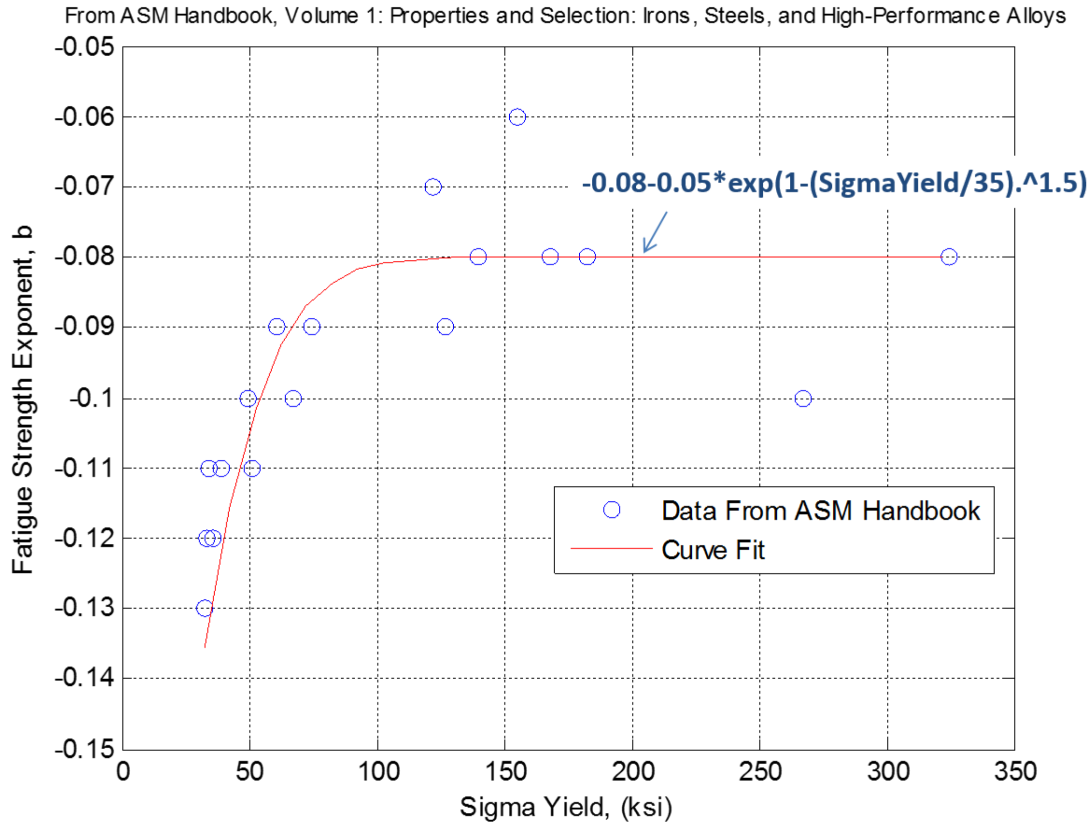

Figure 8. Fatigue Strength Exponent Correlation

extent of this degradation is influenced by variables associated with the EDM process (current, feed rate, etc.). Just as the recast layer adversely affects the fatigue properties of the steel, the HAZ adversely affects the steady-state properties.

During an AEDC analysis effort, fatigue samples were fabricated using conventional machining techniques (milling) and EDM. Each of the samples were tested in the metallurgical lab on the Tatnall-Krouse fatigue-testing machine at the theoretical fatigue stress. The minimum desired number of cycles to failure was 10 million, which was considered infinite fatigue life for these samples. Results indicated that using EDM greatly decreased fatigue life, as shown in Table 1. Figure 9 shows an EDM surface under a microscope. The purpose of this section is not to discourage the use of EDM, since it is the only way to machine current state of the art balance designs, but to provide an example of a factor that reduces fatigue life. In many cases the benefits of geometries achievable by EDM outweigh the reduction in fatigue life, but a balance user needs to be aware of this impact. Countermeasures such as restoring the recast layer or making flexures thicker than required should be incorporated if significant cycles are expected while using the balance.

Table 1. Fatigue Data

Finish	Cycles
Milled	14,264,800+
Milled	13,800,000+
Milled	10,000,000+
EDM	86,700
EDM	122,600
EDM	49,500
EDM	85,700
EDM	101,200
EDM	109,300

"+" in cycles column indicates test was

terminated prior to failure

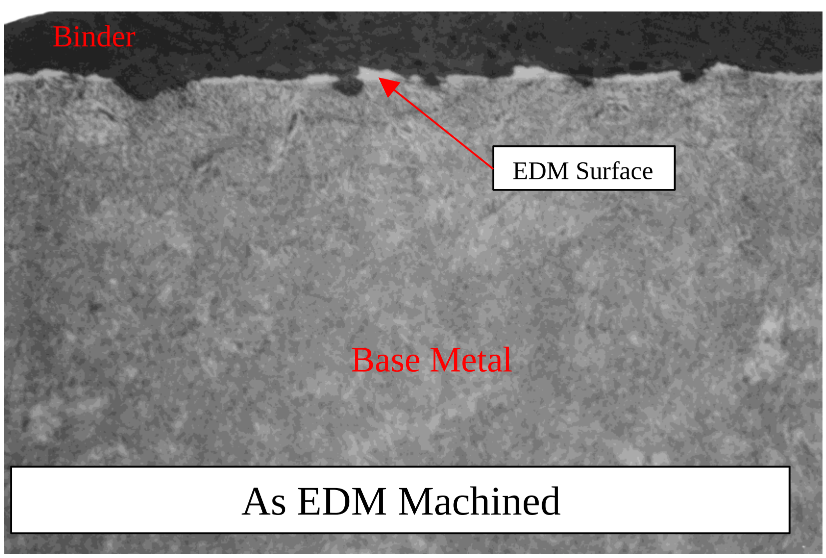

Figure 9. EDM Machined Surface

3.0 BACKGROUND

3.1 LEGACY AEDC BALANCE MONITORING METHOD

AEDC currently implements a balance monitoring process that looks at both the steady state load and the dynamic load. This is achieved by taking the balance signal output and splitting it into two paths. One path will be used for the steady state signal and the other for the dynamic signal. In this system the steady state load is defined as the load that remains after the signal is passed through a low-pass analog and digital filter. These filter settings are typically set to a value of around 1Hz cutoff frequency, thus loads at frequencies higher than 1 Hz are not considered steady state. The dynamic load is defined as the load that remains after the signal has been passed through a high-pass analog filter. This filter is typically set to a value of around 2Hz cutoff frequency, thus loads at frequencies lower than 2Hz are not considered dynamic loads.

Based on the steady state load and the dynamic load two sets of monitoring limits are implemented. For the first limit, the steady state load is compared to the designed balance rated loads and, if the steady state load exceeds the balance rated loads, the model motion is stopped. This static load limit is intended to protect a balance failure due to a single catastrophic loading. It is standard practice to make this limit correspond to a factor of safety (FoS) of 3 on tensile yield strength of the balance material in order to provide additional conservativism on failure. The model motion is automatically stopped, so the test engineer does not have to constantly monitor the balance loads and determine whether an unsafe condition has been met. Stopping the model motion provides the test engineer the option to continue cautiously towards higher loads or terminate the current sequence and move on to the next test sequence. For the second limit the modified Goodman diagram concept is used. As discussed in Section 2.3.2, this concept is derived from failure due to fatigue. Where the first limit is protecting the balance from a single catastrophic event, the second limit is protecting the balance from failure due to smaller magnitude cyclic loadings. For this limit, the steady state load is used as the mean stress and an analog root mean square (RMS) meter is used on the dynamic balance signal to provide the alternating load components. From the diagram it is evident that as the mean stress increases the allowable alternating stress decreases. This diagram is converted from the stress domain into a load domain and then monitored in real-time for exceedance of the allowable alternating stress based on the mean stress. The alternating limit is divided into 3 categories. These are termed a first, second, and third level dynamic limit. The third level dynamic limit corresponds to the infinite life line on a modified Goodman diagram and the second and first level limits are set at some prescribed ratio below the third level limit. If the alternating load exceeds the first level limit a warning is signaled, but no action is taken. If a second level limit is reached the model motion is stopped, just like the action taken on a static limit exceedance. If a third level dynamic limit is reached the model is automatically driven to a safe location to prevent further cumulative damage. The actions taken after any alarm can be changed before the test, but the actions described here are typical.

3.2 SHORTFALLS OF LEGACY METHOD

Although the legacy method was very elegant when designed, there are some shortfalls which can now be addressed with modern computers and technology. The first shortfall discussed is caused by the analog filtering scheme used for the steady state load, and the use of an analog RMS meter for the dynamic load. Having to choose a low pass analog filter to define what the steady state load system will monitor can be problematic. In order to do this one must know the system frequencies that are expected and set the filter appropriately before testing begins. There is a limit to the number of values to which the analog filter can be set. Normally the system frequencies of a model on the end of a long sting attached to a balance are on the order of ~10Hz. In this case a 1Hz cutoff low-pass filter will remove the unwanted model dynamics from the steady state balance loads, and a 2 Hz cutoff high-pass filter will adequately keep them for the dynamic load monitoring. But there are times when a model and sting/balance system's natural frequency ranges from 2Hz to 4Hz. The problem this presents comes from the analog filter roll off as illustrated in Fig. 10 and the fact there is no overlap between the filter settings. The analog filter cards used in 16T trend towards the 6 dB/octave curve shown in Fig. 10. Data from a single analog RMS meter card is presented in Fig. 11, where a

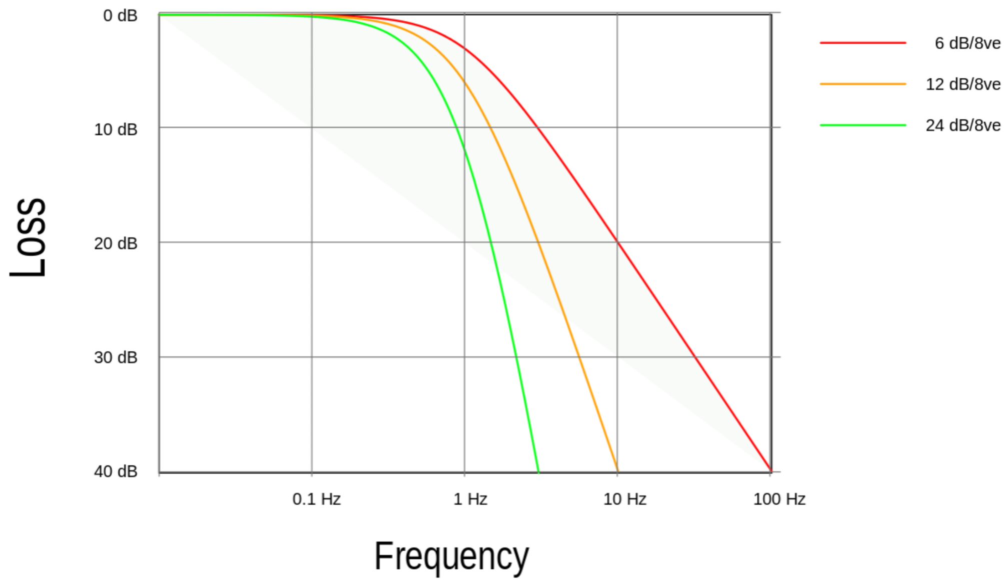

Figure 10. Analog Filter Roll Off Example

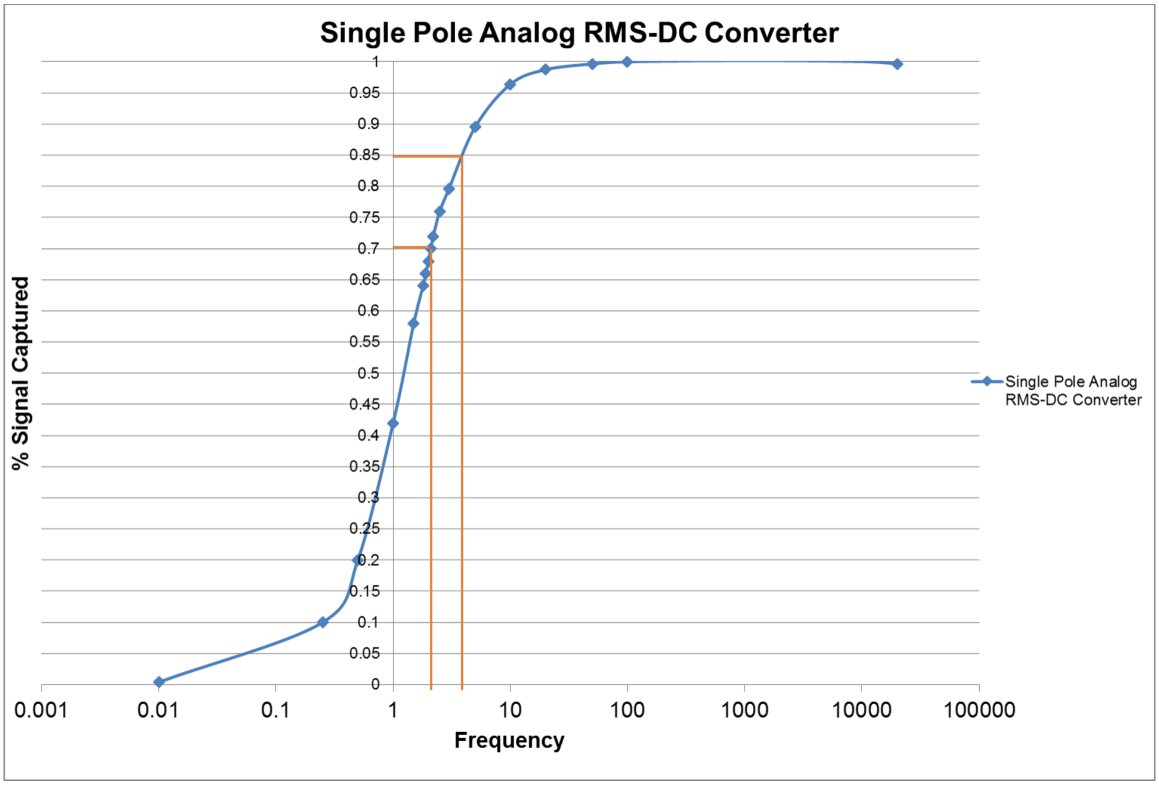

Figure 11. RMS Meter Signal Capture vs Frequency

known frequency and voltage were injected and the output voltage measured. In this case if the high-pass filter remain at the 2 Hz cutoff, approximately 15% of the signal would be lost for a 4Hz frequency and 30% lost for a 2Hz frequency. This system sets up the potential for higher loads to be allowed without realizing it because a significant portion of the signal is not captured. Furthermore, the use of an RMS meter which outputs the balance signal RMS, decreases the magnitude of the dynamic component which must be accounted for to accurately capture the maximum dynamic load. This is trivial if the signal is a sine wave as shown in Fig. 12, where the RMS of a sine wave is a constant 70.7% of the magnitude as defined in Eq. 13:

$$RMS(Sine\ Wave) = \left(\frac{1}{2} \times \sqrt{2}\right) \times Sine\ Wave\ Magnitude \tag{13}$$

There are also similar equations defined for a square wave, triangle wave, etc., but real data does not explicitly follow one of these waves.

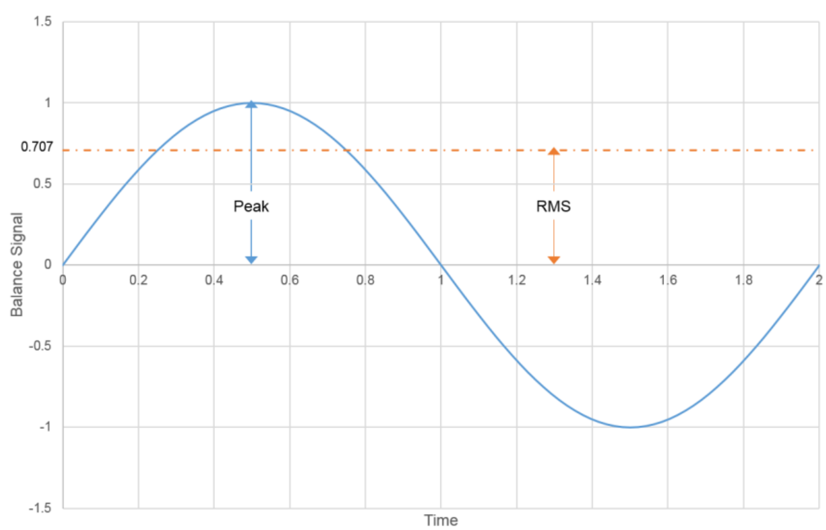

Figure 12. Sine Wave RMS

In the legacy method, it is assumed that the signal resembles a sine wave and thus places the third-level limit at a max allowable RMS value of 70.7% of the load that corresponds to the endurance stress limit. Figure 13 provides two examples of data recorded from strain-gage balances during wind tunnel testing and their corresponding RMS values. This data has been normalized to ± 1 magnitude for convenience in comparing to the 0.707 RMS sine wave assumption. The rolling moment data does exhibit an RMS value of roughly ~70% of the peak when the magnitude of the oscillations is high, but the axial force data sample has an RMS value of 0.3% to 0.6% of the peak even when high oscillations are present. This is troubling because the legacy method relies on a fixed ratio to determine the peak allowable alternating load so 10 to 40% additional alternating load would be allowed unintentionally. Additionally, the RMS meter relies on a preselected time interval on which it determines the RMS. In the cases presented in Fig. 13, that time interval corresponded to 0.441 seconds. So if peak loads were to happen quickly then dampen out, the RMS will smooth this peak out and not signal a limit alarm. Conversely, even if the peak is not smoothed by RMS and a limit is signaled, the signaling of the limit will be delayed because the RMS requires 0.441 seconds of data in this example.

The second shortfall of the legacy method is the dependence on the time domain for setting the window for the RMS alternating load determination. Fatigue failure data is not presented in terms of time, but is presented in terms of cycles. An S-N curve does not specify whether the loads were applied at 0.01,

Figure 13. RMS Ratio of Wind Tunnel Balance Data, a. Rolling Moment, b. Axial Force

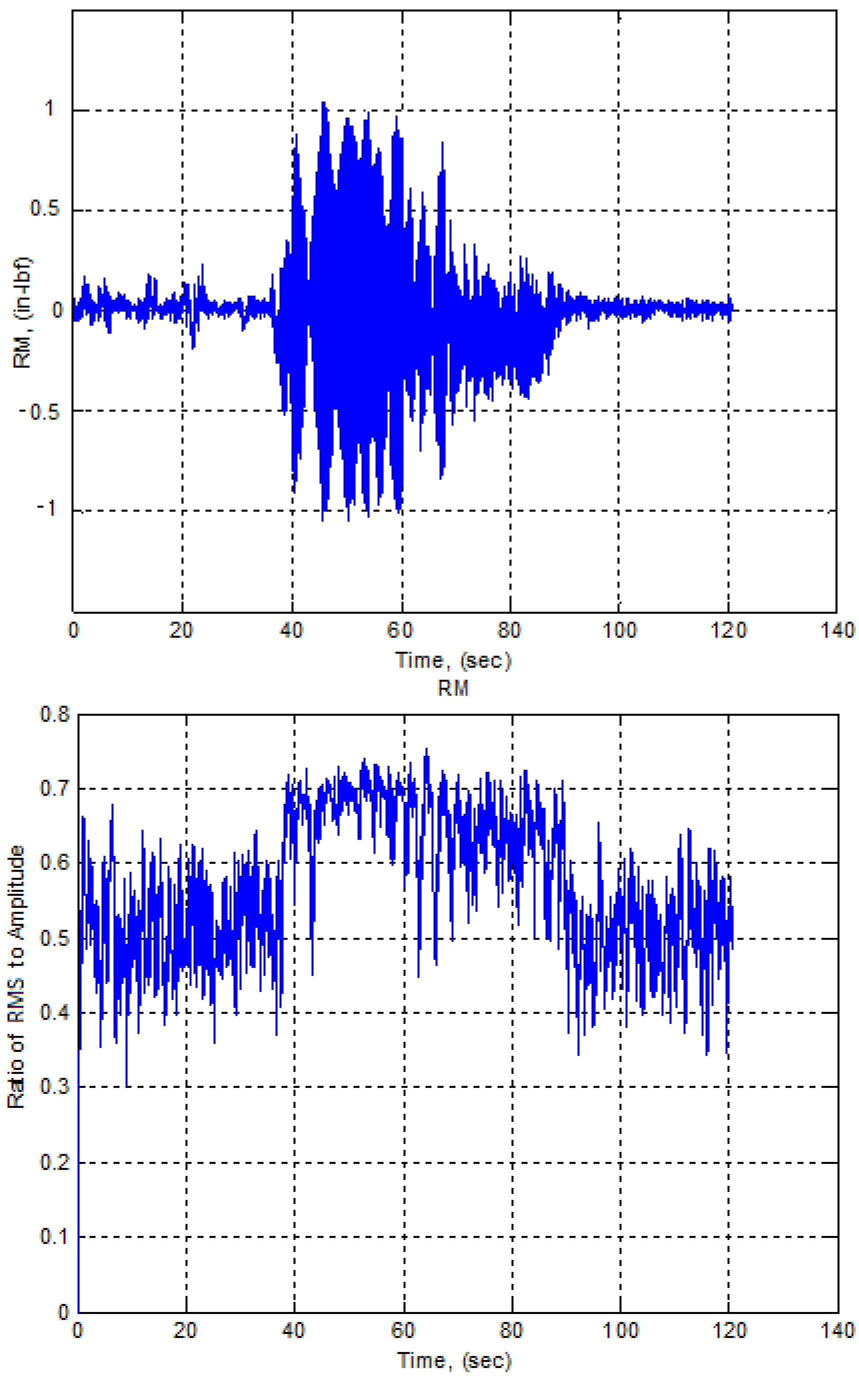

a.

Figure 13. Continued

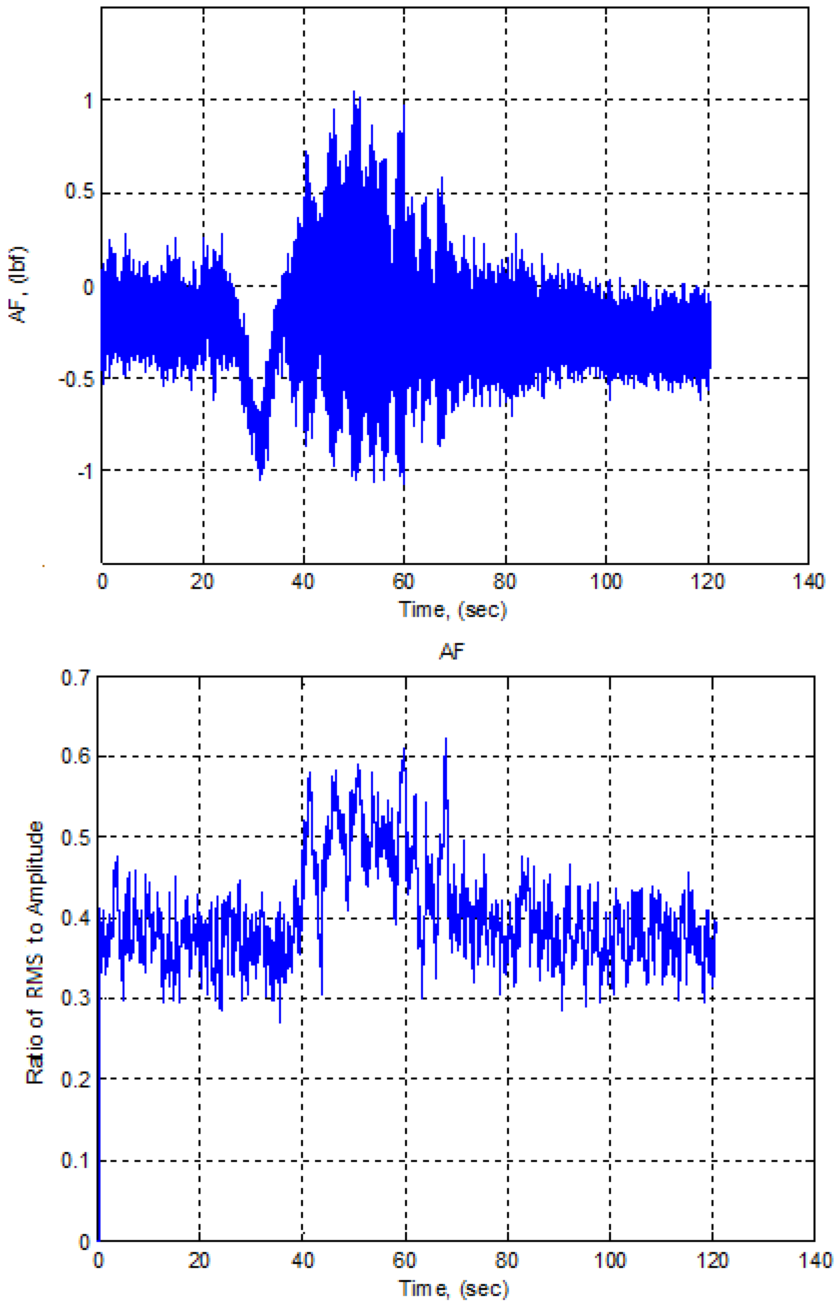

b.

Figure 13. Continued

0.1, 1, 10, 100, or 1,000 Hz. It is simply a function of the number of cycles. The idea of assigning a certain frequency threshold to determine the steady-state mean load to feed the modified Goodman diagram opens up the possibility that lower frequency cycles will not be considered as alternating stress.

The third shortfall of the legacy method is the use of only the primary sensitivity for calculation of the alternating load. Although balance calibrations are primarily a linear behavior, interactions between the different components and higher order effects can be significant in terms of accurately capturing the magnitude of the alternating load. For steady state measurements, accuracies on the order of ± 0.1% of the full scale capacity of the balance are typically desired thus a thorough characterization of the balance using more than the primary sensitivity is required. For monitoring purposes this requirement can be relaxed greatly, but the load calculation should still have accuracies of at least ± 5%. The use of the primary sensitivity alone will not meet this requirement on all components for most balance designs. Results of comparisons of calculating loads from the primary sensitivities, 6x6 matrix, and 6x96 matrix will be provided in Section 5.2.

A fourth shortfall stems from the monitoring being performed in the load domain instead of the stress domain. Since the limits are currently set based on threshold values of individual component loads being crossed, there is no ability to allow these limits to fluctuate based on the other balance load components. In reality, the allowable normal force depends on the magnitude of the side force, axial force, pitching moment, yawing moment, and rolling moment. In other words, the same critical stress level can be reached by an infinite combination of loads. For a given stress limit, if all but one component have a magnitude of zero, then the last component can reach a much higher magnitude than it could if all other components were significantly loaded. This flexibility is not built in to the legacy method.

A final shortfall of the legacy method relates to how the limits are recorded and reported. During a test when either a steady state or dynamic load limit is encountered a message is displayed and a prescribed action is taken. This is good, but knowing that a limit was hit does not give insight into the true severity of the event. In the legacy system, if test data were being recorded when a limit was reached, then the mean and alternating loads could be examined, but only at the sample rate of the steady state data system. Many times an event occurs when test data is not being acquired (i.e. changing test conditions, going to the start of the next model position, etc.), and in this case no information can be determined about the severity. This information is crucially important in determining how much life is left in the balance. If the modified Goodman infinite life line is crossed then some portion of the balance life has been taken away, and to know the amount one must know how far past the line the load was. To make matters worse the S-N curve shown in Fig. 5 is a log scale, so going past the infinite life line by a small amount can result in only having 100,000 or 10,000 cycles of that magnitude left.

3.3 BALANCE CHOOSEN FOR STUDY

The balance chosen for the study was an AEDC 3-piece moment balance which was designed and fabricated in 1971. The AEDC balance designation is 6-.80-.150-.52M. This balance has an old 3-piece design and does not represent the state of the art, but the principles of balance monitoring are generic enough to enable its use on more current designs. This balance was chosen because it represents typical six-component internal balances used at AEDC and its design has no sensitivity restrictions. For more current designs, the geometry and material selection will dictate the level at which the limits are set, but this does not change the general approach that should be taken to monitor a balance. General characteristics of the balance are presented in Table 2. This balance was fabricated from 13-8 H1025 stainless steel. Table 3 presents the material properties of 13-8 stainless steel (REF 17). A photo of the balance is provided in Fig. 14. Autodesk Inventor 2015 was used to create a 3-D CAD model, which would subsequently be used during the FEA. The 3-D CAD representation of the balance is presented in Fig. 15. Note that each side of the balance has a shallow taper. On the aft end of the balance the taper is inserted into a sting piece and securely seated. The forward taper is attached to the wind tunnel model.

3.4 DATA COLLECTED

The 6-.80-.150-.52M six-component strain-gage balance was recently used during a recent AEDC 16T wind tunnel test. In order to not interfere with

Table 2. Balance Characteristics

Design Loads						Length (in)	Diameter (in)
NF (lb)	PM (in-lb)	SF (lb)	YM (in-lb)	AF (lb)	RM (in-lb)		
150	450	100	300	40	120	6.22	0.8
250	0	167	0	40	120		

Table 3. 13-8 Stainless Steel Material Properties

Property	**H 950**	**H 1000**	**H 1025**	**H 1050**	**H 1100**	**H 1150**
UTS, ksi (Mpa)	220 1517)	205 (1413)	185 (1276)	175 (1207)	150 (1034)	135 (931)
0.2% YS, ksi (Mpa)	205 (1413)	190 (1310)	175 (1207)	165 (1138)	135 (931)	90 (620)
Elong. % 2" (50 mm)	10	10	11	12	14	14
Hardness, Rc	45	43	41	40	34	30
Bhn	430	400	385	372	313	283
Endurance Limit ksi	100	100	100	100	100	100

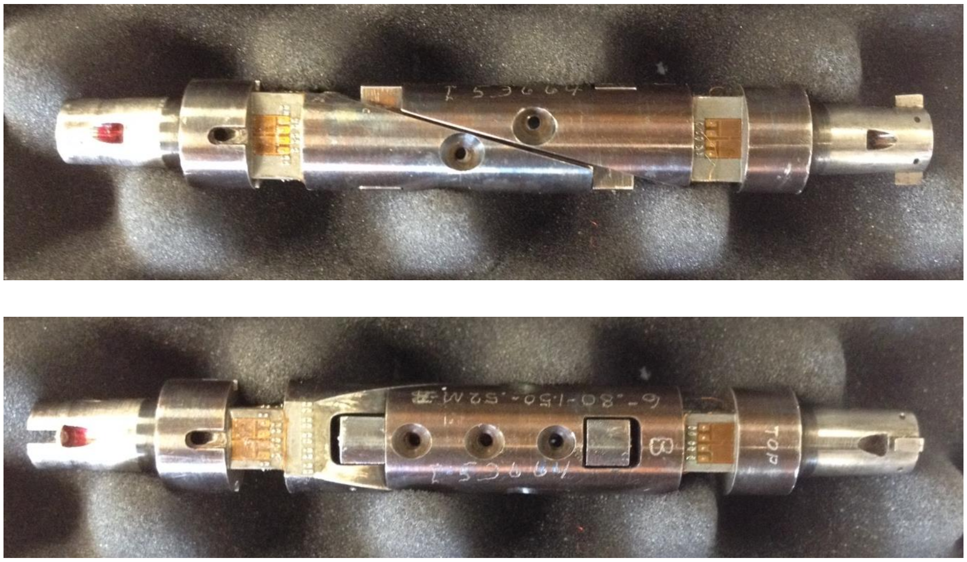

Figure 14. Balance Photos

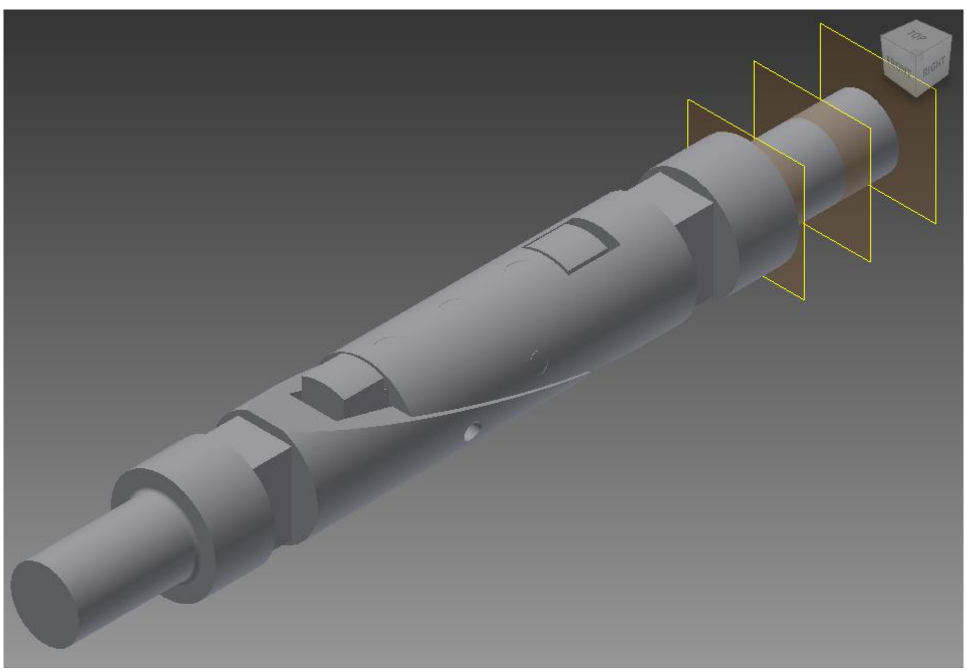

Figure 15. CAD Model

the wind tunnel test, an auxiliary stand-alone high speed data recording system was brought in to record the balance outputs at ~5,000 samples/sec for the entire test. The data output from each of the 6 Wheatstone bridges was stored in μV and was not analog or digitally filtered in any way. Simultaneous to this auxiliary storage of the balance data, the legacy 16T balance monitoring system was operating as it does for any test using a balance. During the test three dynamic events were flagged by the legacy balance monitoring system. After the testing was completed, twenty second data slices were extracted from the 5,000 sample/sec data surrounding the three events flagged by the legacy balance monitoring system. This data served as the data used for analysis and simulations which led to the development of a new balance monitoring method.

4.0 APPROACH

4.1 OUTLINE OF APPROACH

The shortfalls of the legacy balance monitoring process allow room for development of a method that has the pros of the legacy method but improves upon the shortfalls. Simulation tools made use of ANSYS® Workbench, MATLAB®, and Microsoft® Excel to develop algorithms using the data collected from AEDC 16T to illustrate the outcomes of the new monitoring methodology. The simulation tools were used to compare the legacy method to the new method. A comparison discussion is presented on the following areas:

- Legacy and new method abilities
    - When are limits reached
    - Time to determine limit exceedance
- Load calculation
- Load limit determination
- Remaining Balance Life

The approach of the comparison analysis was sequential. Initially an “apples to apples” comparison was performed where the same data were used to compare the two methods. Both methods calculated the load from the μV data using only the primary sensitivity. The same limits were used to determine whether an exceedance has occurred. This provided insight to whether there are inherit benefits to the new methodology, or if all of the benefits are simply gained from the load limit determination and the load calculation. After this was examined, the load calculation and load limit determination pieces will be discussed and compared. Finally, the remaining life of the balance is discussed.

4.2 NEW METHOD APPROACH

The new method makes use of current technology levels to provide a balance monitoring approach to improve upon the shortcomings of the legacy balance monitoring approach. This method does not make use of any analog filters to break the signal into a steady state and dynamic component. Breaking the signal into two components was done out of necessity when the legacy method was developed because continuously recording the entire signal or digitally calculating an RMS would have been impractical. Now sample rates can easily capture the entire signal, and computer storage space is ample to store all the data. This eliminates the implicit need for a priori knowledge of the data frequency content in order to set filters, because the raw signal is recorded for decomposition of the signal into a mean and alternating component.

Additionally, instead of using a low-pass value as an input for monitoring against a single catastrophic load failure, the actual transient peak load was used for this threshold. Instead of monitoring an RMS of the signal to determine the alternating portion of the signal, a peak finding algorithm was employed and peak pairs were identified. This eliminates the need for the 0.707 assumption and captures the alternating load regardless of frequency. As an alternative to using a 6x96 matrix for the steady state loads and the diagonal elements of the 6x6 (primary sensitivities) for the dynamic component, the 6x96 matrix can be used on the entire signal. This can be dropped to the full 6x6 to eliminate the iterative nature of the calculation if sufficient accuracy is captured by the primary sensitivities and interactions.

The new method has limits determined in terms of stress instead of in terms of load. This enables the allowable individual balance component loads to vary as a function of the other components, since all components feed a stress limit equation. Having this flexibility ensures safety, while also allowing the balance to be used to its full capability instead of arbitrary only considering an all loads simultaneously applied condition.

Finally, the severity of the limit exceedances is tracked using Miner's rule, Goodman-Basquin equation, and a rainflow cycle counting algorithm (REF 18). Having this information provides the test engineer with data to make an informed decision on whether to continue testing as is, change the testing direction, or stop testing until the balance is inspected for damage. This information is not calculated in real-time, but is needed within a few minutes to facilitate a quick decision while the tunnel continues to burn power.

4.3 SAMPLE RATE DETERMINATION

Ideally all of the analog signal is captured so that no load information is lost, but at some point the analog signal needs to be digitized. The process of digitizing the analog signal only allows some finite number of samples per second to be acquired from the analog signal. Even if it is possible to record and store the data at 1 MHz if no additional value is added over a slower rate, then the slower rate should be used. The perfect sample rate is one that is fast enough to reconstruct at least 95% percent of the signal, but slow enough to allow for monitoring calculations to occur in a real-time fashion and provide reasonable file size for post-test analysis.

Initially a modal analysis was performed in ANSYS workbench 14.5 using a 3-D CAD model of the balance and sting build-up to determine the resonant frequencies. This may sound contradictory to previous statements that the frequency information is not needed in the new method. Within the realistic possibilities of an AEDC 16T setup this is true, but if frequency information is known it can be exploited to optimize the methodology. Results of this modal analysis are presented in Fig. 16 and 17. This serves as a way to approximate the frequencies of interest before any data is collected. For this hardware, the analysis calculated expected frequencies ranging from 9Hz to 60Hz.The first and second modes are a simple yaw and pitch bending motion, and the fifth and sixth modes were an “s” bending motion primarily in the axial plane. 60 Hz being the highest predicted frequency is beneficial because these frequencies are low, thus resulting in a potentially low sample rate requirement. Using the Nyquist Criteria (REF 19) the minimum sample rate that could be used would be 120 Hz. At AEDC a factor of 10 of the desired frequency content is typically used as a rule of thumb to provide better resolution to the signal, which increases the sample rate to 600 Hz.

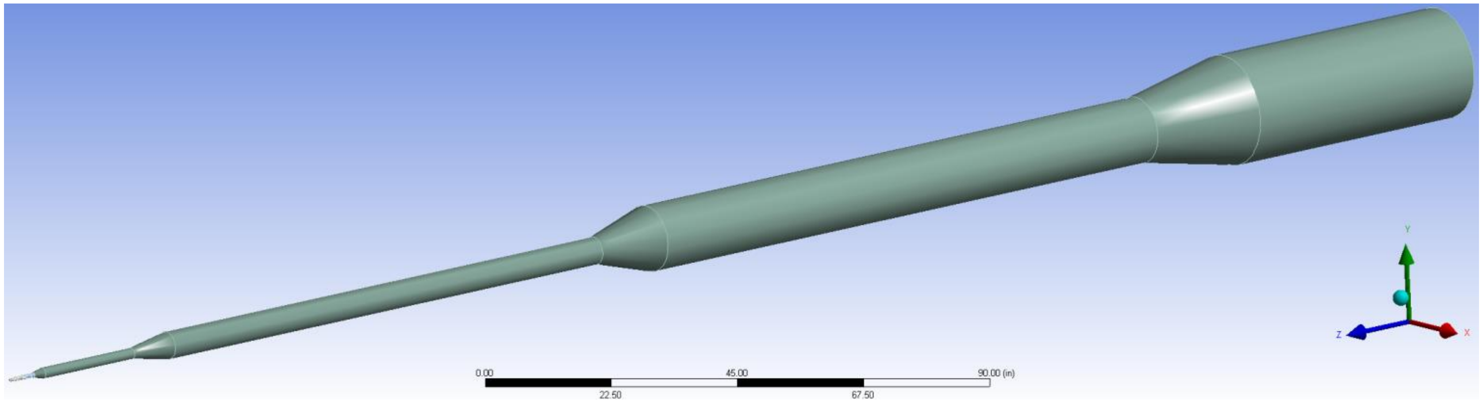

Figure 16. Modal Model of Balance and Sting

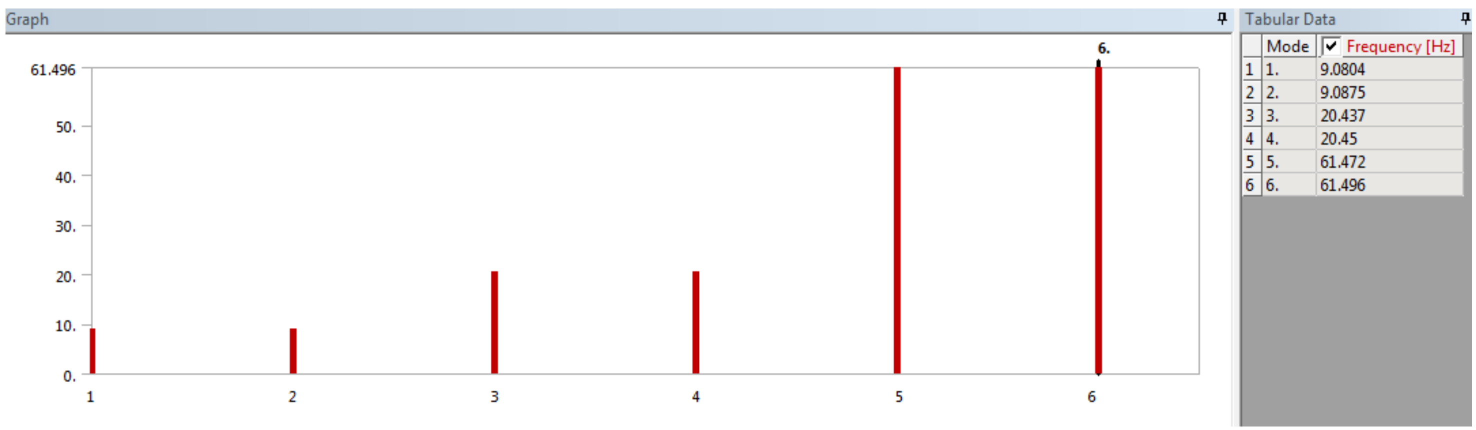

	Mode	Frequency [Hz]
1	1.	9.0804
2	2.	9.0875
3	3.	20.437
4	4.	20.45
5	5.	61.472
6	6.	61.496

Figure 17. Frequencies for Each Mode

In this case 5 KHz data was already acquired, which based on the modal analysis should be more than adequate. Since the data was already acquired, it was used to determine frequencies measured during testing. This provided evidence for the sample rate choice, instead of relying on simulated results. This type data would not normally be available, but similar sting build-ups could use it as a guideline for AEDC 16T's balance data frequency. This data was downsampled at 20 Hz, 100 Hz, 500 Hz, 1000 Hz, and left alone at 5,000 Hz. In order to understand the alternating component of the stress, the peaks of the signal must be accurately identified. Since the axial component had the highest predicted frequency content, the axial force bridge will be used to determine what sample rate will be adequate. Figure 18 shows time histories of axial force, where each of the downsampled frequencies was used and the peaks of the downsampled signal identified. The actual data is in blue, and the red circles are where peaks exist in the downsampled data. The 20 Hz and 100 Hz data is insufficient because many of the peaks of the original data are not determined. Looking at the 500 Hz data, it is greatly improved over the 100 Hz, but if one looks closely there are still some missing peaks. The 1,000 Hz data identifies all the peaks, and by definition the 5,000 Hz data does as well. In this example the 1,000 Hz proves to be sufficient, so it is used instead of over sampling at the 5,000 Hz.

To provide more insight into what rate should be used, a fast Fourier transform (FFT) was performed on the data to understand the frequency content.

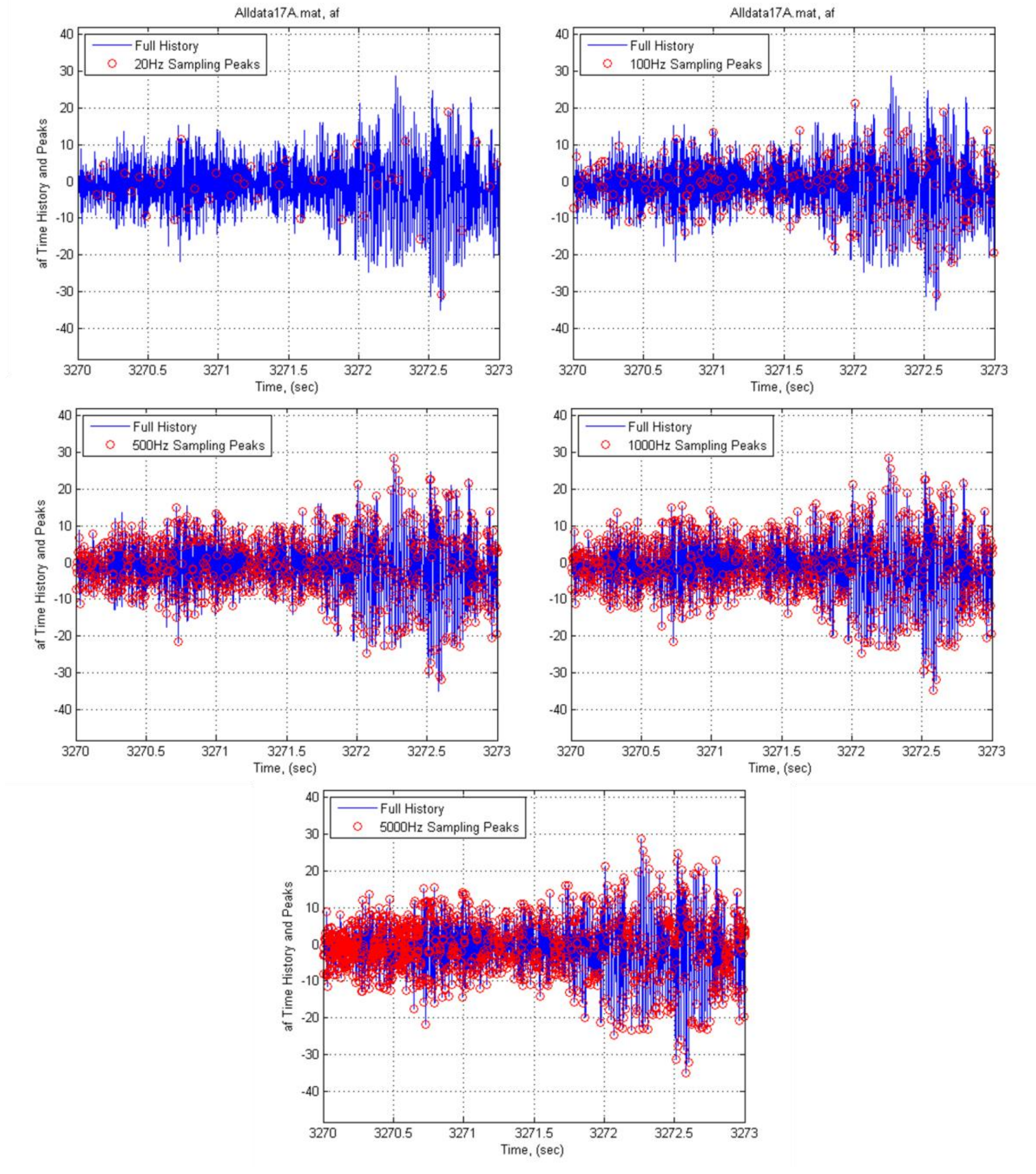

Figure 18. Various Downsampled Data Rates

Figure 19 shows an FFT for each balance channel. These FFTs prove that axial force indeed has the highest frequencies and will be the driving factor. With the dominant axial force frequency at ~55 Hz, it was determined that a sample rate of 1,000 Hz would be the minimum. A lower sample rate could be used if less resolution is acceptable, but for this work the higher resolution is desired.

4.4 CYCLE COUNTING METHODOLOGY

A cycle can simply be considered an event in which two load/stress reversals occur. The first question to answer in this section is, “What is a significant cycle?” From the FFTs performed in section 4.2, one could easily take the first mode frequency and multiply it by the number of air-on hours the balance was tested in order to determine the number of cycles to which the balance was subjected. For a typical wind tunnel test, which can last for 150 air-on hours with a frequency of 10Hz, the number of strain reversal cycles would be 5,400,000+. But the number of the cycles is practically meaningless if all of them occur in the infinite life region of the modified Goodman diagram. So, this means that at a minimum, cycles which exceed the infinite life line should be accounted for and counted in determining the remaining life of the balance.

The next problem to address is that balance data does not look like fatigue data. If it did, the problem would be simplified because the cycles could be summed and compared to an S-N curve. In wind tunnel data, the mean and magnitude of the alternating load varies. Figures 20 and 21 show a standard fatigue test cycle and a representative set of wind tunnel data that does not have

Figure 19. FFT of Balance Data, a. Forward Pitching Moment, b. Aft Pitching Moment, c. Forward Yawing Moment, d. Aft Yawing Moment, e. Rolling Moment, f. Axial Force

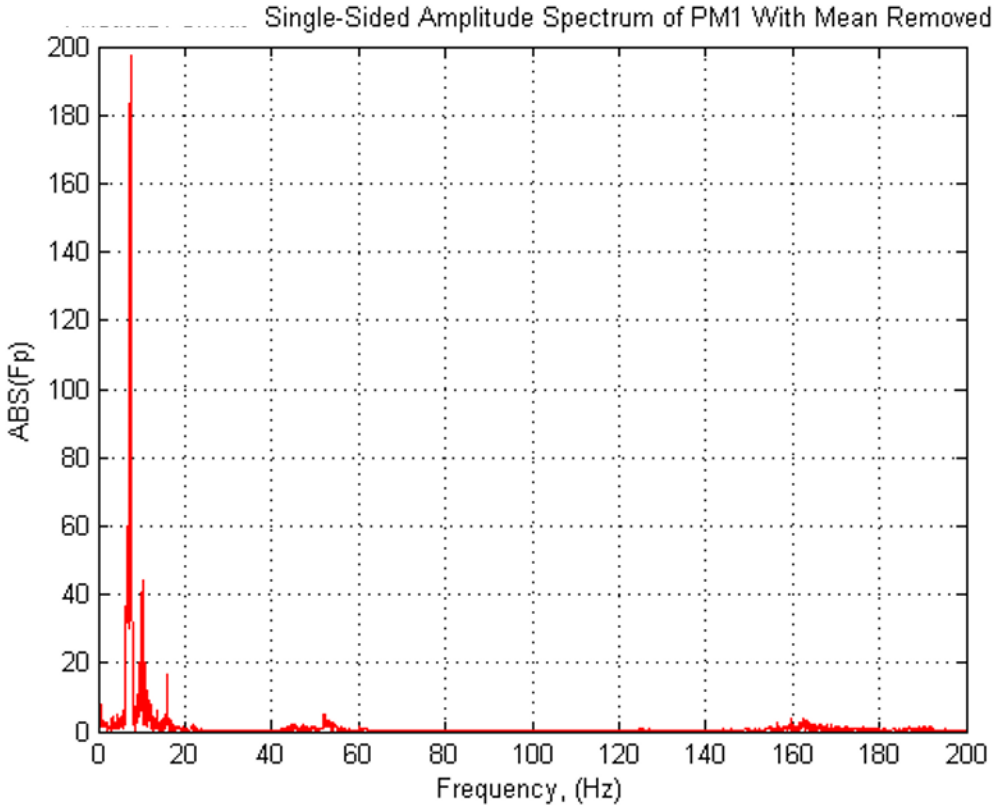

a.

Figure 19. Continued

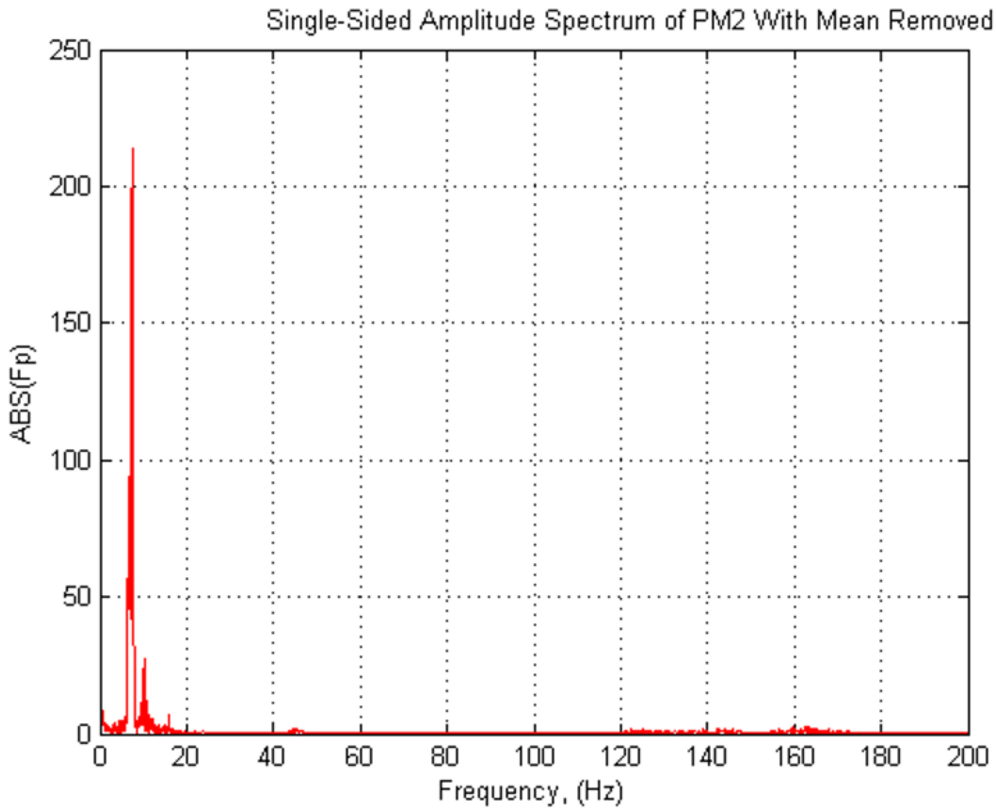

b.

Figure 19. Continued

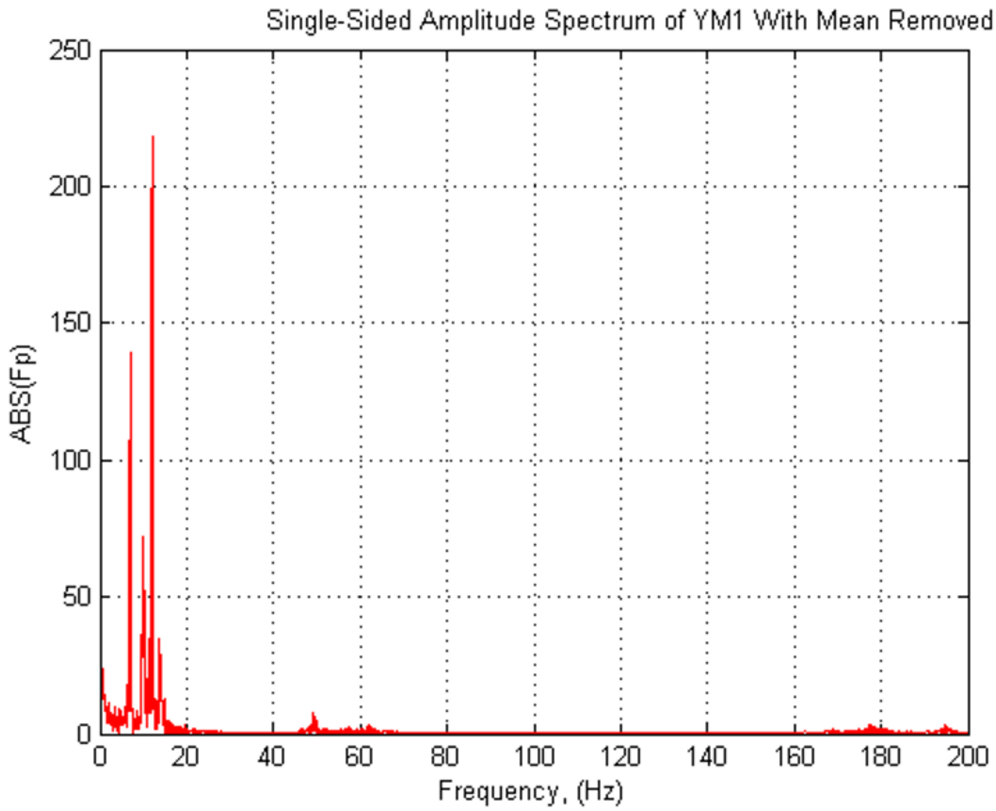

c.

Figure 19. Continued

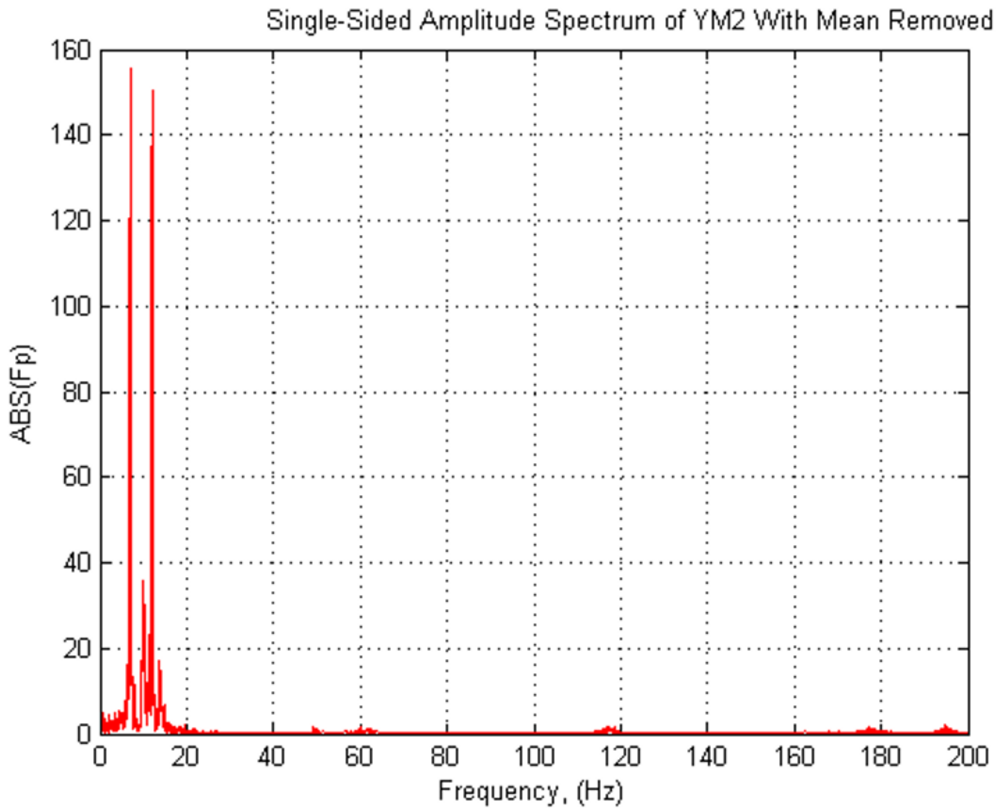

d.

Figure 19. Continued

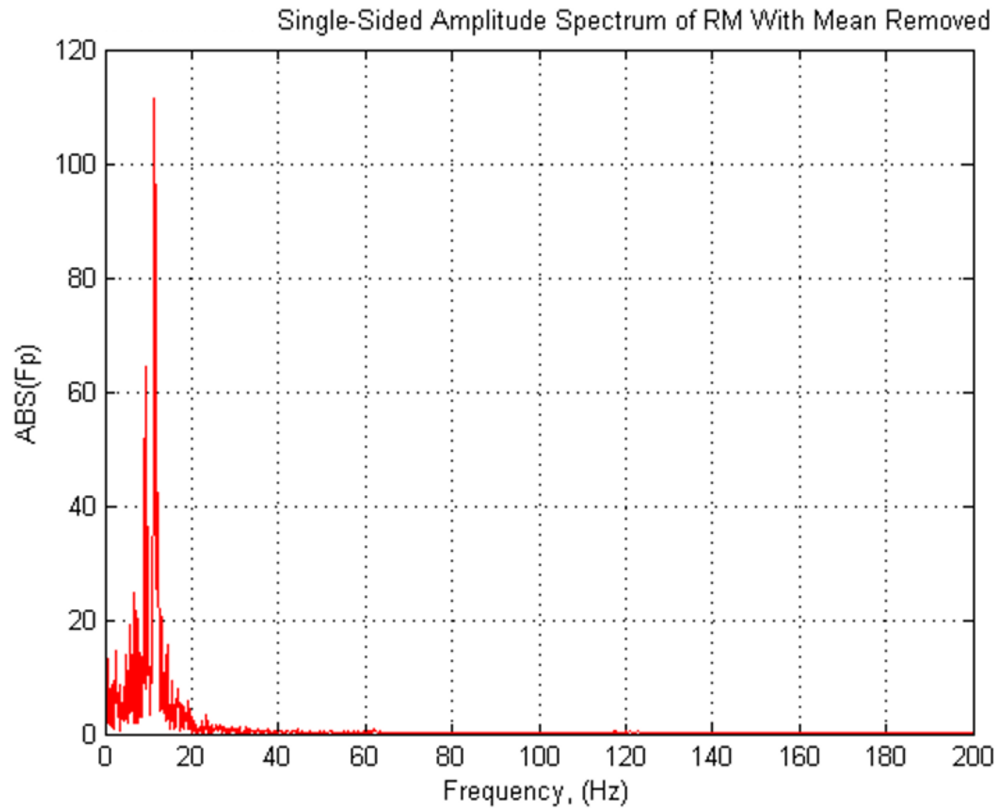

e.

Figure 19. Continued

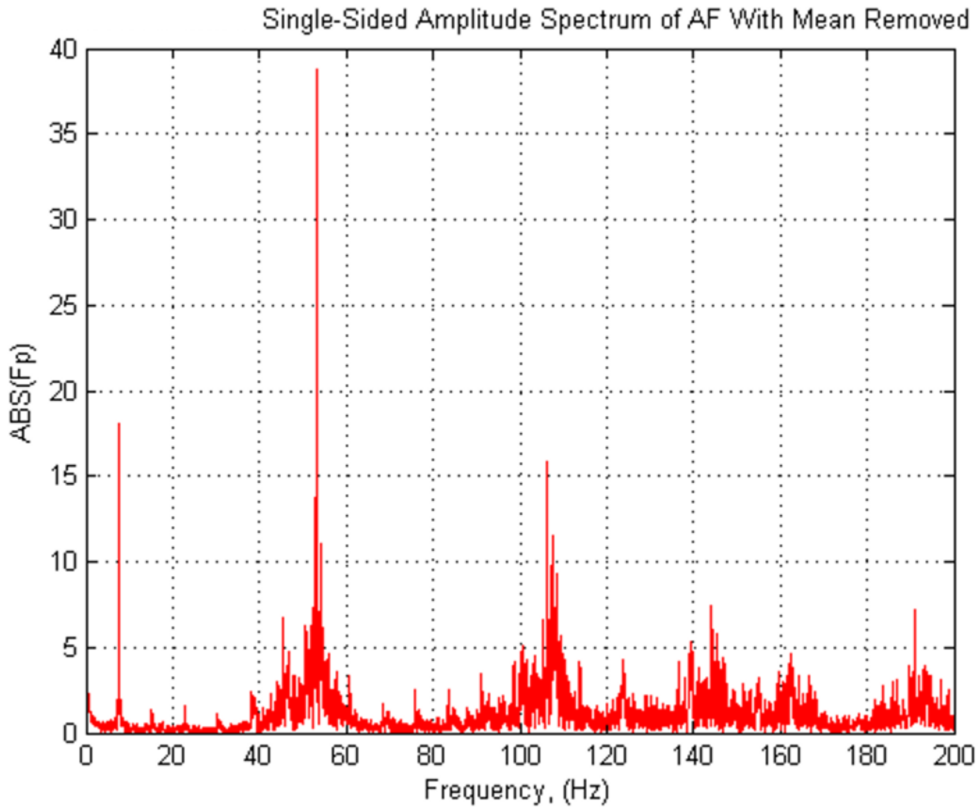

f.

Figure 19. Continued

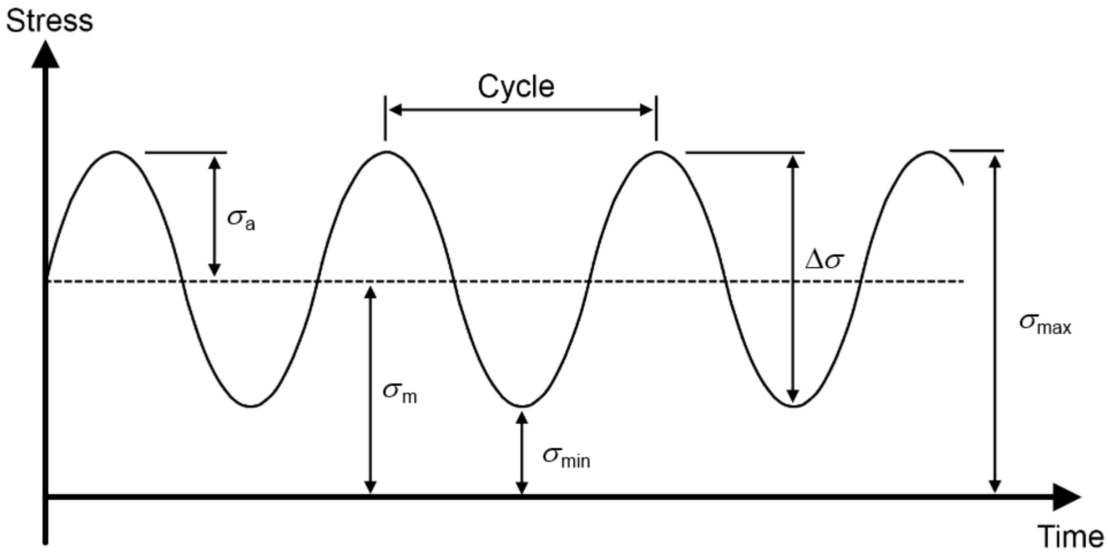

Figure 20. Typical Fatigue Test Time History

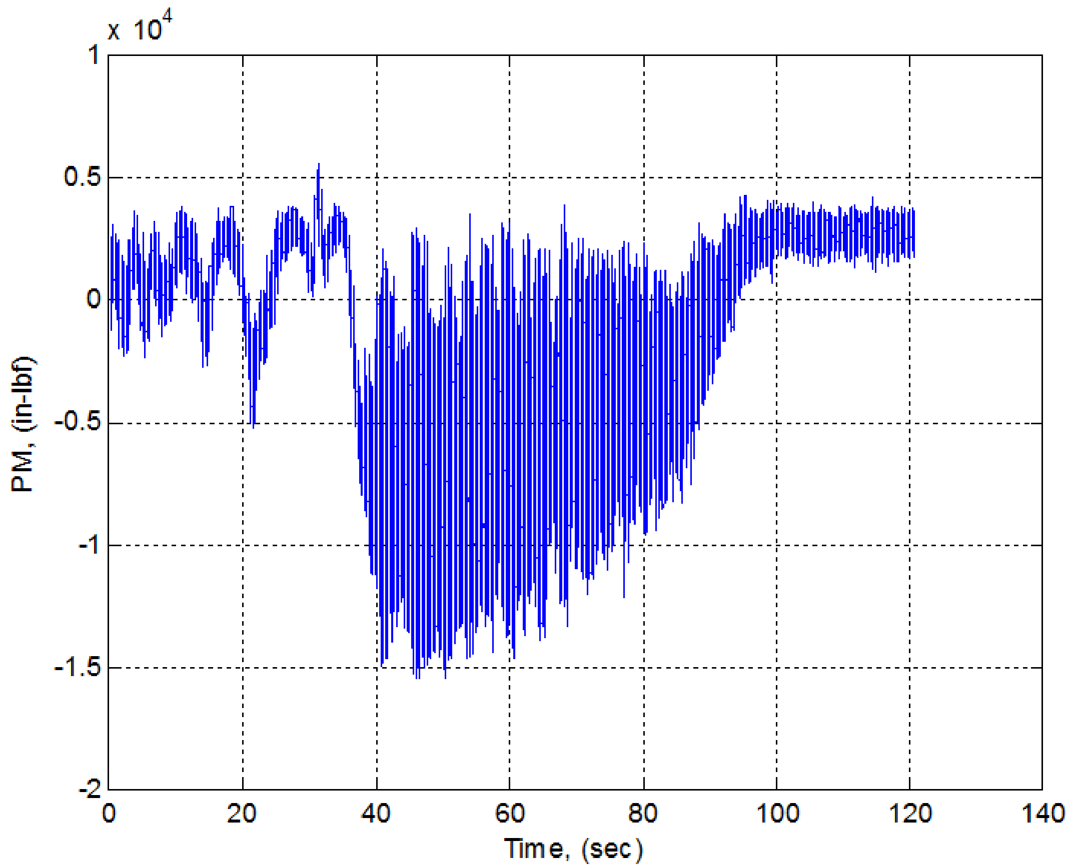

Figure 21. Representative Wind Tunnel Test Time History

a consistent magnitude from one load reversal to the next. This is a common problem for application of fatigue analysis on real-world systems, and is addressed by the ASTM E1049 standard (REF 18). In this method, referred to as rainflow counting analysis, the relative peaks and valleys are determined from the data and then counted as half cycles. Figure 22 illustrates an example of how this is done. Each time a half cycle is greater than the infinite life line on the Modified Goodman, Eq. 12 is used and the half cycle is counted. When the next significant half cycle is found the process is repeated and the new half cycle is summed with all previous cycles using Eq. 11. As every half cycle is summed with the others, the Test Engineer will be able to estimate what percent of the balance’s life has been used.

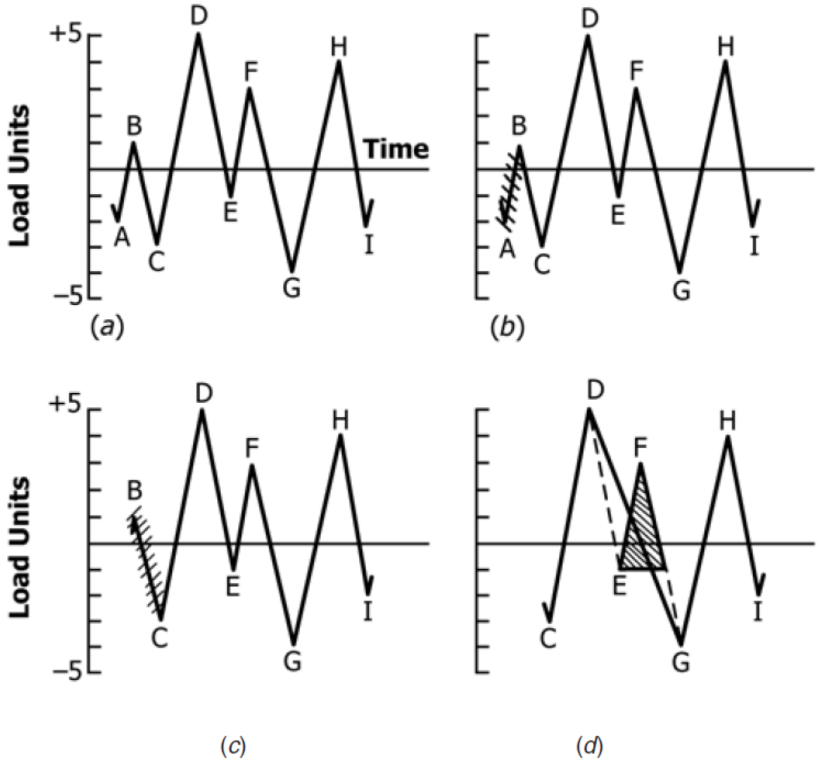

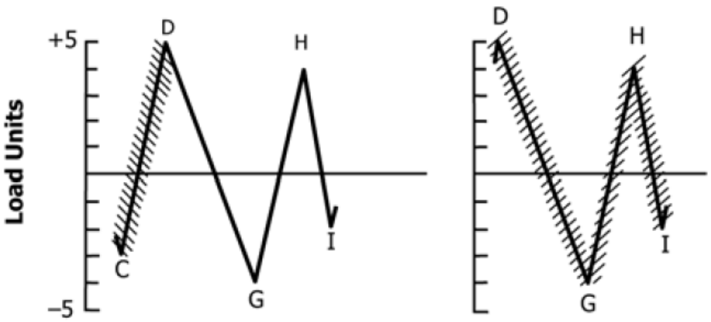

Range (units)	Cycle Counts	Events
10	0	
9	0.5	D-G
8	1.0	C-D , G-H
7	0	
6	0.5	H-I
5	0	
4	1.5	B-C , E-F
3	0.5	A-B
2	0	
1	0	

(e) (f)

Figure 22. Rainflow Counting Example (REF 18)

5.0 RESULTS

5.1 LEGACY AND PROPOSED METHOD COMPARISON

Using the same data, a simulation was setup to directly compare the abilities of the legacy method and the proposed method. The first comparisons presented used the same load limits and only used the primary sensitivities in order to calculate the balance bridge loads. Figure 23 compared the RMS signal to the transient data for the three events that the 16T test engineer classified as dynamic events. Note that only the first event actually had an alarm trigger from the legacy balance monitoring system. Figure 23 indicates several areas of concern. Firstly, although the RMS method detected a limit, it took nearly a second before this was signaled. Secondly, on the first run PM1 also crossed the rated load threshold, but because the RMS value was lower than the limit and the steady state mean signal was only ~300 in-lbs, no limit was flagged on the legacy system. Finally, the second and third runs had areas of concern, where the peak values exceed the rated load limit of the balance components, but the legacy method did not set off any alarms.

Next the transient data (blue on Figures) was decomposed into alternating and mean components for plotting on the legacy dynamic monitoring curves. Figure 24 provides the legacy monitoring curves for this balance. Note that the maximum value on the y-axis is 70% because an RMS is used. When the transient signal was decomposed and plotted on a comparable curve, only the third level was examined which needed to be increased back to 100% since an

Figure 23. Transient Peak vs RMS Trigger, a. Run 1, b. Run 2, c. Run 3

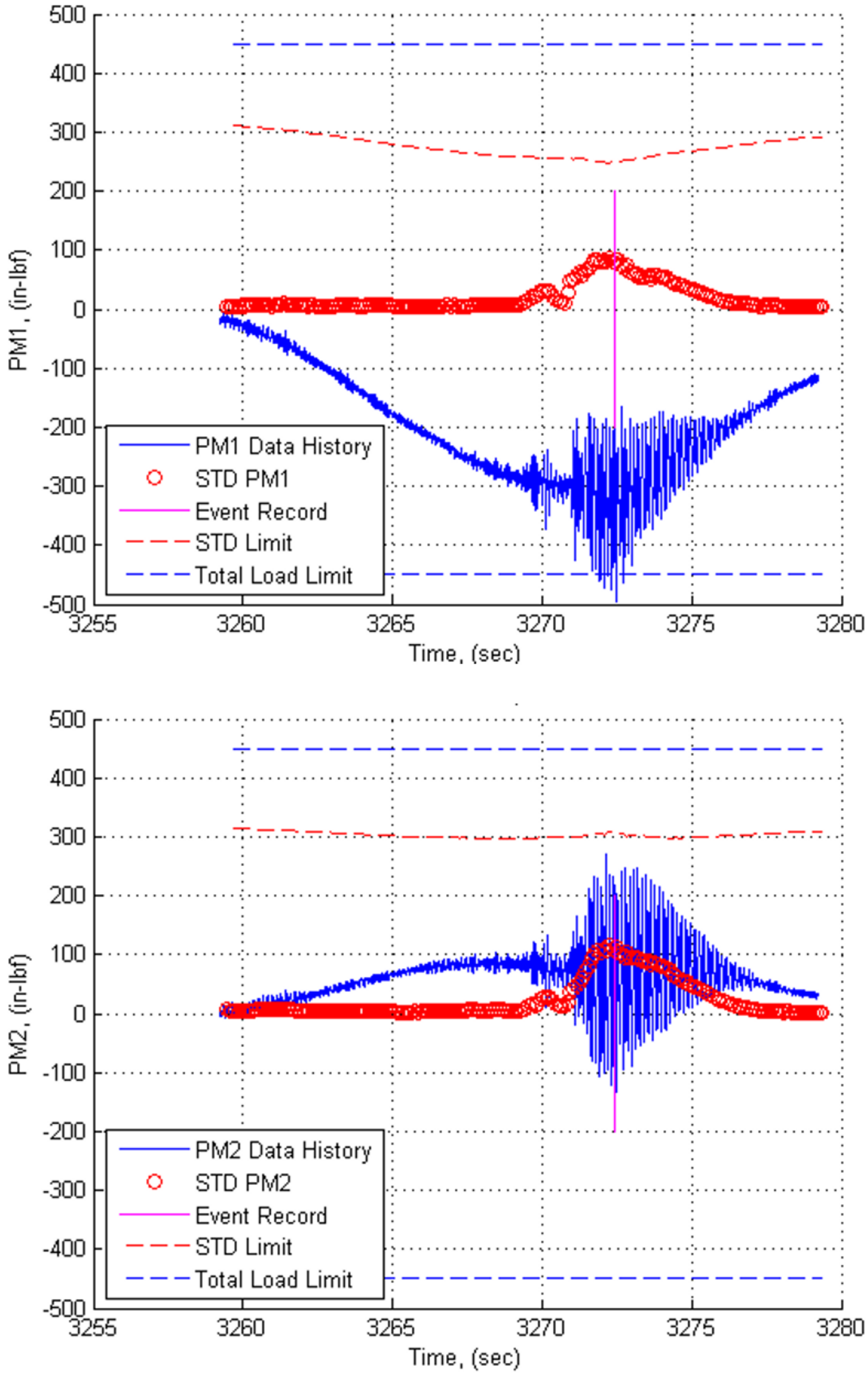

a.

Figure 23. Continued

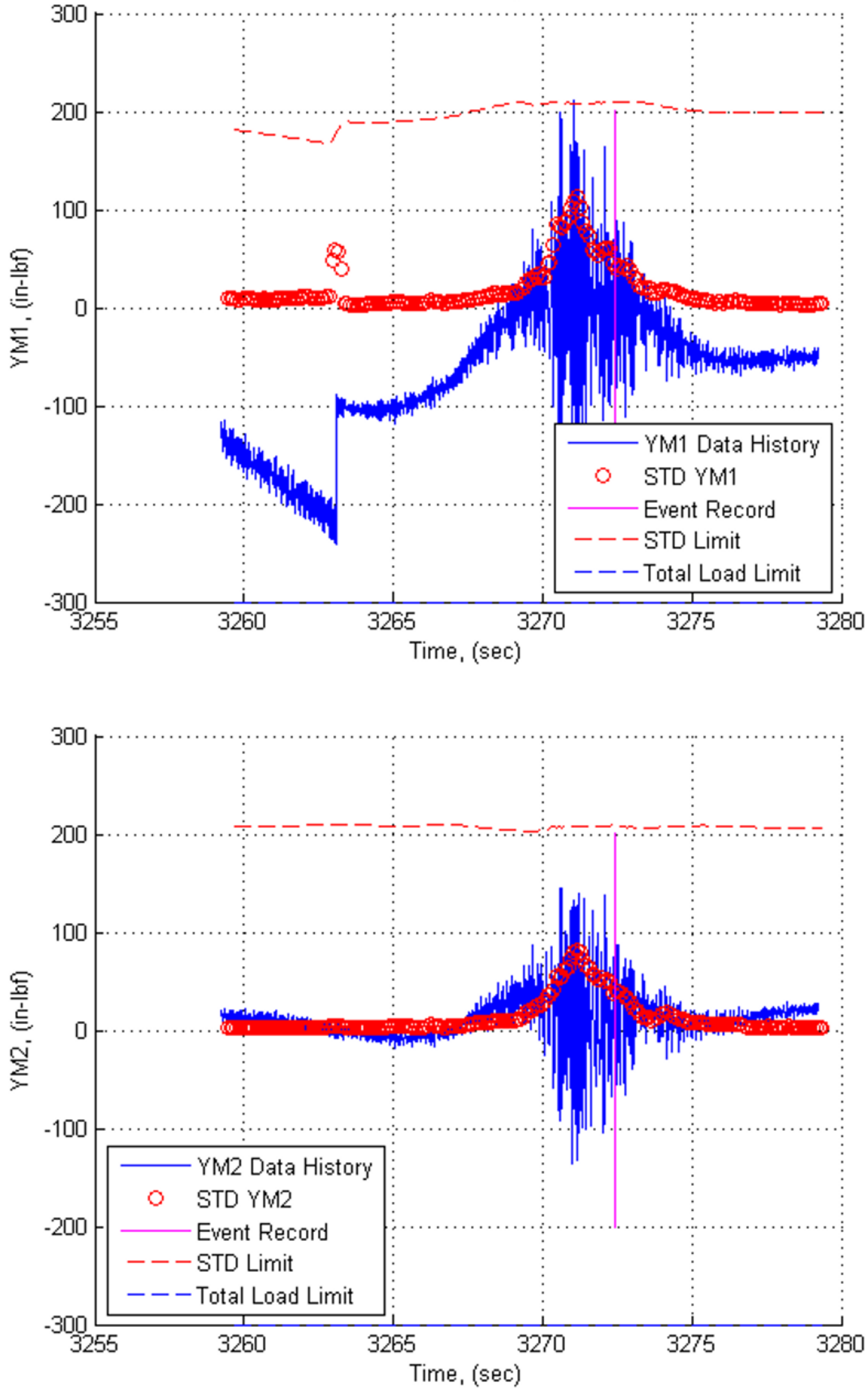

a.

Figure 23. Continued

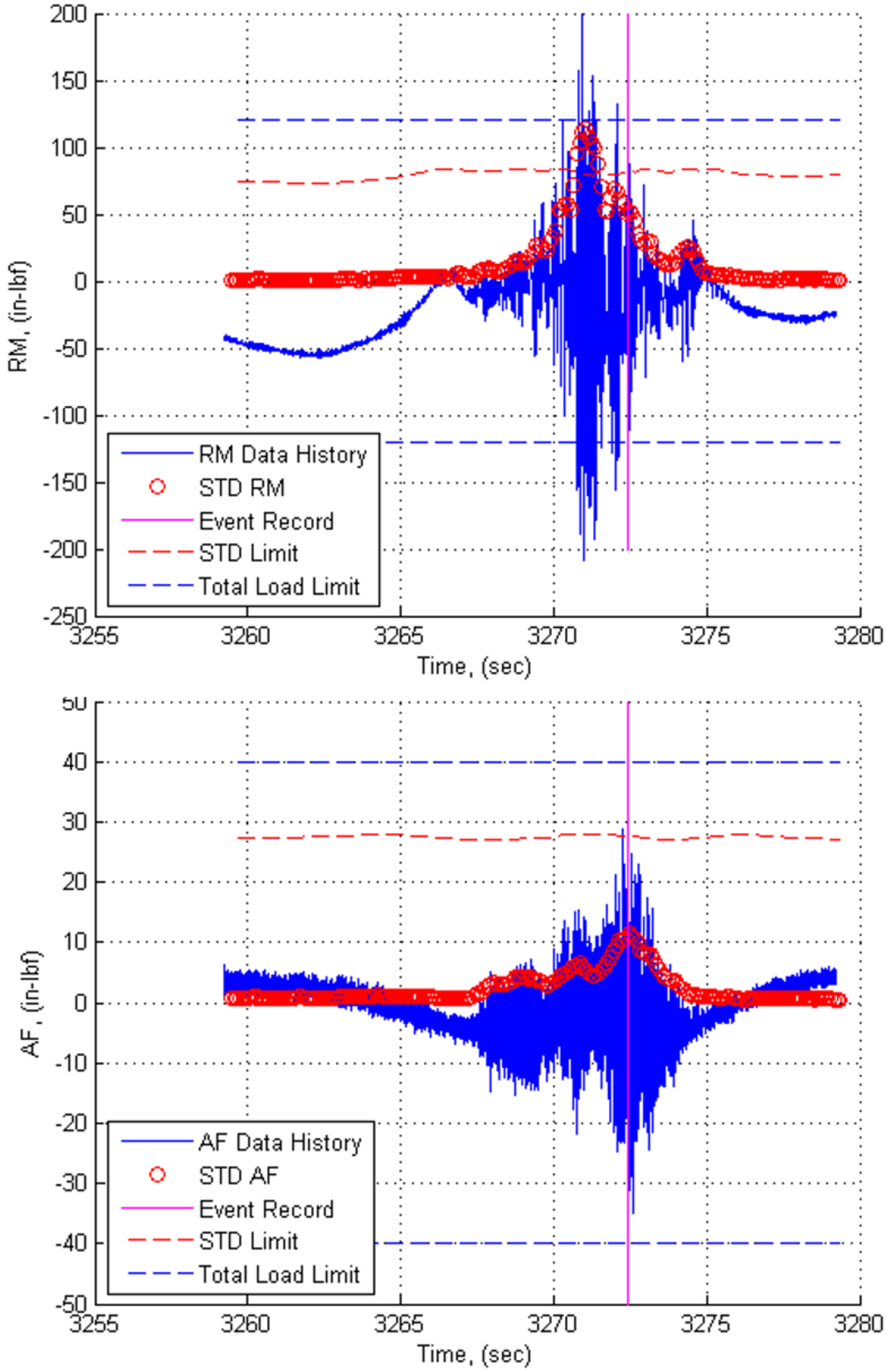

a.

Figure 23. Continued

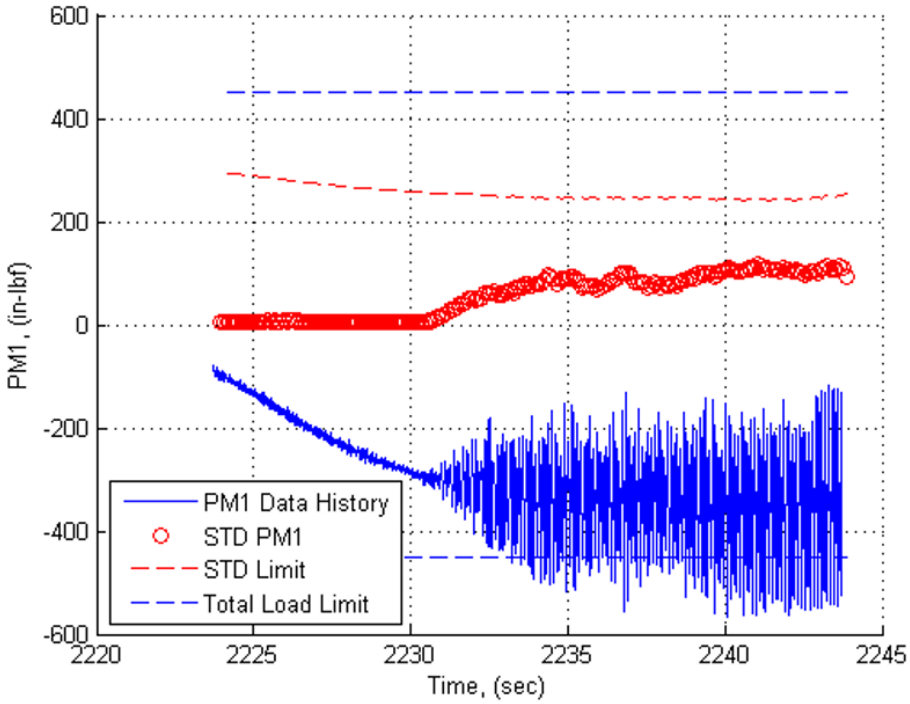

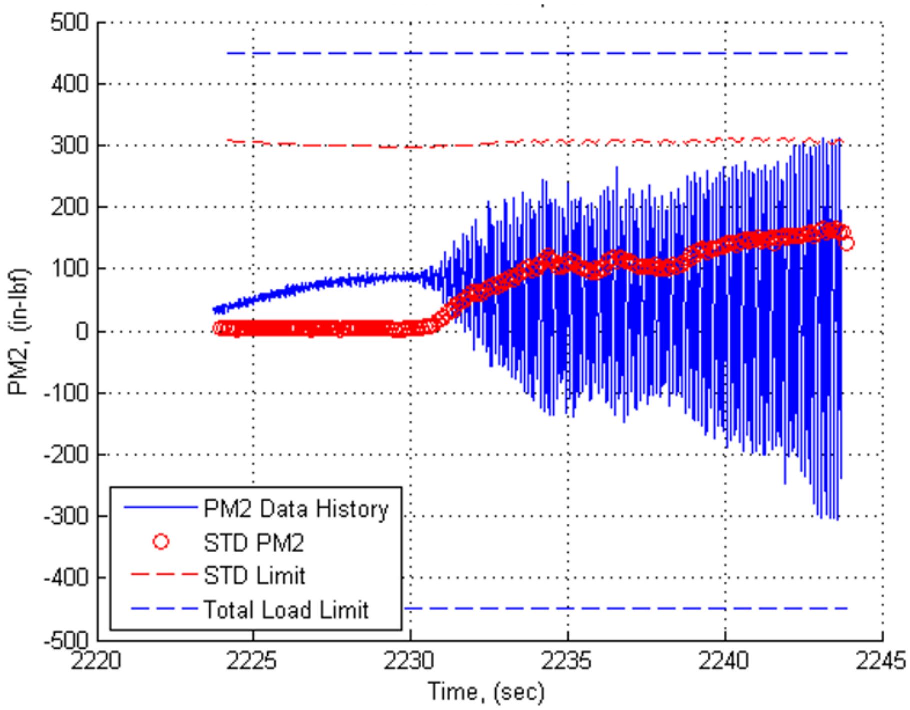

b.

Figure 23. Continued

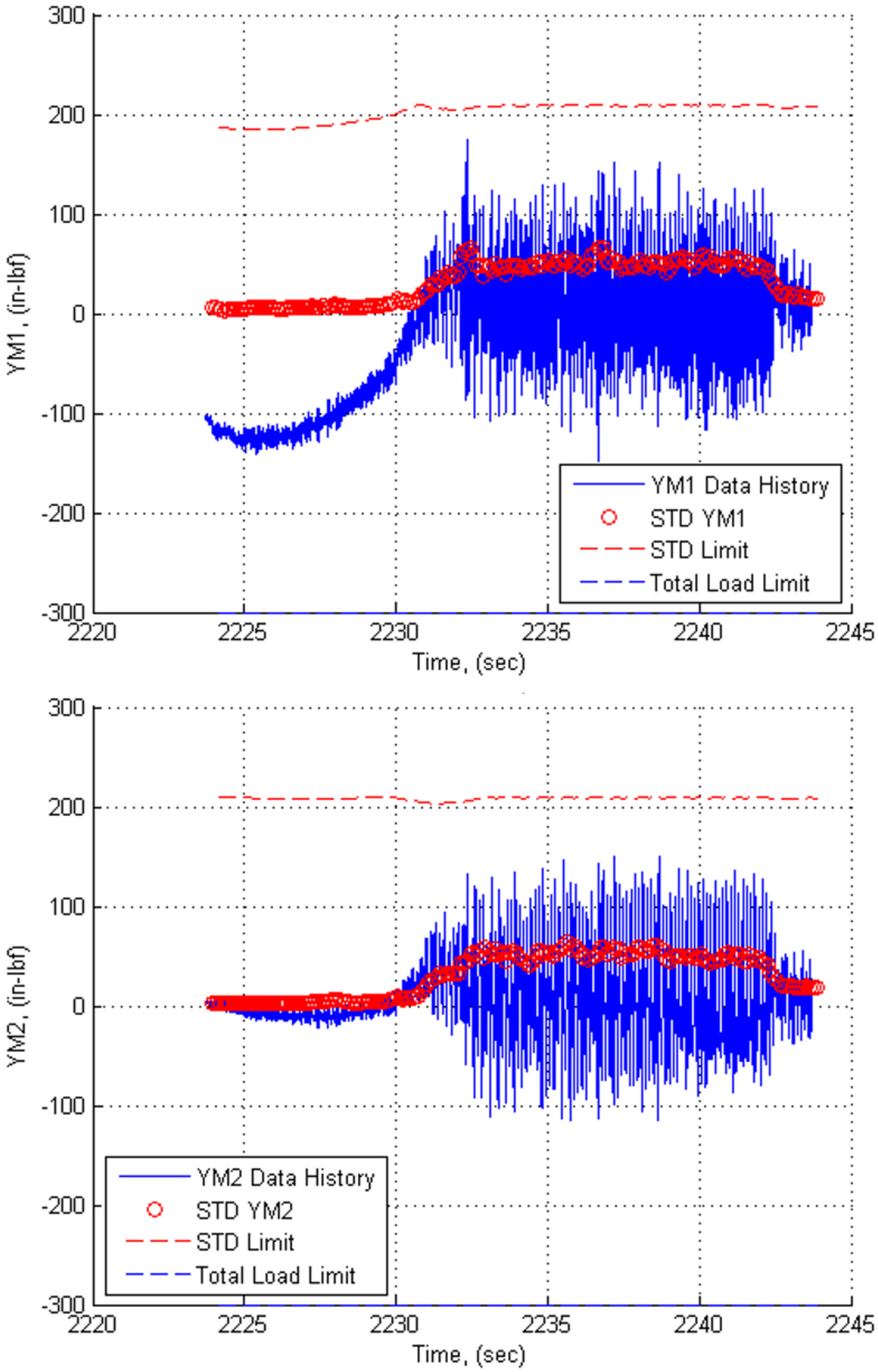

b.

Figure 23. Continued

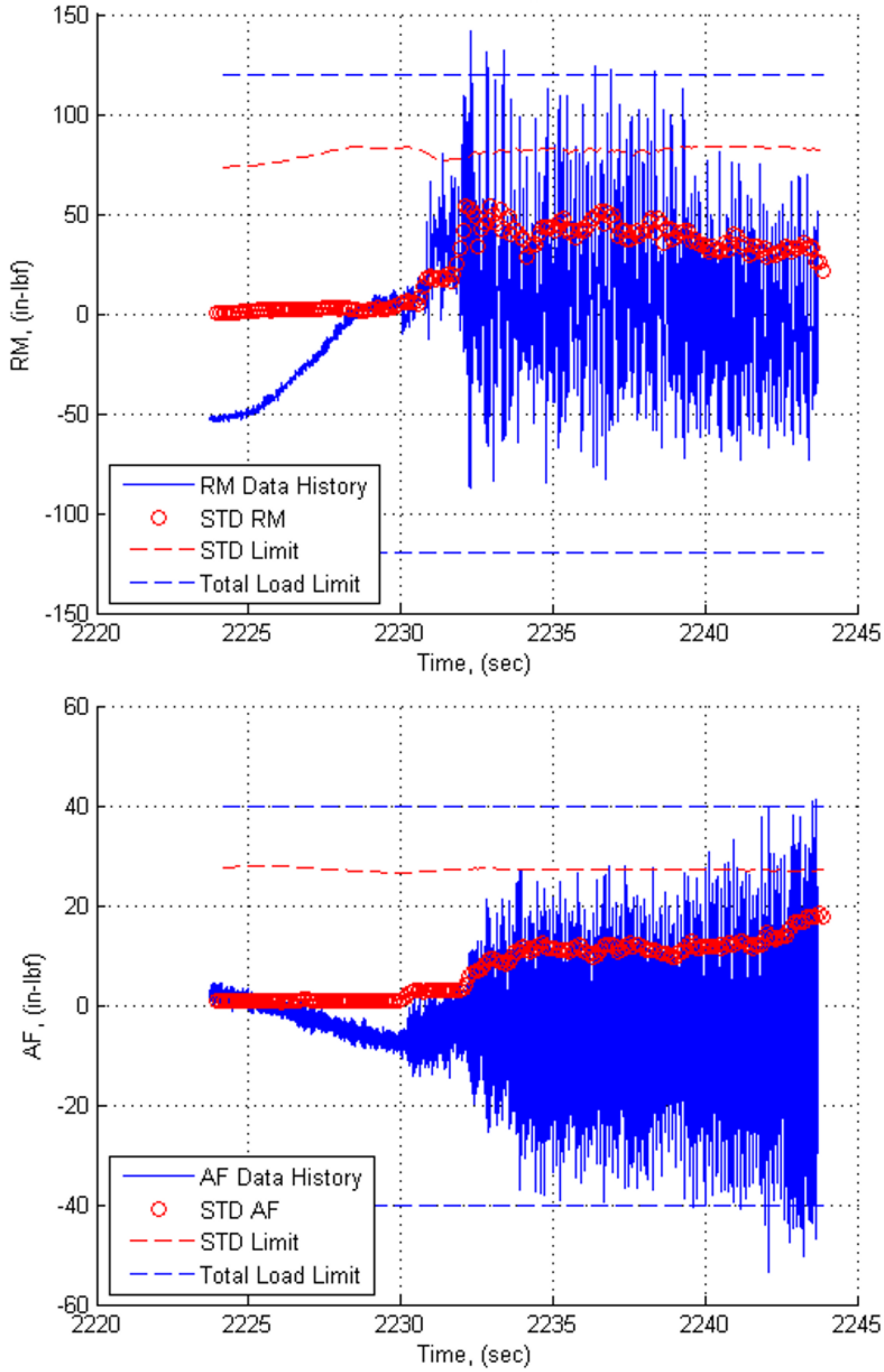

b.

Figure 23. Continued

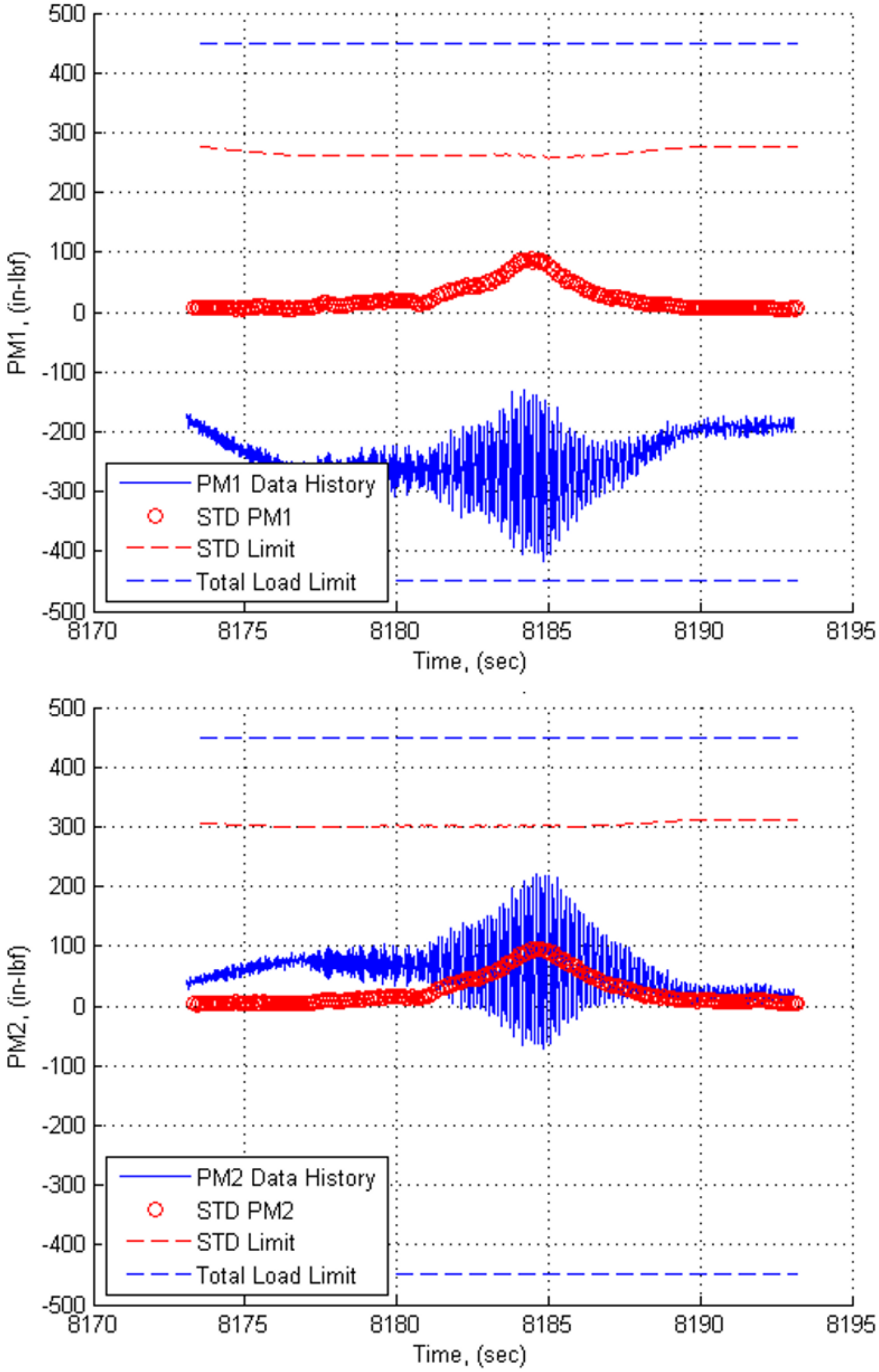

c.

Figure 23. Continued

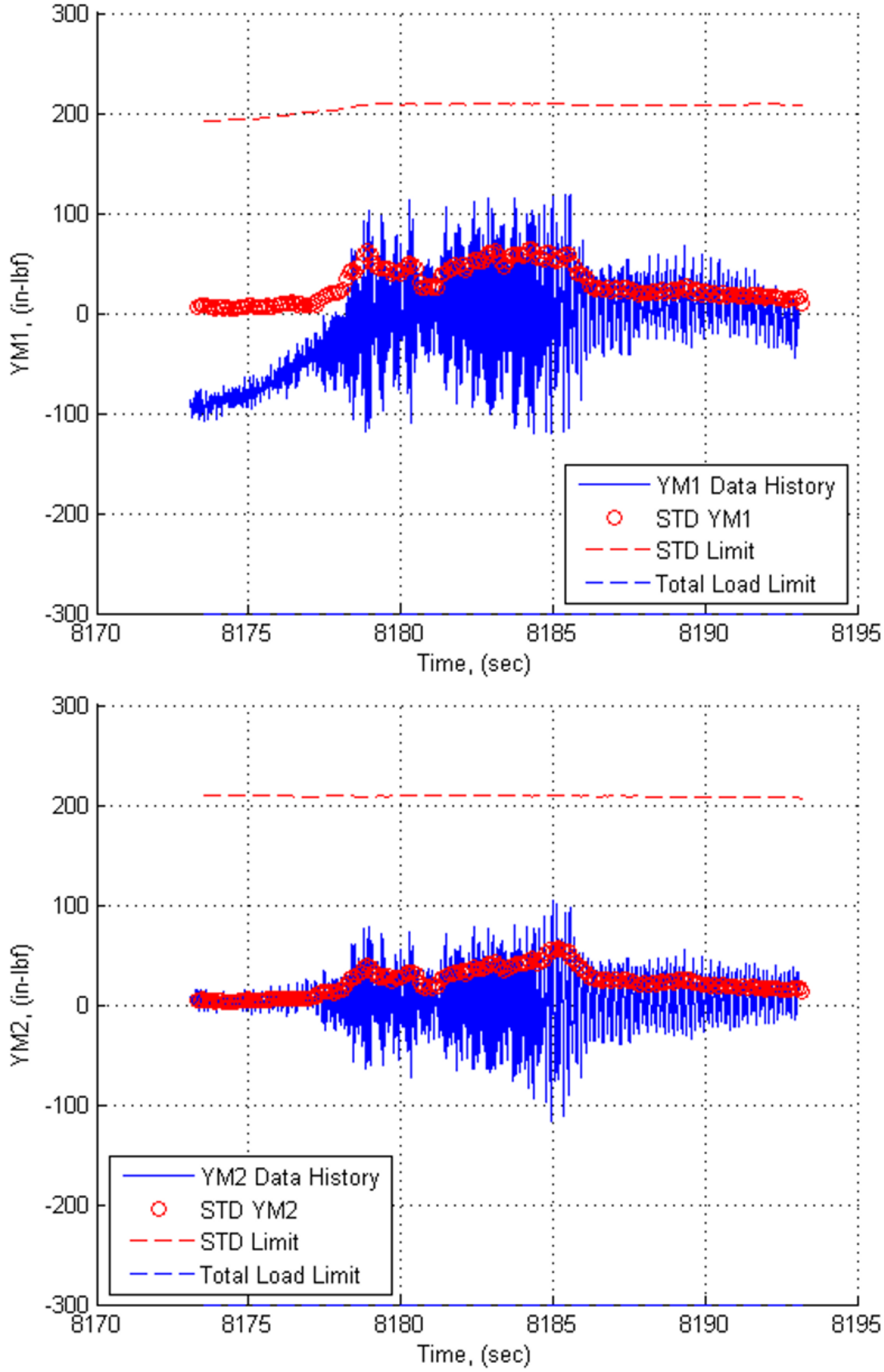

c.

Figure 23. Continued

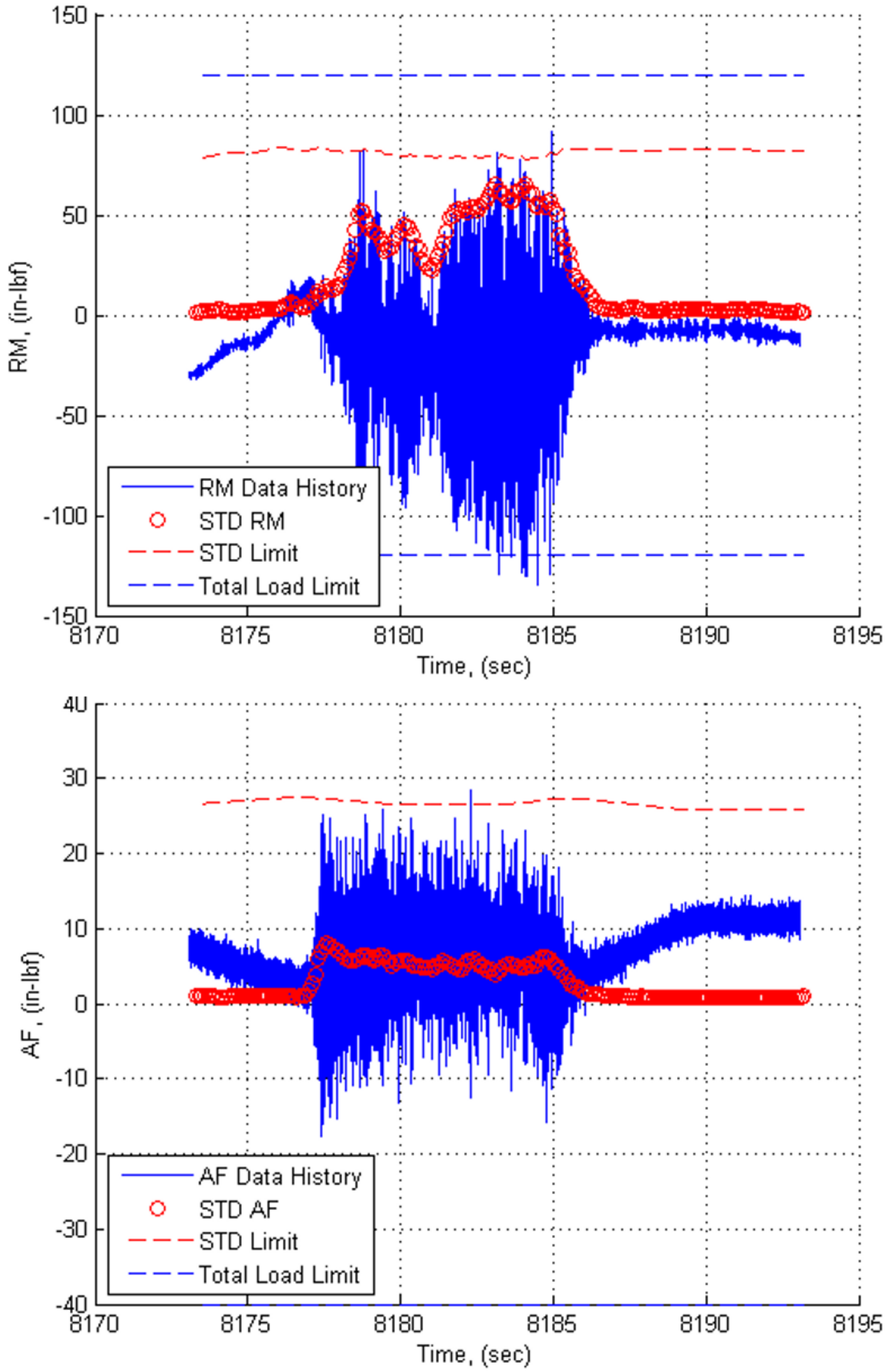

c.

Figure 23. Continued

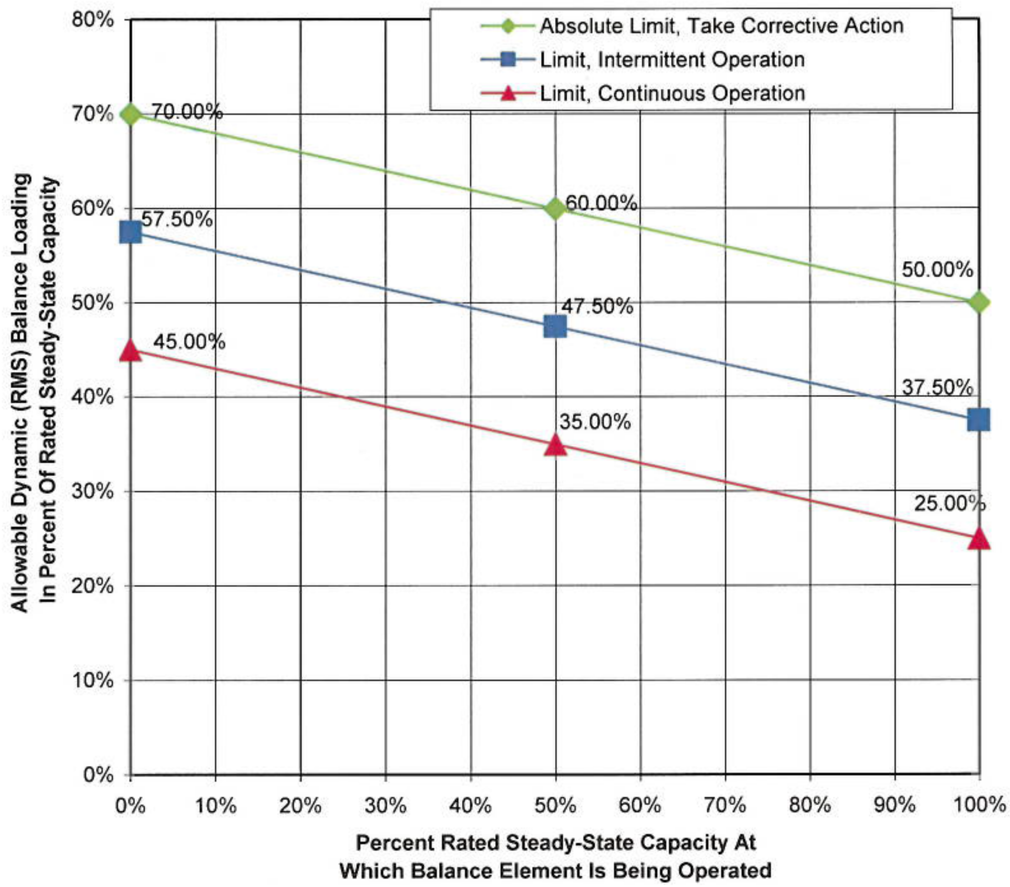

Figure 24. Legacy Dynamic Monitoring Curves

RMS wasn't used. In order to decompose the signal, an algorithm to find peaks was written in MATLAB®. This algorithm searched through the data and identified each point as either an "up", "down", or "peak". The peaks were then used to identify when stress reversals occurred and were paired to calculate a mean and alternating component. Figure 25 is an example of a 0.5 second data slice illustrating how the mean and alternating components were calculated from the peak finding algorithm. Since axial force was demonstrated previously, Figure 26 shows full time histories for each of the other five components with the peaks identified. These plots provided confidence that the sample rate was sufficient, and the peak finding algorithm was working properly as all the peaks were identified. Figure 27 displays each balance component signal broken into the alternating and mean loads using 1000 Hz downsampling. The figure shows that Run 1 had cases which crossed the infinite life line on the rolling moment component. Run 2 had axial force and rolling moment crossings, and Run 3 contained no points which crossed the infinite life line.

5.2 LOAD CALCULATION

Although using a 6x96 balance calibration matrix provides the most accuracy, the ability to perform the iterative calculation at 1,000+ Hz can be challenging. As previously discussed, the primary sensitivity coefficient is multiplied by the bridge output to get a calculation of the dynamic load sensed by the balance in the legacy method. This is done because of the significant savings in calculating the product of two numbers versus the iterative process

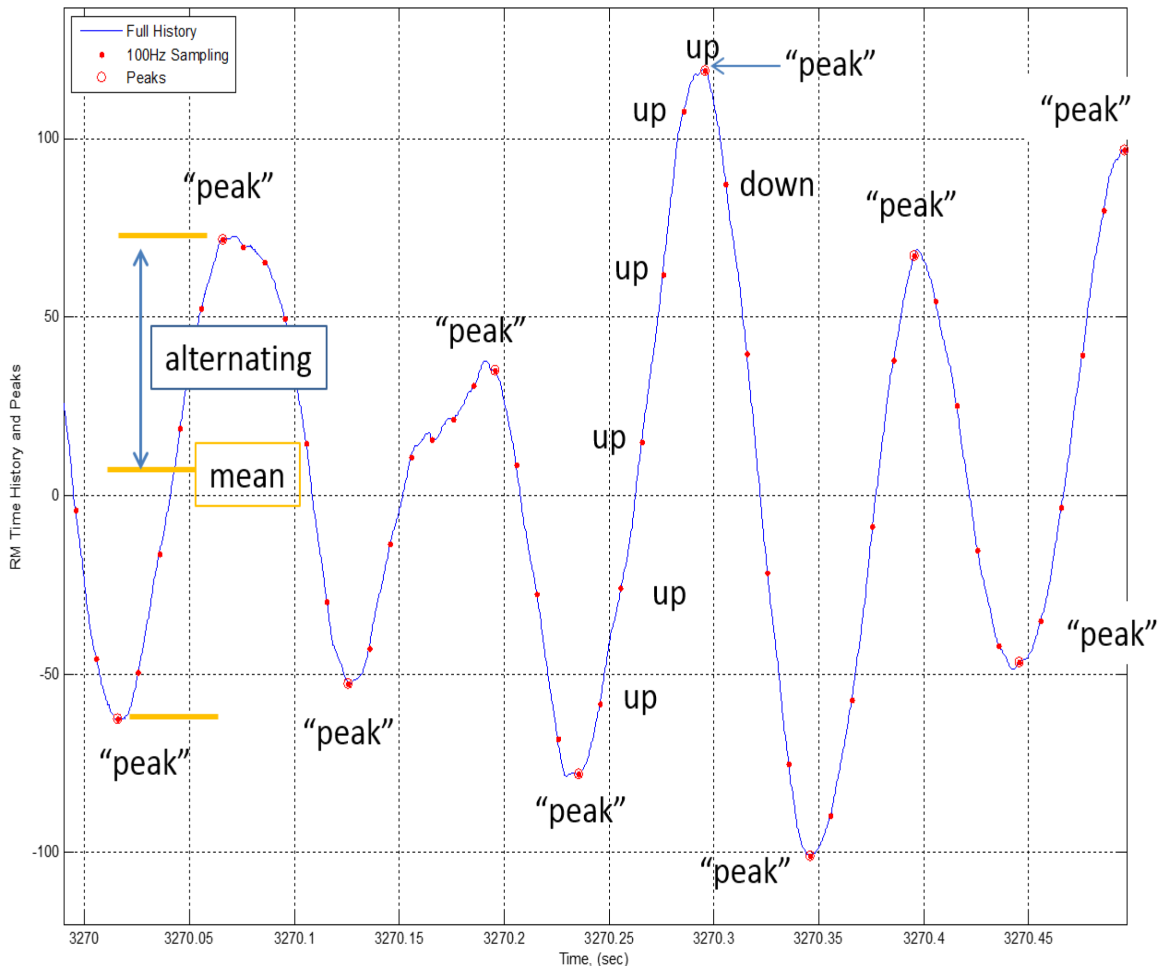

Figure 25. Example of Peak Finding Algorithm

Figure 26. Peak Selection at 1000Hz Example

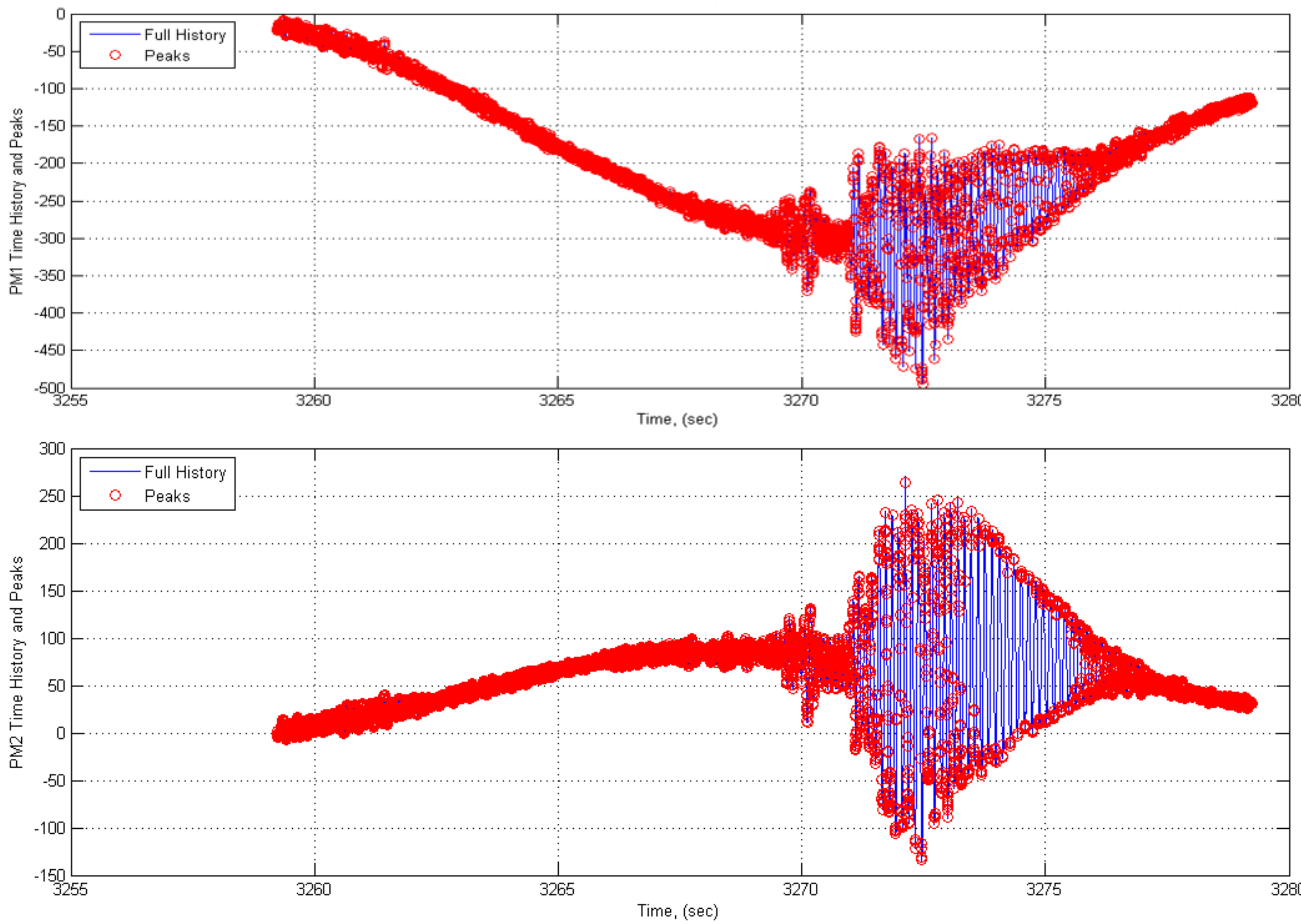

Figure 26. Continued

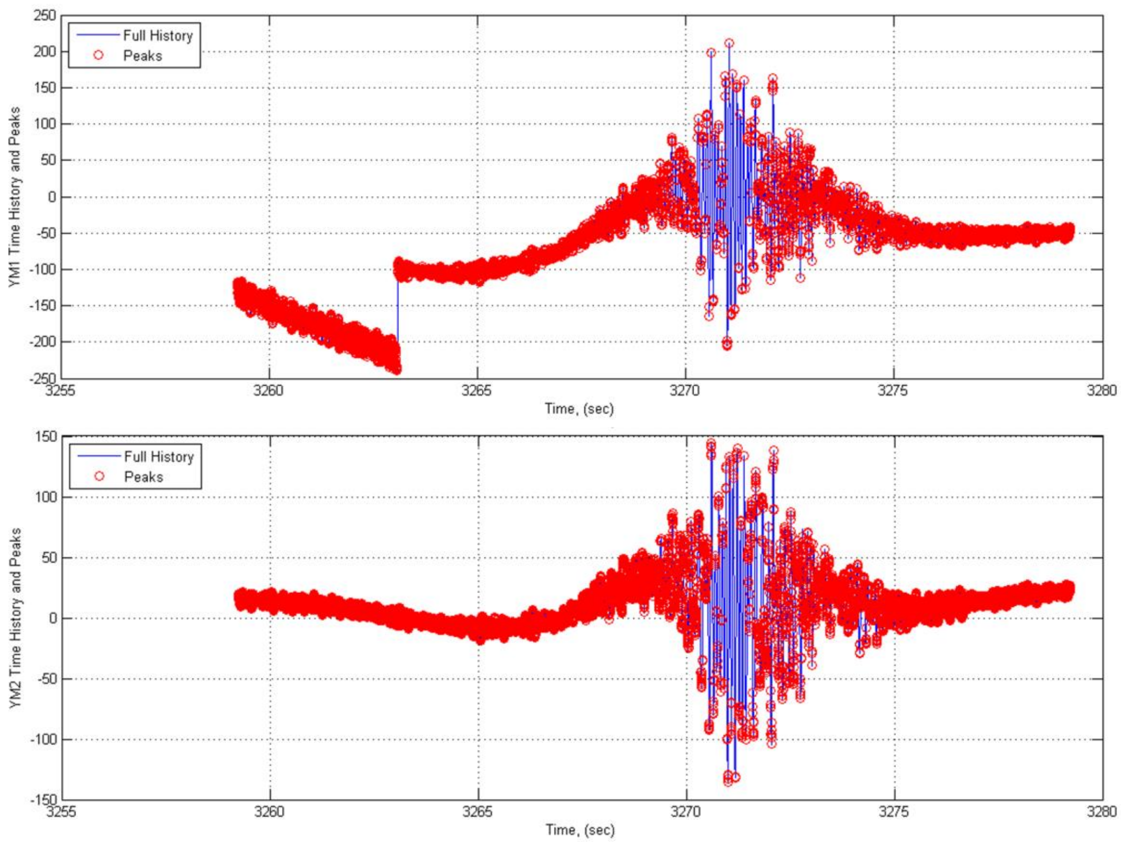

Figure 26. Continued

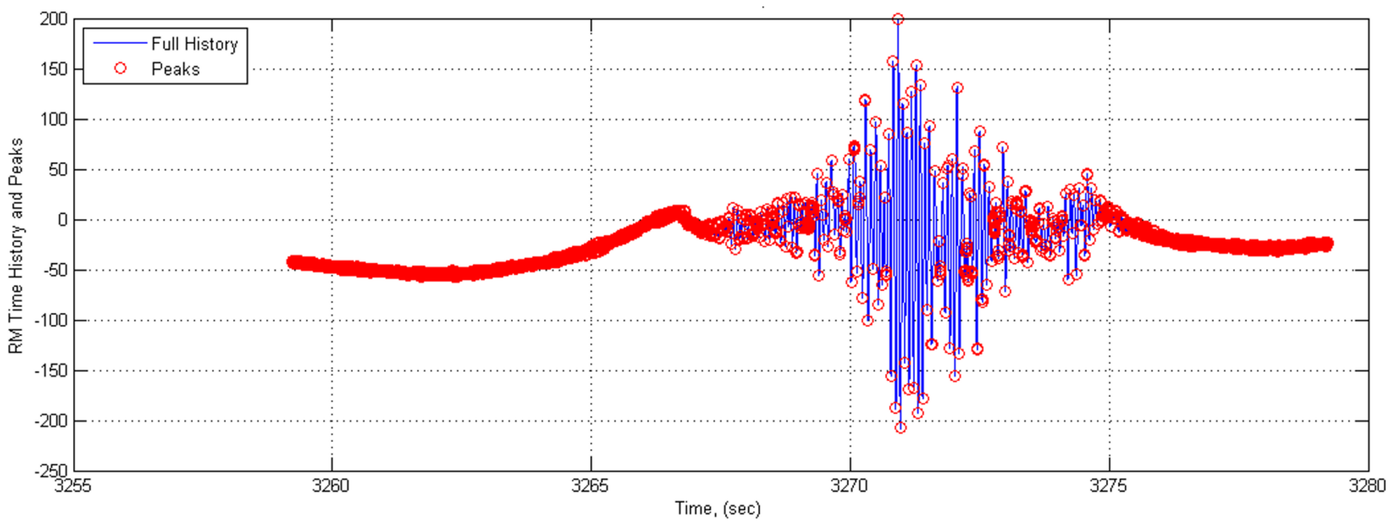

Figure 26. Continued

Figure 27. Legacy Modified Goodman Chart Displaying New Method

Calculations, a. Run 1, b. Run 2, c. Run 3

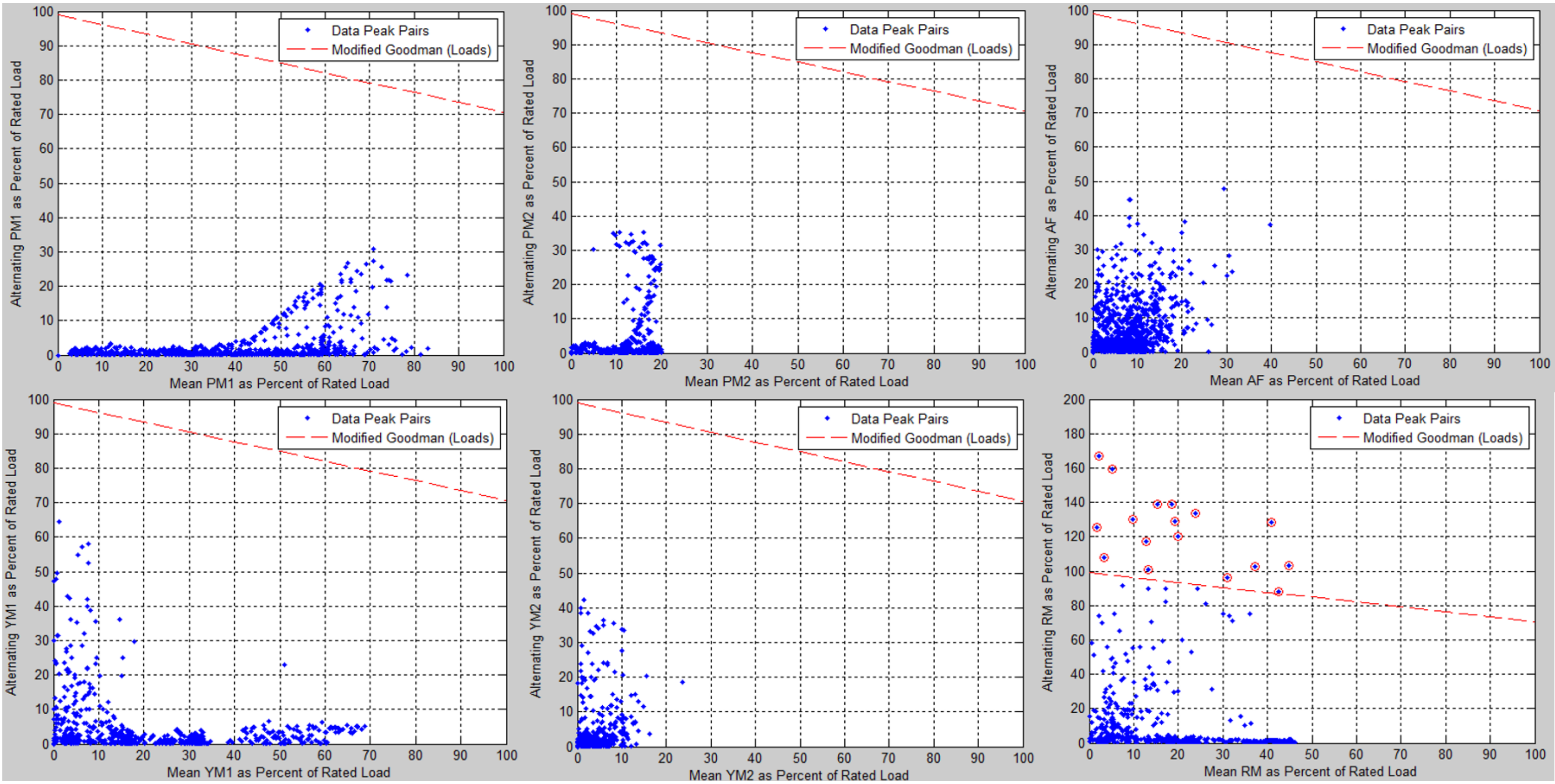

a.

Figure 27. Continued

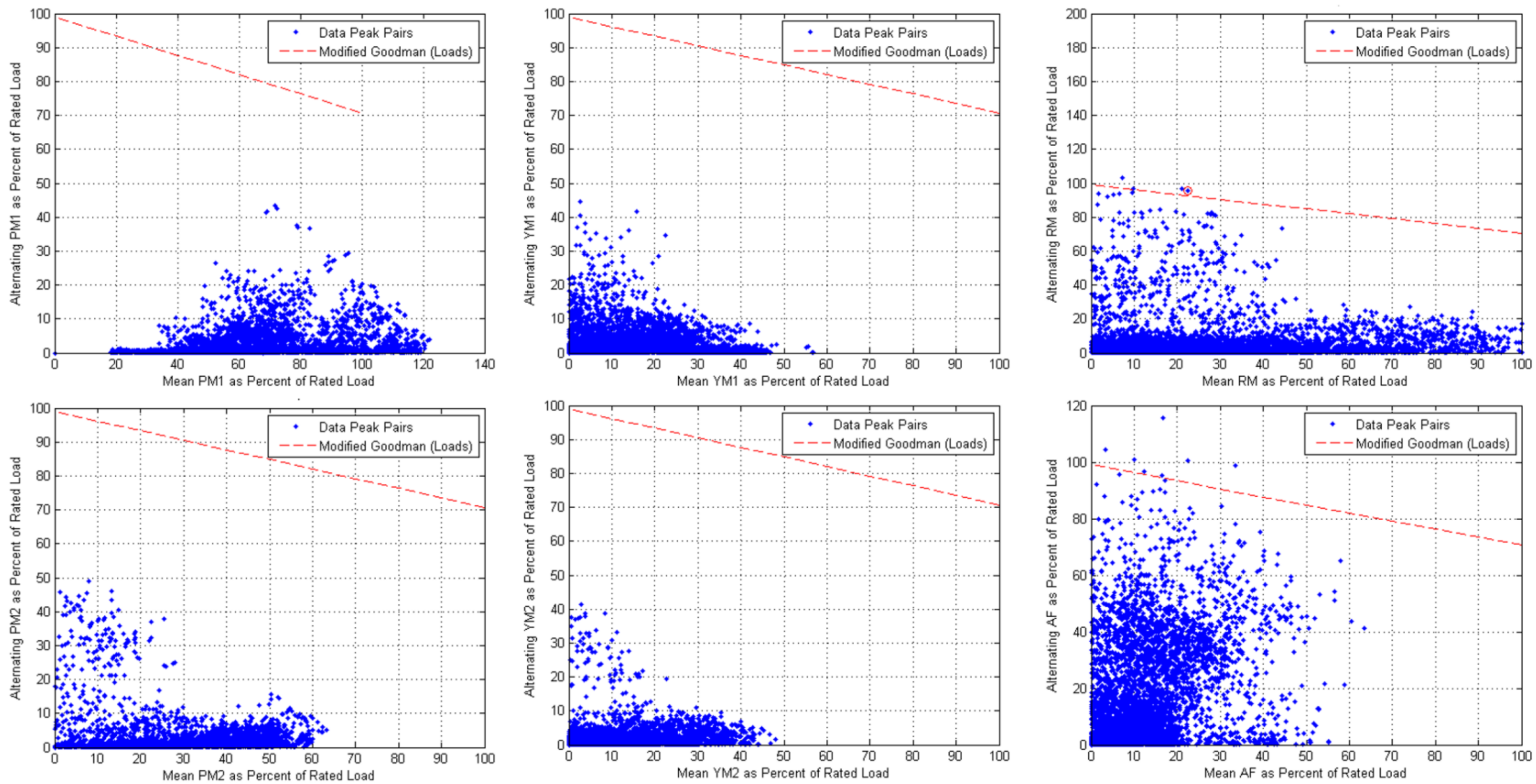

b.

Figure 27. Continued

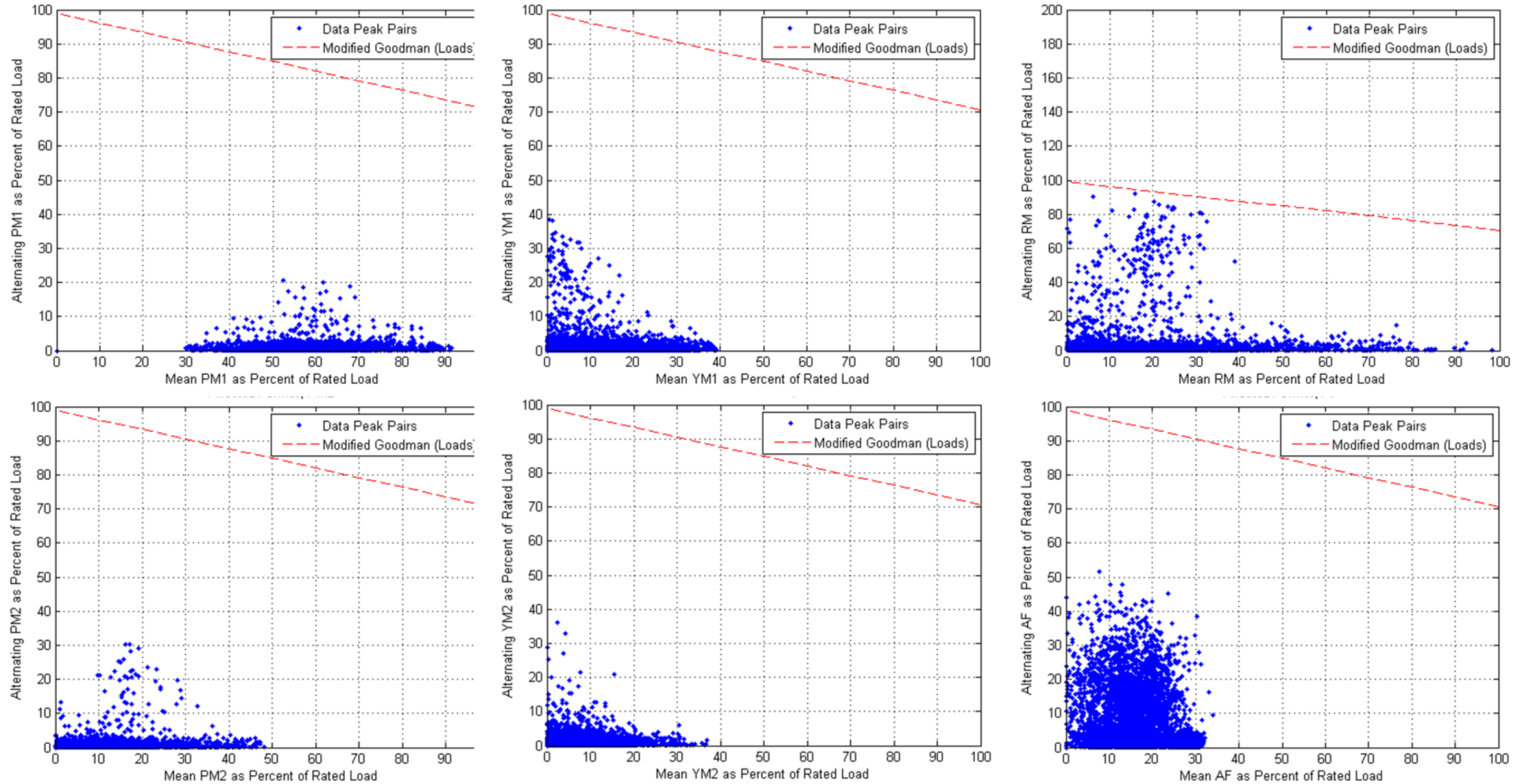

c.

Figure 27. Continued

required to use all 6x96 possible balance calibration coefficients. In some cases the use of the primary sensitivity alone could yield results that are better than 95% of the total load being applied. This is considered good enough for an engineering solution for monitoring the dynamic balance output. Unfortunately, this is not the case for all balance designs.

Without significantly increasing the complexity of the calculations, the 6x6 matrix can solve for the load. With the addition of the linear interaction terms, balances that have machining or alignment errors can also be characterized. The improvement of using the 6x6 instead of the primary sensitivities will be significant in these kind of balances. Table 4 shows the results of calculating a load from the primary sensitivities, primary interaction 6x6 matrix, and the full non-linear calibration matrix for two different balance types. Significant increases occur in both the standard deviation of all the residuals and the maximum error if only the primary sensitivities are used for balance B. The table shows the results of the load calculations for comparison purposes. The results were normalized by dividing by the full scale capacity of each component. The legacy dynamic monitoring calculation uses only the primary sensitivity, so this is a shortfall that should be corrected in the new method. This comparison shows that the 6x6 is much better than the primary sensitivity, and that the 6x96 only provides marginal gains if ± 5% is the target. Because the 6x6 calibration matrix showed significant improvement over the primary sensitivity, and the fact that it does not require an iterative scheme to solve like the 6x96 does, the 6x6 matrix calculation was

Table 4. Comparison of Load Calculation Methods

		Balance A		Balance B	
		2*σ/FS	worst error/FS	2*σ/FS	worst error/FS
Prime Sensitivity	NF	0.85%	4.49%	0.39%	1.53%
	PM	0.08%	0.43%	3.90%	19.13%
	SF	1.39%	5.46%	1.61%	7.33%
	YM	0.72%	3.62%	4.87%	16.07%
	RM	0.64%	2.41%	0.33%	1.23%
	AF	3.83%	12.85%	13.70%	72.95%
6x6	NF	0.00%	0.02%	0.01%	0.08%
	PM	0.01%	0.09%	0.04%	0.36%
	SF	0.01%	0.02%	0.07%	0.55%
	YM	0.07%	0.40%	0.06%	0.17%
	RM	0.10%	0.58%	0.11%	0.44%
	AF	0.78%	2.47%	0.82%	2.09%

chosen for the simulation models.

5.3 LOAD LIMITS

The entire balance monitoring method hinges on properly determining the limits on which to monitor the balance. Historically balances were designed and analyzed using the same fundamental stress equations that FEA uses, but these hand calculations were limited to sections where the designer expected the loads to be high, and the geometry was relatively simple. FEA allows thousands or millions of nodes to be examined at all locations of the balance and can uncover new areas of stress concentrations. The designers knew that stress concentrations existed, but without full understanding of the actual stress levels Factors of Safety (FoS) values of 3 on yield strength and 4 on ultimate strength were implemented (REF 20). FEA has the potential to better identify the stress concentrations which may in turn allow lower FoS to be used while still remaining safe. The other advantage of FEA is the ability to easily perform simultaneous load cases to identify what physical locations of the balance should be monitored, and can be used to streamline this node monitoring selection process.

5.3.1 FEA

After the 3-D geometry model was created, a static structural analysis was performed in ANSYS Workbench 14.5. As previously mentioned, the 3-D balance models were constructed in Autodesk Inventor 2015. Although this balance has screws holding the three pieces together, the stress analysis was simplified with the assumption that these connections were bonded, since a stress analysis including the tightness of the screws is beyond the scope of this work.

The first step was to set up the boundary conditions and applied loads. For the analysis a fixed support was placed on the sting mounted taper side of the balance. This type of constraint assumes that this portion of the balance was fixed to “ground”. This is a valid assumption because the stiffness of the sting is much larger than the stiffness of the balance. Next, remote normal, side, and axial forces were placed at the balance moment reference center and were fixed to the forward taper. A remote force was used because all loads applied to the model were transferred to the balance through the forward taper attachment, which was well forward of the balance reference center where the loads were calculated. Finally pitching, yawing, and roll moments were applied about the balance axis. Figure 28 shows the fixed constraint and loads applied to the balance model.

The forces and moments were parametrically varied in order to determine which stress node locations of the balance were the most critical for monitoring. Initially, the approach examined 8 load cases to identify the critical nodes. Table 5 provides these loads, which were the maximum rated loads for each component and the two combined load cases for which the balance was designed.

The default mesh created by ANSYS was initially used to ensure that a solution could be achieved. Further mesh refinements were performed in areas of high stress areas identified by the default mesh. Finally, a mesh convergence study was performed to determine the point at which continuing to make the mesh size smaller impacted the results by less than 5%. Figures 29 and 30 illustrate the results of the mesh convergence study and the final mesh. As shown in Fig. 29, no significant difference in the maximum Von Mises stress was seen by increasing the number of mesh elements from 25528 to 89708, thus the fewer element model was used to simply the analysis and reduce computational time. The highest stress nodes and locations for each of the initial 8 cases are provided in Table 6 and a graphical representation of these nodes is shown in Fig. 31.

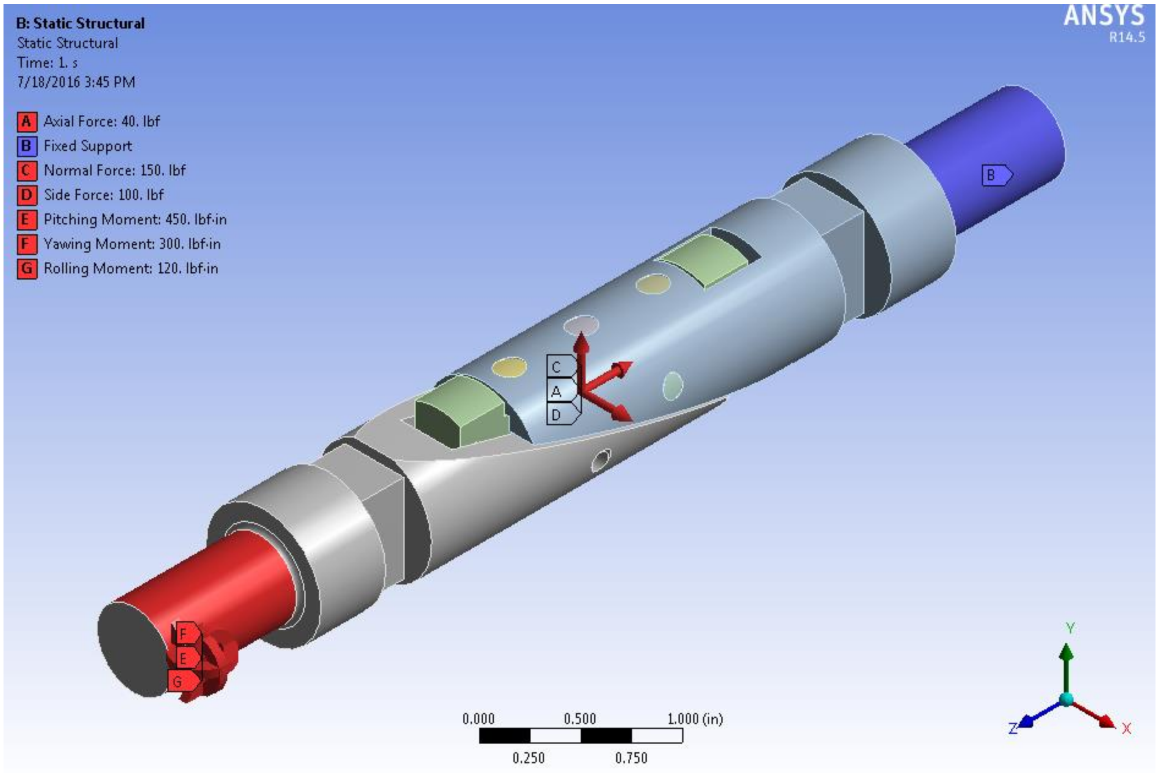

Figure 28. Balance Model with Loads and Fixed Support Constraint

Table 5. Initial FEA Load Cases

Load #	AF (lb)	NF (lb)	SF (lb)	PM (in-lb)	YM (in-lb)	RM (in-lb)
1	-40	0	0	0	0	0
2	0	150	0	0	0	0
3	0	0	100	0	0	0
4	0	0	0	450	0	0
5	0	0	0	0	300	0
6	0	0	0	0	0	120
7	-40	150	100	450	300	120
8	-40	250	167	0	0	120

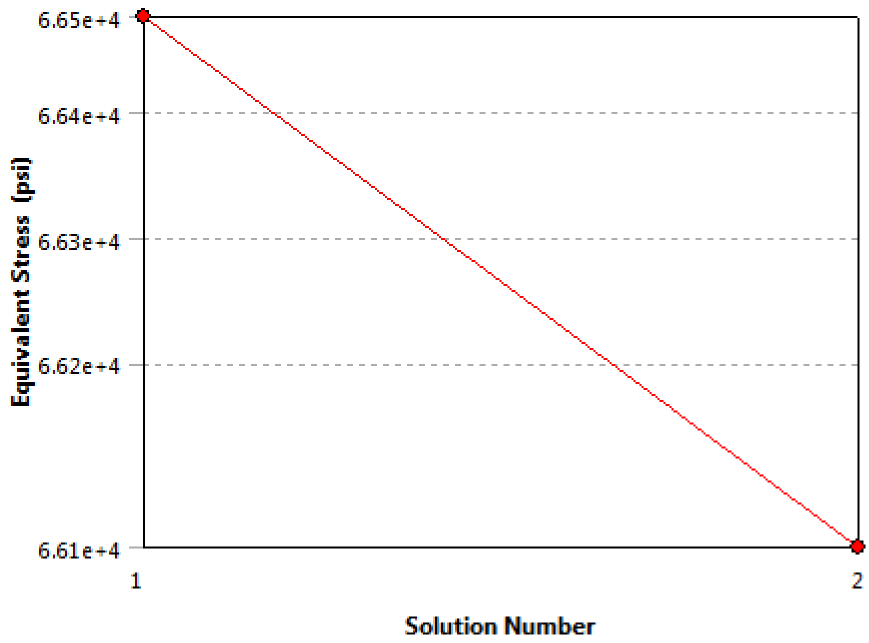

	Equivalent Stress (psi)	Change (%)	Nodes	Elements
1	66476		25528	14232
2	66054	-0.63792	89708	55958

Figure 29. Mesh Iterations

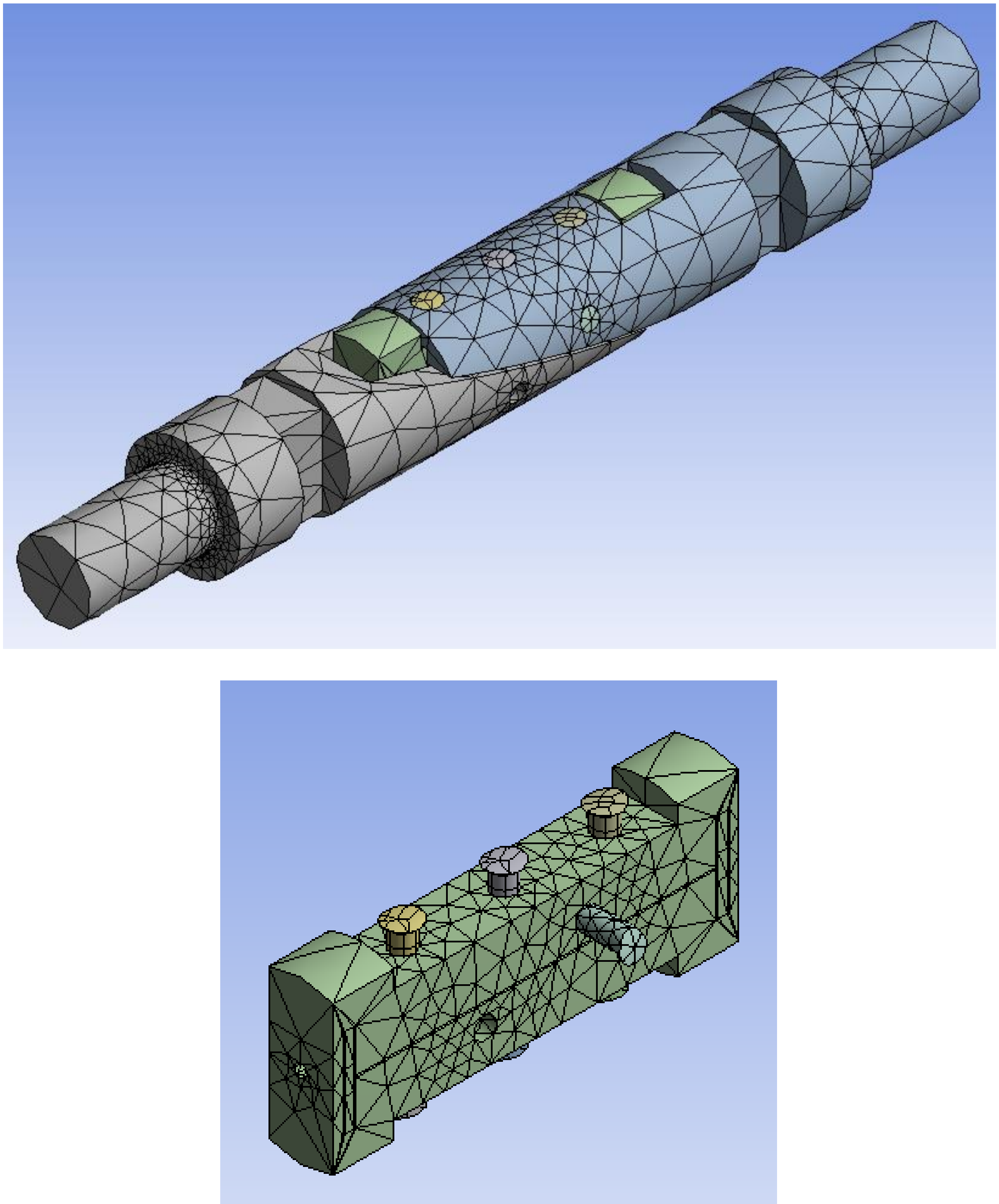

Figure 30. Final Mesh

Table 6. Critical Nodes From Initial FEA Load Cases

Load #	Node	X	Y	Z	Type
1	11807	0.000	0.220	0.944	Axial
2	5797	0.065	0.252	-2.240	Normal
3	5770	-0.249	-0.074	-2.240	Side
4	5797	0.065	0.252	-2.240	PM
5	5770	-0.249	-0.074	-2.240	YM
6	11739	0.160	-0.220	-0.898	RM
7	11739	0.160	-0.220	-0.898	Combined
8	5797	0.065	0.252	-2.240	Center Combined

Figure 31. Graphical Critical Nodes, a. Axial Force, b. Normal Force (top), Side Force (bottom), c. Pitching Moment (top), Yawing Moment (bottom), d. Rolling Moment (top), Combined (bottom), e. Combined Center

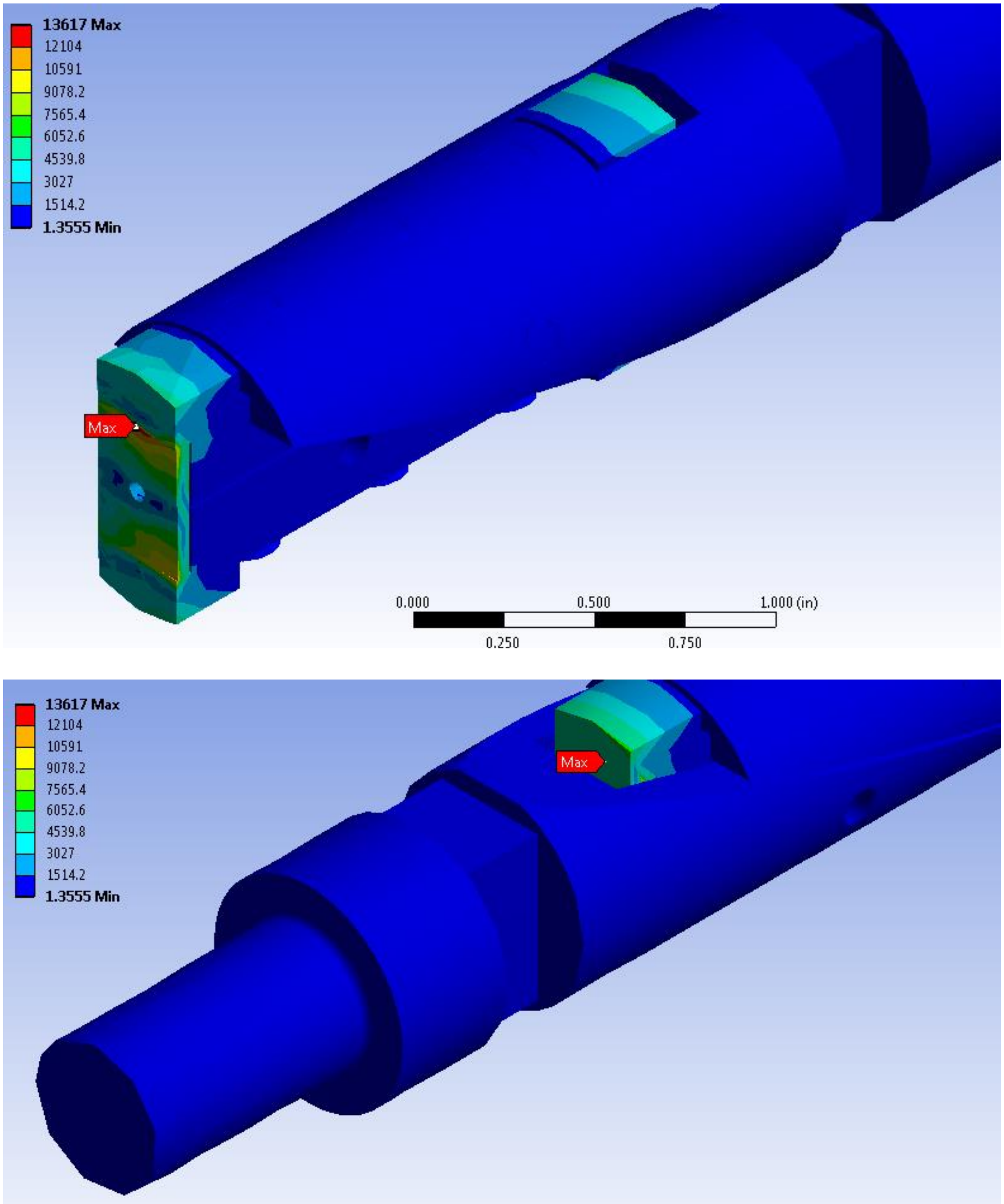

a.

Figure 31. Continued

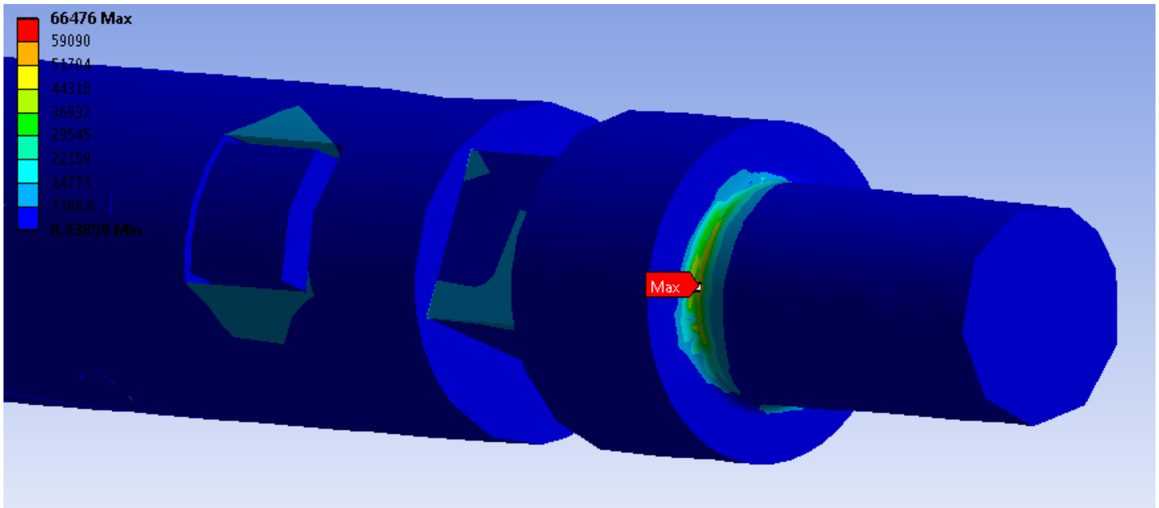

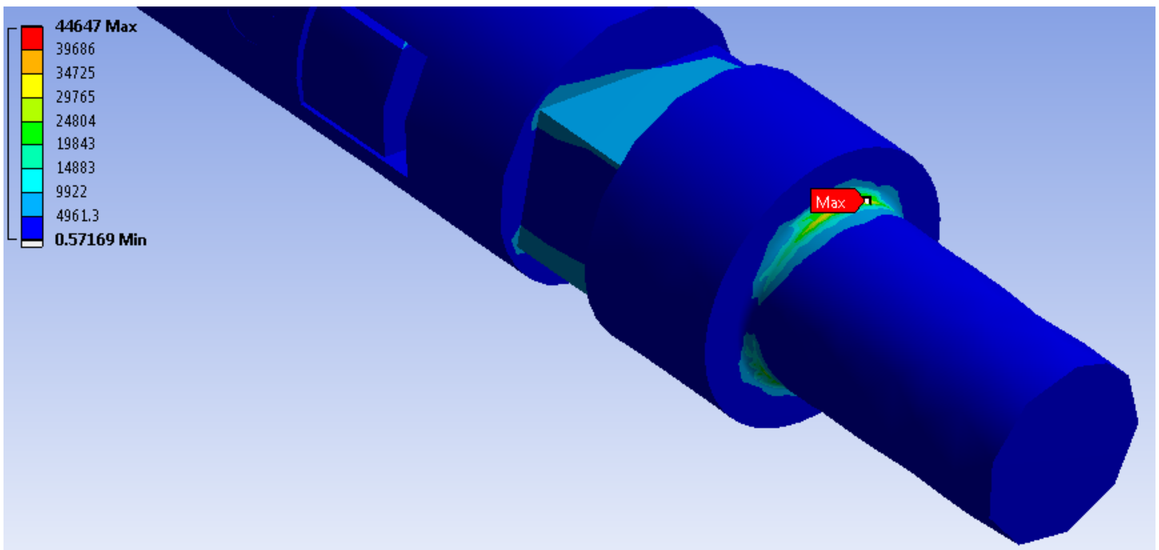

b.

Figure 31. Continued

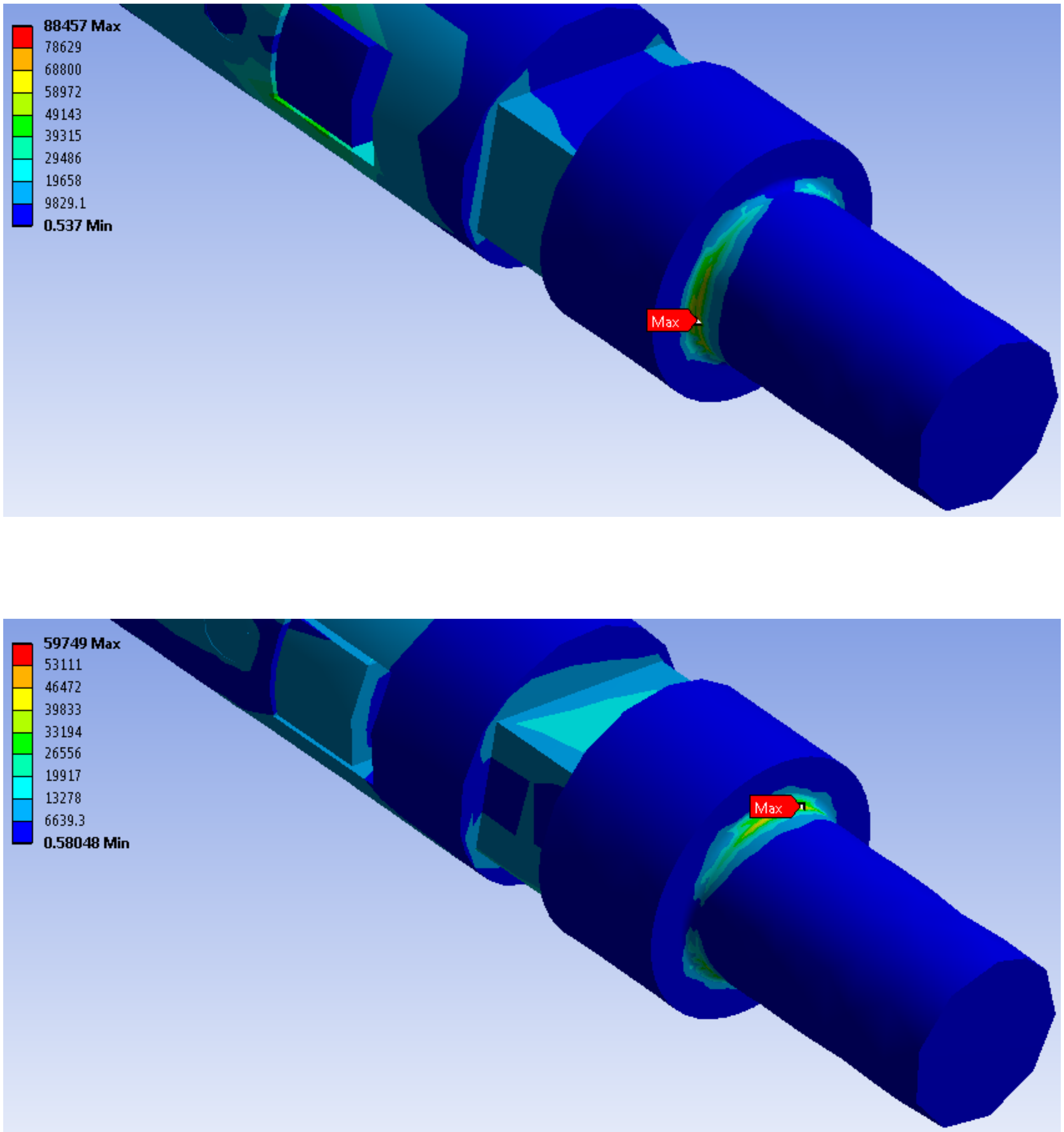

c.

Figure 31. Continued

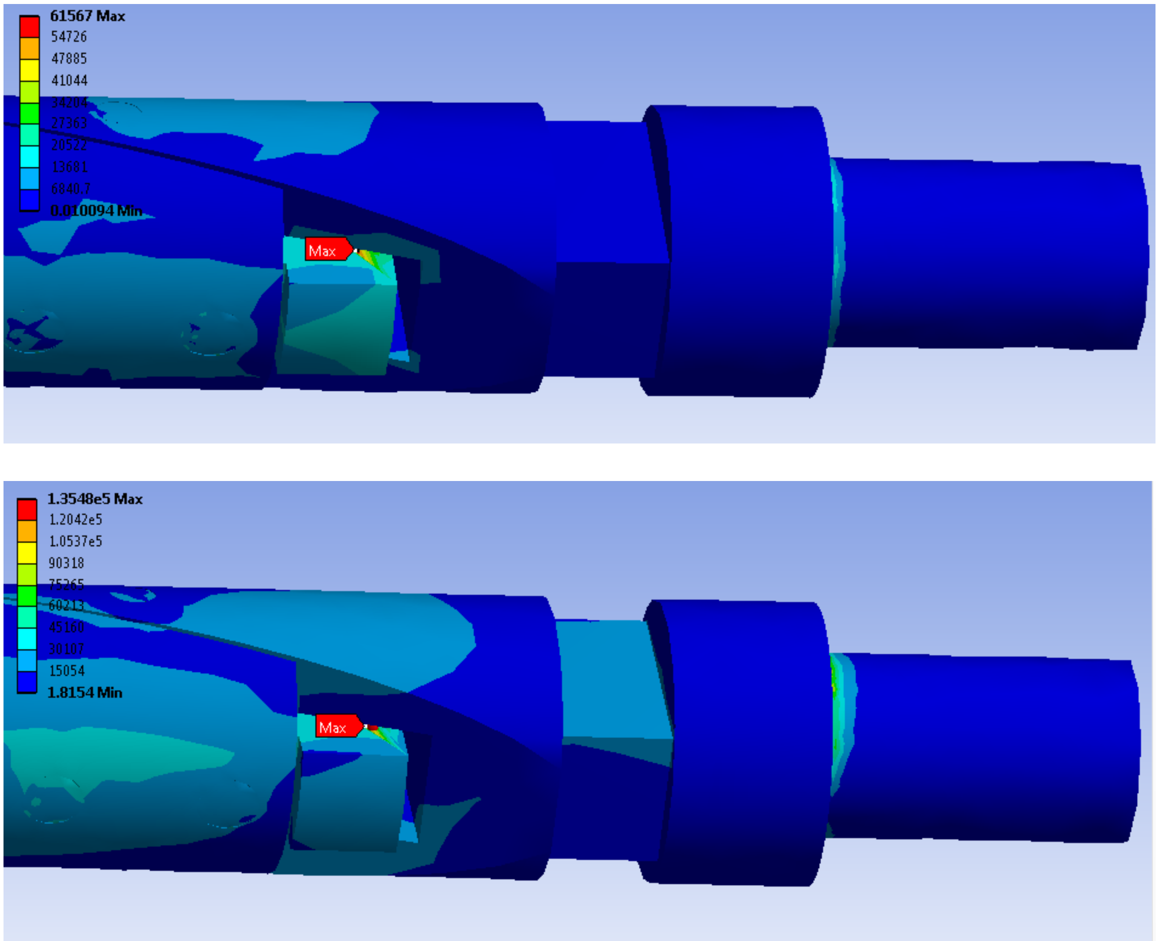

d.

Figure 31. Continued

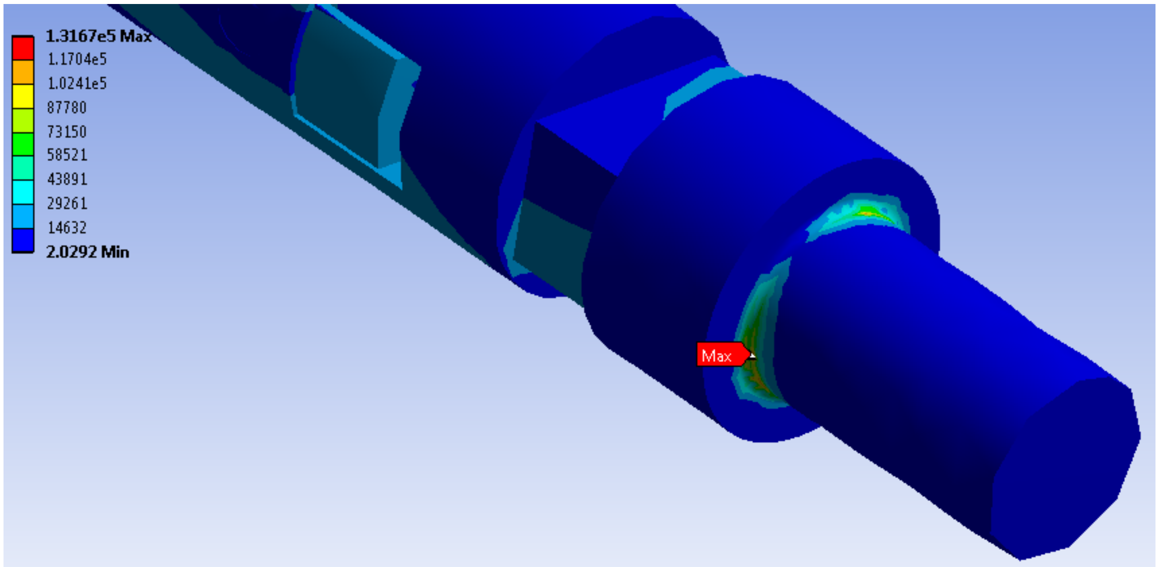

e.

Figure 31. Continued

5.3.1.1 Hand Calculations

Hand calculations of stress are used to guide the analysis of maximum loads which can be handled by the balance. These can also serve as a bench mark for FEA computations. Typical locations which are analyzed using hand calculations are the sting taper attachment point and the flats where the gages are located. Figure 32 provides some geometric properties required to calculate bending stress at the sting attachment taper. The diameter of the taper is 0.52 in., and the maximum normal force and side force are 150 lbf and 100 lbf, respectively. Additionally the maximum pitching moment and yawing moment of 450 in-lbf and 300 in-lbf, respectively, need to be considered. Since the balance resolves loads about the center, the only additional information required is the distance from the balance center to the station shown in Fig. 32. This distance is 3.86 inches for the chosen balance. To calculate the bending stress, Eq. 5 is used, where:

M = [(3.86 * NFmax + PMmax)^2 + (3.86 * SFmax + YMmax)^2]^0.5

c = gage diameter / 2

I = 0.0036 in^4

So, σ_b = 89.32 ksi, which holds a FoS of 2.07 on yield. Next the forward pitching moment and yawing moment beam were examined as depicted in Fig. 33. Again the same bending moment calculation can be used. Since this part contains a rectangular cross section, maximum stress will occur at the corner based on the principle stress. The width is 0.408 in and the height is 0.612. The distance from the balance center to the furthest part of the beam is 1.76 in. Therefore:

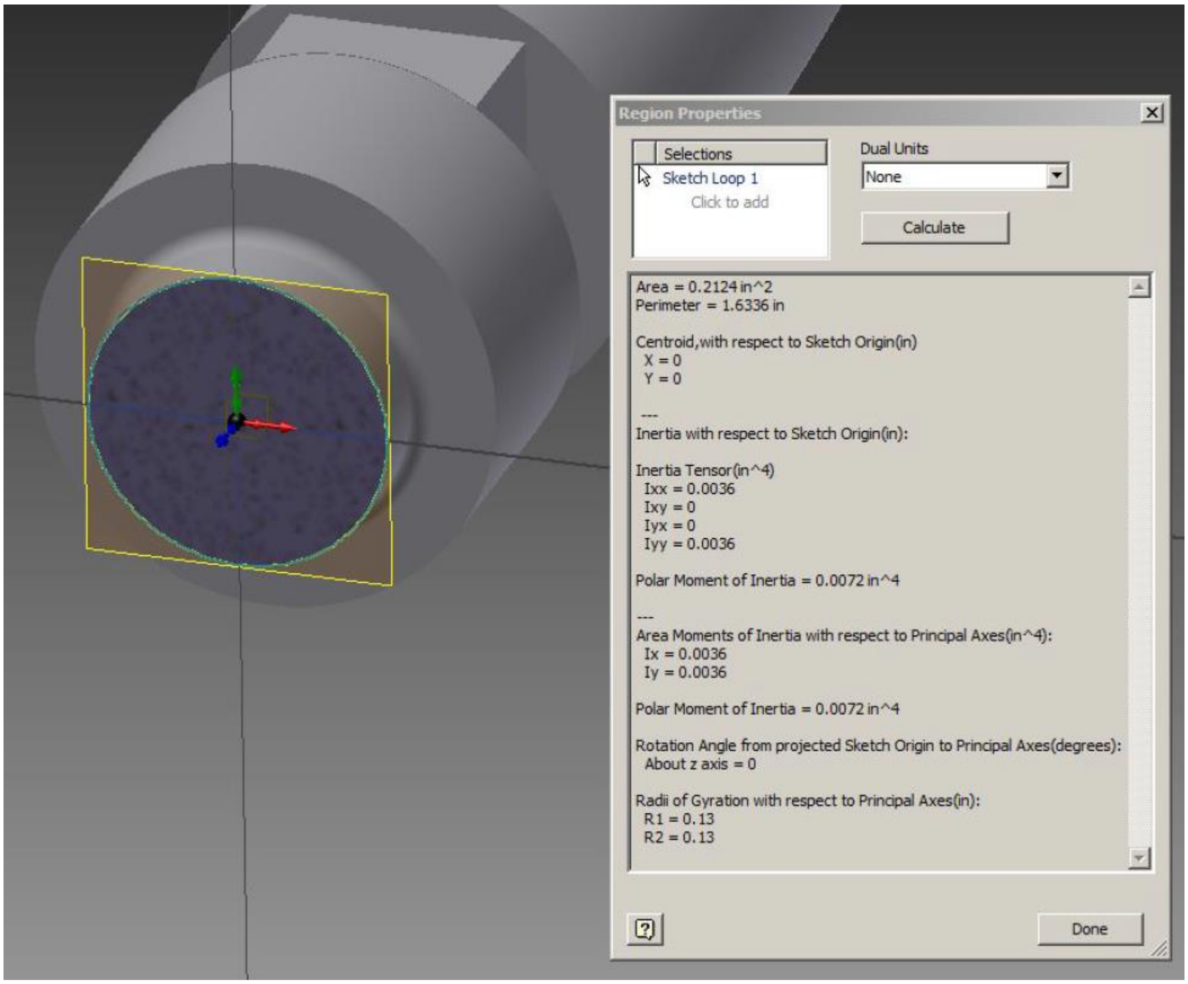

Figure 32. Cross Section of Forward Taper

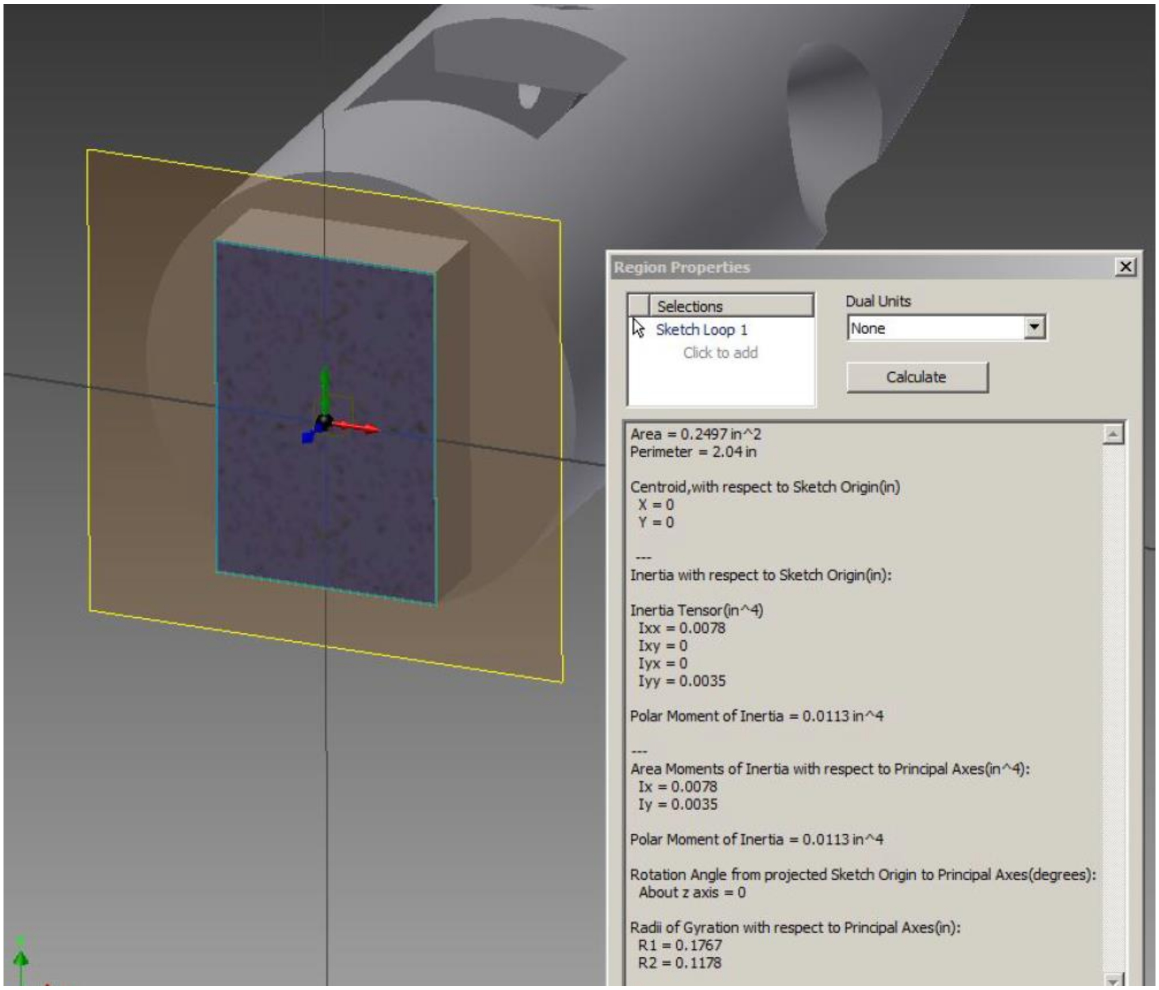

Figure 33. Cross Section of Pitching/Yawing Moment Beam

M_{PM} = [(1.76 * NFmax + PMmax), M_{YM} (1.76 * SFmax + YMmax)^2]^0.5

c_{Normal} = height / 2, c_{Side} = width / 2

I_{Normal} = (b * h^3) / 12 = 0.00346 in^4, I_{Side} = 0.00779 in^4

So, $\sigma_b = \sigma_{PM} + \sigma_{YM}$ = 28.4 ksi + 28.1 ksi = 56.5 ksi, which holds a FoS of 3.28 on yield. Since this balance is symmetric about the balance center the same stress would be calculated on the aft pitching and yawing moment beams.

Next the same load cases were performed using FEA and the results are compared. Table 7 compares the results from the hand calculations to those from the FEA model. Note that agreement exists when compared at the same location which provides some confidence in the FEA results, but note that FEA calculated higher stress on the taper where the fillet was. The hand calculation did not consider this stress concentration, but the FEA picked up on it.

5.3.2 CREATING LOAD MONITORING EQUATIONS

As previously discussed the modified Goodman diagram is the basis for understanding whether cycles are considered significant or not. Because the balance will directly measure loads and not stress, it is important to construct a relationship that calculates the critical node stresses based on the measured

Table 7. Hand vs FEA Calculations

Load	Location	Hand Calc	FEA	FEA at Fillet	% diff at location	% diff at Fillet
NF = 150 SF = 100 PM = 450 YM = 300	Fwd Taper Gage	89,320	90,271	95,619	1.1%	6.6%
	Aft Taper Gage	89,320	90,439	96,819	1.2%	7.7%
	Pitch/Yaw Beam	56,467	57,430	58,609	1.7%	3.7%

balance loads. The overall starting point in this process was to construct a modified Goodman diagram. The construction process began with knowing the ultimate tensile, yield tensile, and endurance limit strength. For 13-8 H1025 these values are 185 ksi, 175 ksi, and 100 ksi respectively. Using these values, the standard modified Goodman diagram, as shown in Fig. 34, was constructed. In Fig. 35 this diagram has been constructed with maximum allowable alternating stress on the x axis. The last step before converting from the stress axes to the load axes is to determine what safety factor should be applied to the mean stress. The AEDC strength and design handbook for the propulsion wind tunnels (PWT) states that a factor of safety of 3 on tensile yield should be used. Using this guideline Fig. 36 shows the max allowable alternating stress diagram with the factor of safety of 3 on yield strength applied.

With the legacy load monitoring method, the next step is to convert this chart from a mean stress vs alternating stress to a mean load vs alternating load for each balance component. This is then normalized by the maximum or rated load for each component. The alternating load axis incorporates the sinusoidal load assumption and accounts for the fact that the measurement is coming from an RMS meter. The results of these steps were seen in Figure 24 which provided an example of the legacy method load limits in chart form. The 3rd level line represents the infinite life line and the 2nd and 1st limits were derived by reducing the 3rd level limit by 25% and 50% respectively. As discussed earlier, the additional limits offer the ability to provide a warning as the infinite life line is

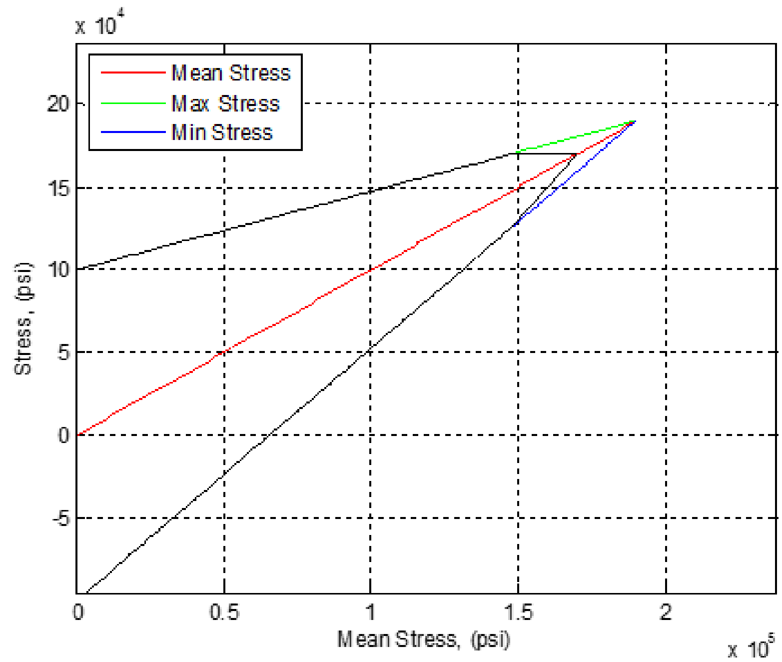

Figure 34. 13-8 Stainless Steel Modified Goodman Diagram

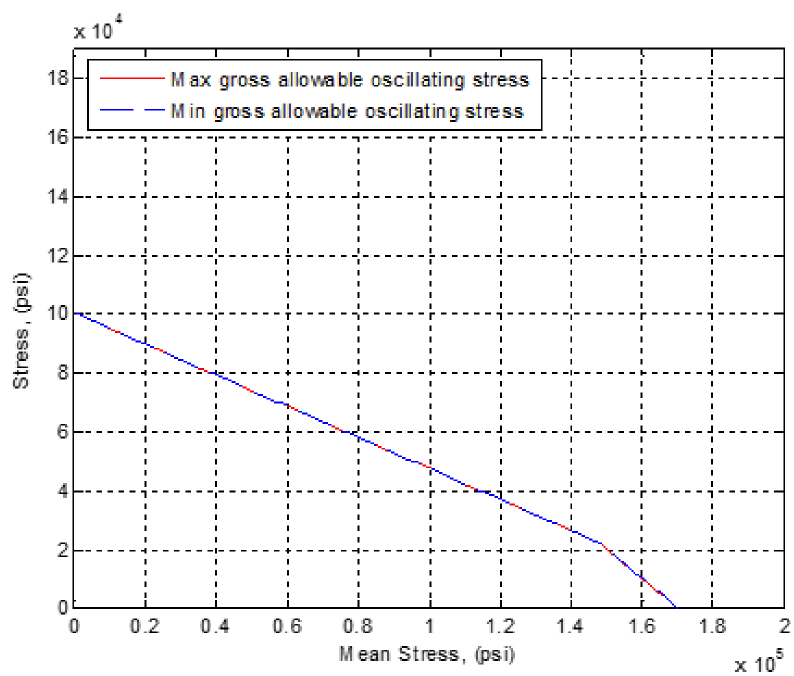

Figure 35. 13-8 Stainless Steel Max Allowable Alternating Stress

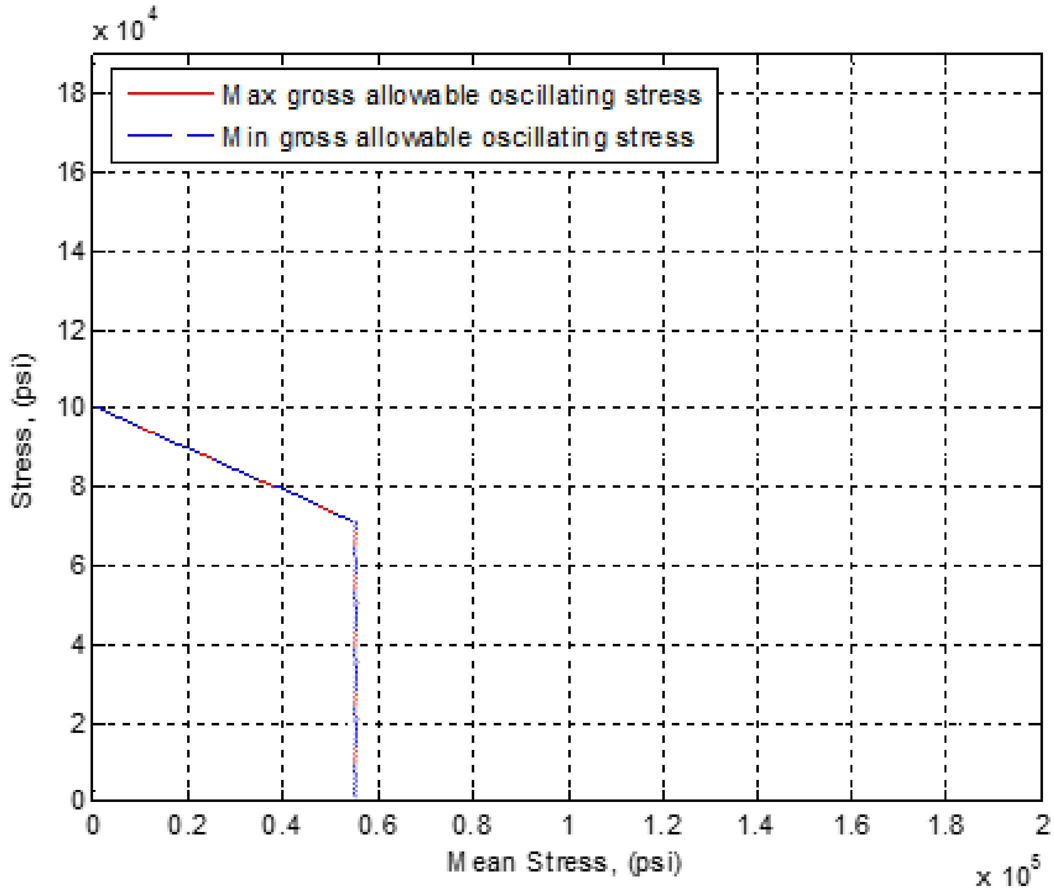

Figure 36. Max Allowable Alternating Stress with Factor of Safety

approached.

In the proposed method once the modified Goodman and allowable alternating stress curves are created, the next step is to create an equation that can be compared to the curves in real-time and alert the control room staff if limits are exceeded. There is no need to convert to the load domain since stress equations can be explicitly written as functions of the balance load components. Hand calculations could be used to perform this step, but it is recommended that a parametric FEA be used to speed up the process and allow for easily computing multi-component load scenarios. Additionally the FEA provides insight into the stress concentration factors of complex geometries that the hand calculations would not incorporate. The initial FEA load cases provided in Table 5 were used to begin the investigation of the relationship between component loads and Von Mises stress. Stress coefficients were derived by dividing the worst case node stresses by the appropriate component loads. Previous research found that the use of superposition to compute the worst case stress for each node based on the balance loads was sufficient for some balance designs (REF 2). This approach can be used for this balance type using the single component maximum load cases and the combined load case.

A new approach where the balance stress was modeled using a global response surface mathematical model was also implemented. For this research, design of experiments (DOE) methodologies were used to determine which FEA test points should be used to characterize the load/stress relationship. Because of its efficient nature and ability to accommodate 2nd-order models, a central composite design (CCD) was chosen (REF 21). Figure 37 provides a graphical representation of a CCD with three factors, and Table 8 shows the CCD test points which were used as inputs into FEA as variable parameters, and it also contains the output results.

A statistical analysis of variance (ANOVA) was performed on the results to determine which factors are significant by calculating an F-statistic (f-value) and probability value (p-value). The overall model has an f-value of 79 and a p-value of nearly 0 which means the model is definitely significant. Reference 21 provides more detail, but a rule of thumb is that p-values less than 0.05

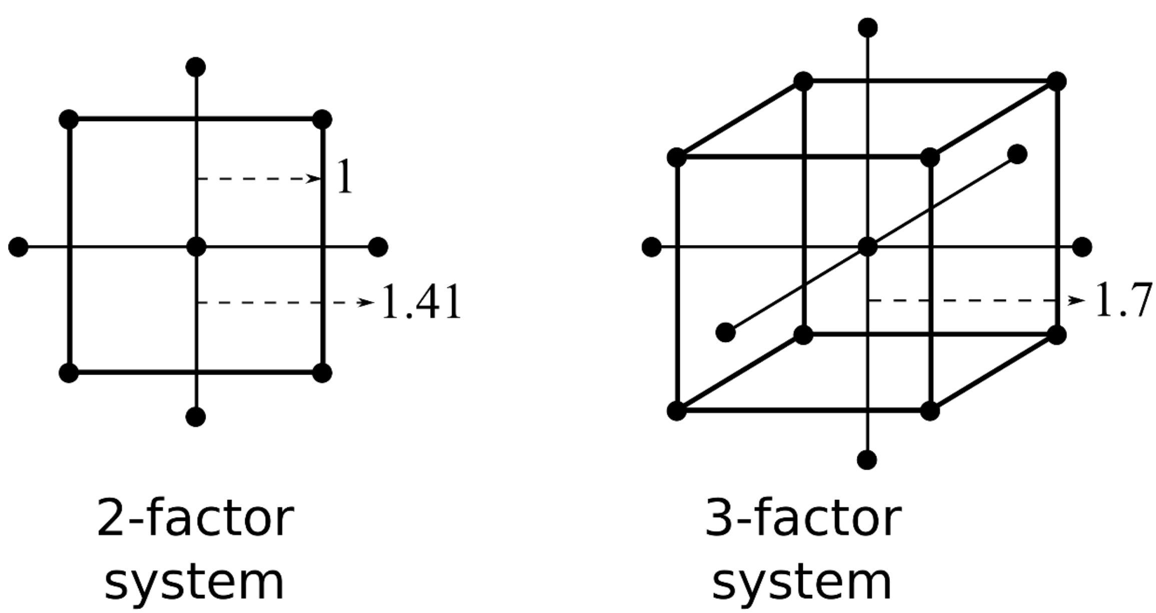

Figure 37. CCD Graphical Representation

Table 8. CCD Load Cases and Results

Load Case	AF (in-lb)	NF (in-lb)	SF (in-lb)	PM (in-lb)	YM (in-lb)	RM (in-lb)	FEA max Von Mises (psi)
1	-40	-150	-100	-450	-300	120	118,518
2	40	-150	-100	-450	-300	-120	135,476
3	-40	-150	-100	-450	300	-120	125,809
4	40	-150	-100	-450	300	120	124,286
5	-40	-150	100	-450	-300	-120	147,310
6	40	-150	100	-450	-300	120	143,212
7	-40	-150	100	-450	300	120	136,162
8	40	-150	100	-450	300	-120	112,357
9	-40	-150	-100	450	-300	-120	181,717
10	40	-150	-100	450	-300	120	184,057
11	-40	-150	-100	450	300	120	152,816
12	40	-150	-100	450	300	-120	151,856
13	-40	-150	100	450	-300	120	159,370
14	40	-150	100	450	-300	-120	160,457
15	-40	-150	100	450	300	-120	157,416
16	40	-150	100	450	300	120	157,323
17	-40	150	-100	-450	-300	-120	157,323
18	40	150	-100	-450	-300	120	157,416
19	-40	150	-100	-450	300	120	160,457
20	40	150	-100	-450	300	-120	159,370
21	-40	150	100	-450	-300	120	151,856
22	40	150	100	-450	-300	-120	152,816
23	-40	150	100	-450	300	-120	184,057
24	40	150	100	-450	300	120	181,717
25	-40	150	-100	450	-300	120	112,357
26	40	150	-100	450	-300	-120	136,162
27	-40	150	-100	450	300	-120	143,212
28	40	150	-100	450	300	120	147,310
29	-40	150	100	450	-300	-120	124,286
30	40	150	100	450	-300	120	125,809
31	-40	150	100	450	300	120	135,476
32	40	150	100	450	300	-120	118,518
33	0	-267.6	0	0	0	0	118,607
34	0	267.6	0	0	0	0	118,607
35	0	0	0	-802.9	0	0	157,824
36	0	0	0	802.9	0	0	157,824
37	0	0	-178.4	0	0	0	79,658
38	0	0	178.4	0	0	0	79,658
39	0	0	0	0	-535.3	0	106,604
40	0	0	0	0	535.3	0	106,604
41	-71.4	0	0	0	0	0	24,295
42	71.4	0	0	0	0	0	24,295
43	0	0	0	0	0	-214.1	109,846
44	0	0	0	0	0	214.1	109,846

indicate that individual terms are significant. The ANOVA results are provided in Table 9. This table shows a somewhat odd result that none of the main effects, A through F, are significant, but many significant terms do exist. Using the ANOVA table only significant contributors and those required to support model hierarchy were chosen for the math model. Table 10 provides the final selected parameters and their corresponding coefficients. Table 11 provides the statistical characteristics of the chosen math model. Finally, additional validation points are calculated using FEA and the mathematical model. Table 12 provides the validation points FEA, math model calculations, and statistical summary results. These results are quite good considering that limited number of data points used to make the model, and this data provides credence that a single math model equation could be developed to monitor the overall balance health. This is not sufficient for counting cycles on each node, but does simplify real-time monitoring. In post processing, the stress can be broken down into the individual node components and summed appropriately.

5.4 REMAINING LIFE ESTIMATES

Once the load limits are known and the data is acquired, the remaining life of the balance can be estimated. As previously discussed, the Goodman-Basquin equation and Miner's rule are the tools used in this balance monitoring methodology. Figure 27 graphically depicts the information that will be used for estimating the remaining life. Points that exceeded the modified Goodman line were input into the Goodman-Basquin equation. Figure 38 is an example of this

Table 9. Full Model ANOVA Table

Source	Sum of Squares	df	Mean Square	F Value	p-value Prob > F
Model	57,248,567,946	27	2,120,317,331	79	1.20875E-17
A-AF	90,387	1	90,387	0	0.954230644
B-NF	2,312,927	1	2,312,927	0	0.771749404
C-SF	495,900	1	495,900	0	0.893074049
D-PM	81,618	1	81,618	0	0.95650491
E-YM	252,532	1	252,532	0	0.923576684
F-RM	12,740,821	1	12,740,821	0	0.497688279
AB	49,912	1	49,912	0	0.96597972
AC	368,040,515	1	368,040,515	14	0.001117826
AD	20,590,949	1	20,590,949	1	0.39004475
AE	181,891,371	1	181,891,371	7	0.015642762
AF	881,679,125	1	881,679,125	33	6.67272E-06
BC	51,517,248	1	51,517,248	2	0.178904143
BD	8,673,412,222	1	8,673,412,222	323	2.01163E-15
BE	1,501,898,731	1	1,501,898,731	56	1.02425E-07
BF	139,845,301	1	139,845,301	5	0.031696865
CD	706,665,730	1	706,665,730	26	3.00493E-05
CE	47,374,985	1	47,374,985	2	0.196735787
CF	78,916,190	1	78,916,190	3	0.099468701
DE	55,748,643	1	55,748,643	2	0.16268084
DF	6,041,703	1	6,041,703	0	0.639661675
EF	227,180,813	1	227,180,813	8	0.007719861
A^2	3,386,975,895	1	3,386,975,895	126	4.89649E-11
B^2	13,787,563,542	1	13,787,563,542	513	1.04308E-17
C^2	2,029,821,993	1	2,029,821,993	76	7.05749E-09
D^2	22,439,372,391	1	22,439,372,391	835	3.69094E-20
E^2	6,547,908,920	1	6,547,908,920	244	4.54192E-14
F^2	7,347,556,170	1	7,347,556,170	273	1.27616E-14
Residual	644,904,663	15	26,871,028		
Cor Total	57,893,472,609	43			

Table 10. Chosen Model ANOVA and Coefficients

Source	Sum of Squares	df	Mean Square	F Value	p-value Prob > F	Coefficients
Model	56966380324	20	2848319016	95.24174764	2.11344E-22	
A-AF	17,008,921		17,008,921			1.082E+01
B-NF	2,353,608		2,353,608			1.084E+00
C-SF	337,320		337,320			9.062E-01
D-PM	51,579		51,579			8.033E-02
E-YM	115,549		115,549			1.827E-01
F-RM	12,838,059		12,838,059			-4.482E+00
AC	296,952,107		296,952,107			-4.360E-01
AE	212,276,530		212,276,530			-2.098E-01
AF	798,688,004		798,688,004			5.701E-01
BD	8,681,087,045		8,681,087,045			-2.430E-01
BE	1,525,802,273		1,525,802,273			1.512E-01
BF	116,245,589		116,245,589			6.720E-02
CD	788,534,073		788,534,073			-1.077E-01
EF	224,789,165		224,789,165			7.359E-02
A^2	3,559,644,894		3,559,644,894			-4.527E+00
B^2	13,789,578,561		13,789,578,561			1.001E+00
C^2	2,024,890,192		2,024,890,192			1.049E+00
D^2	22,428,289,581		22,428,289,581			1.731E-01
E^2	6,542,390,090		6,542,390,090			2.109E-01
F^2	7,338,924,412		7,338,924,412			1.387E+00
Residual	927,092,286		29,906,203			
Cor Total	57,893,472,609					

Table 11. Chosen Model Statistics

Std. Dev.	5468.656		R-Squared	0.983986
Mean	138271.9		Adj R-Squared	0.973655
C.V. %	3.955003		Pred R-Squared	0.954816
PRESS	2.62E+09		Adeq Precision	44.65488

Table 12. Math Model Confirmation Points Results

Confirmation	AF	NF	SF	PM	YM	RM	FEA (ksi)	Predict (ksi)	Error (ksi)
1	150	450	-100	-300	-40	120	241.7	246.8	-5.1
3	150	450	100	300	-40	120	163.9	168.4	-4.5
4	150	-450	100	-300	-40	120	163.0	162.4	0.6
5	-150	450	100	300	40	120	161.0	167.1	-6.1
7	0	0	100	0	0	0	44.6	57.4	-12.8
8	0	0	0	0	300	0	59.7	65.9	-6.1
9	0	150	0	0	0	0	66.5	71.1	-4.6
10	0	0	0	450	0	0	88.5	81.9	6.5
12	0	0	0	0	0	120	61.6	66.3	-4.7

stdev	5.24
average	-4.09

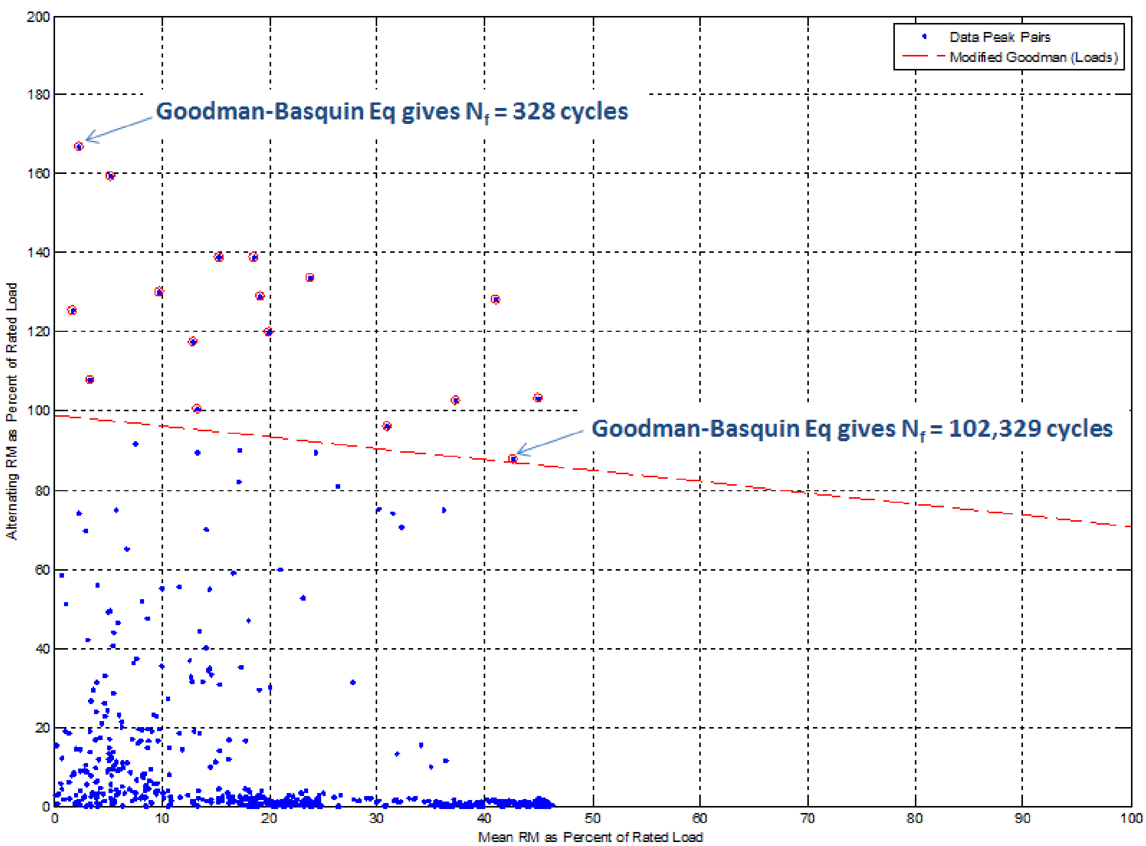

Figure 38. Goodman-Basquin Life Estimate

with two of the calculation results included on the plot. The point at the top left indicates the load condition experienced at that time could only be performed another 328 times before the balance would fail. This single point has reduced the life of the balance by 1/328 = 0.003 or 0.3%. Summing all the points that are significant from the three dynamic events via Miner's rule indicates this balance has an estimated 99.3% of fatigue life remaining. This calculation was performed using the legacy load limits and assuming that all of the significant cycles could be summed together as if occurring at the same node. The same exercise was done using the math model developed in the previous section. This resulted in an estimated 99.4% of fatigue life remaining, but again this does not break it down into an individual node components. It should also be noted that each of these calculations used the peak-to-peak pairs that were identified using the peak finding algorithm. Although the peak-to-peak method is sufficient for online data monitoring, rigor should be added to the post test process by using a rainflow counting algorithm. This method takes all the identified peaks and rearrange them so the maximum stress and minimum stress are considered to have occurred in a back to back fashion. This algorithm continues until new pairs of peaks are identified that make up the actual alternating stress history. Figure 39 shows how the rainflow algorithm would identify the mean and alternating stress on the previously used example. It can be seen that nearly the same maximum data pairing is identified, but much of the rest of the plot looks different.

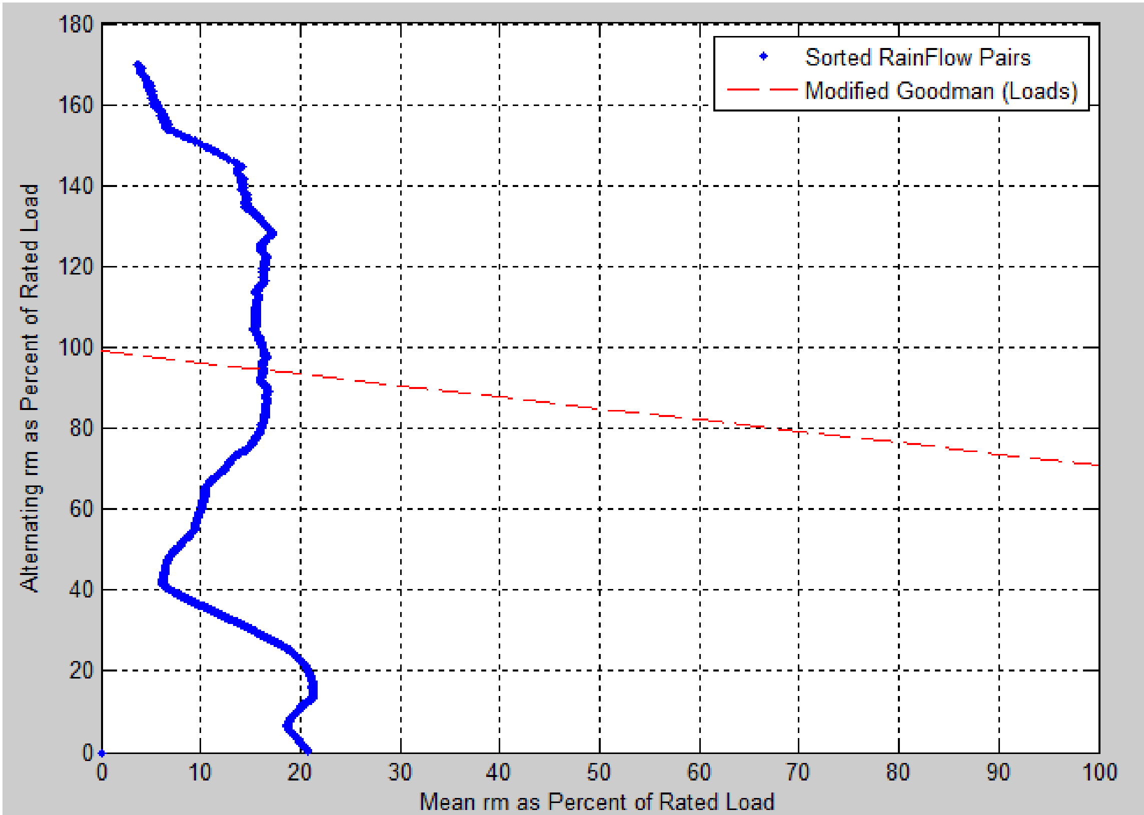

Figure 39. Rainflow Sorted Pairs

Using the rainflow pairs, the final remaining fatigue life estimate is 98.5% which is significantly less than the peak-to-peak alternating stress method.

6.0 CONCLUSIONS AND RECOMMENDATIONS

A new balance monitoring methodology has been developed for use at AEDC. This method built upon the positives of the legacy method, but improved on the deficiencies. The following conclusions are drawn:

1. The new method improves the accuracy of the balance monitoring signal. By eliminating the analog RMS meter the potential to lose as much as 30% of the signal, based solely on the hardware setup frequency, is removed. Additionally, errors as large as 20% are erased by no longer assuming the data will be sinusoidal. Accuracy is further improved by up to 70% by using at least a 6x6 balance calibration to capture interaction terms.
2. The new method does not use a low-pass and high-pass frequency filter to divide the balance signal into a steady state and dynamic component. Instead a peak-finding algorithm is used, which allows analysis to be done in the cycle domain. This improvement will prevent low cycle fatigue failures which were previous ignored because of the filtering in the legacy system.
3. The new method monitors the balance in terms of stress not load. This gives improved flexibility on the allowable loads applied to the balance. Instead of being limited to one set of rated loads, the balance is limited to a rated stress. Because it is monitoring loads, the legacy method has the

potential to limit a balance from using its full capacity, and the new method eliminates this possibility.

4. Finally, the new method provides additional information that the legacy method did not. First, all of the balance data is recorded for the entire time the balance is hooked up. This removes the possibility of a dynamic event information being missed. The legacy system still alerts a dynamic event even if the data is not stored, but no severity information or further analysis can be performed. The Goodman-Basquin results provide this severity information. This information gives the wind tunnel test engineer the ability to differentiate the harshness of dynamic events. Furthermore, this information is summed using Miner's rule to provide remaining life estimates. All of these additional information sources provide insight which was previously not available.
5. The legacy method is insufficient to identify stress exceedances and has a poor ability to capture transient exceedances that do not have a sustained alternating component. The new method identifies these transient events to protect the balance.

This remaining life calculations should be used as preventative maintenance. The concept of preventive maintenance brings up an interesting point. What about the AEDC balance inventory which has seen years of testing and does not have recorded dynamic data or estimated remaining life predictions for its previous use? How should these balances be used? Whether a balance is new and its entire history has been recorded or it is from 1971 like the balance selected for this study, the recommendation is to use the remaining fatigue life estimates presented in this thesis as a guideline. The starting point of the balance can be estimated based on inspection and calibration histories. The fact is that fatigue failure is extremely hard to predict. The concluding thought is it that it is better to put metrics in place to know whether a balance is heading towards failure quickly or slowly than to not have anything. Even if all failures are not prevented, keeping these metrics will prevent some failures which is an improvement. In this way, the estimated life predictions can be qualitative and serve as information to the Test Engineer on the risk of continuing to test if high stresses are regularly being encountered.

Although the methodology presented here brings substantial improvements over the legacy method, the presented methodology is far from perfect. Much work can still be done in this area. Specifically, the interpretation of FEA results needs refinement, and these results must be seamlessly incorporated into the balance monitoring effort. The balance used in this study was relatively simple and allowed for convergence of the results and mesh size. In some balances, stress concentration points make it difficult to reach mesh size convergence. The incorporation of a stress mathematical model simplifies the process of incorporating the FEA results, but the errors shown were larger than desired. More study here could provide value. Additionally, this method does not address non-linear fatigue failure theories which attempt to account for path

dependencies of the loads experienced and other time dependent phenomena.
To provide more accuracy these will have to be considered.

LIST OF REFERENCES

1. Grenat, Gerard, et al., “Real-time PC monitoring of strain-gauge balances in ONEARA’s large wind tunnels using finite elements design tools.” Forth International Balance Symposium, 2004
2. Bennett, Henry H., “Wind Tunnel Balance Safety of Flight System”, 7th International Symposium on Strain-Gage Balances, 2010.
3. Miller, N. L., “A Six-Component Internal Strain Gage Balance System”. North American Aviation Inc. 1948
4. http://www.ruag.com/aviation/subsystems-products/engineering/aerodynamics/instrumentation/strain-gauge-balance/
5. http://www.mmtool.com/aero.html
6. http://www.nlr.org/capabilities/balance-design-and-manufacturing/
7. http://www.vishaypg.com/docs/25506/25506.pdf
8. http://www.omega.com/literature/transactions/volume3/strain.html
9. “Calibration and Use of Internal Strain-Gage Balances with Application to Wind Tunnel Testing”, AIAA R-091-2003, 2003
10. Lindeburg, Micheal R. “Mechanical Engineering Reference Manual”. 12th ed. Belmont, CA: Professional Publications, 2006.
11. Vis, De D., et al. “Fatigue Lifetime Estimation of Structures Subjected to Dynamic Loading.” AIAA Journal, Vol. 24, No. 8, 1986.
12. Maleque, M.A. “Materials Selection and Design”. Springer, 2013
13. https://www.comsol.com/multiphysics/material-fatigue

14. Shigley, Joseph E. “Mechanical Engineering Design”, 5th ed. McGraw-Hill Mechanical Engineering, 1988.

15. L. Yang and A. Fatemi, “Cumulative Fatigue Damage Mechanisms and Quantifying Parameters: A Literature Review,” J. of Testing and Evaluation, Vol. 26, 1998.

16. ASM International Handbook Committee. “ASM Handbook, Volume 01 - Properties and Selection: Irons, Steels, and High-Performance Alloys”, ASM International, 1990.

17. Deel, O. L. and Mindlin, H. “Engineering Data on New Aerospace Structural Materials.” AFML-TR-72-196 Volume II, 1973.

18. ASTM E1049 Standard, “Standard Practices for Cycle Counting in Fatigue Analysis.” ASTM International, 2011.

19. Grenander, Ulf . "The Nyquist frequency is that frequency whose period is two sampling intervals." Probability and Statistics: The Harald Cramér Volume. Wiley. 1959.

20. “Test Article Design and Strength Requirements – AEDC/PWT Wind Tunnels 16T/16S/4T”, AEDC-HDBK-03-01, Aerospace Testing Alliance, October 2003.

21. Montgomery, Douglas C. “Design and Analysis of Experiments”, 6th ed. Wiley, 2004.

VITA

David L. Yoder was born in Huntsville, Alabama in September 1984 to Mr. Leon Yoder and Mrs. Pam Yoder. He obtained his Bachelor of Science degree in Mechanical Engineering from Tennessee Tech University, Cookeville, TN in 2006. After graduation he was hired to work at the Arnold Engineering Development Complex, Arnold AFB, TN serving as a wind tunnel Project Engineer. He attended the University of Tennessee Space Institute starting in 2013.